

COORDINATION COMPLEXES OF HEXADENTATE
PHTHALAZINE HYDRAZONE LIGANDS

CENTRE FOR NEWFOUNDLAND STUDIES

**TOTAL OF 10 PAGES ONLY
MAY BE XEROXED**

(Without Author's Permission)

TAO WEN

COORDINATION COMPLEXES OF HEXADENTATE

PHthalazine HYDRAZONE LIGANDS

BY

(E)

Tao Wen, B.Sc. (Hons.)

A thesis submitted to the School of Graduate
Studies in partial fulfillment of the
requirements for the degree of
Master of Science

Department of Chemistry

Memorial University

June 1988

St John's

Newfoundland

Canada

Permission has been granted to the National Library of Canada to microfilm this thesis and to lend or sell copies of the film.

The author (copyright owner) has reserved other publication rights, and neither the thesis nor extensive extracts from it may be printed or otherwise reproduced without his/her written permission.

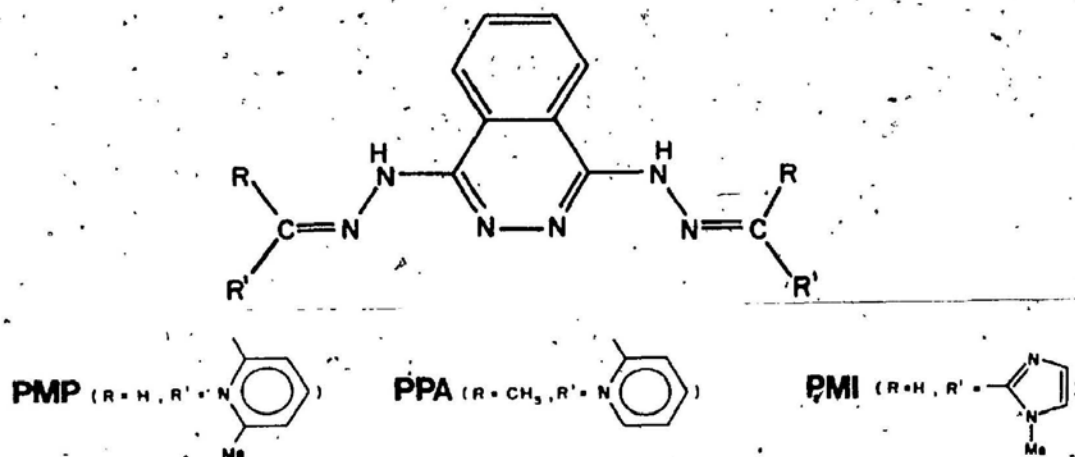
L'autorisation a été accordée à la Bibliothèque nationale du Canada de microfilmer cette thèse et de prêter ou de vendre des exemplaires du film.

L'auteur (titulaire du droit d'auteur) se réserve les autres droits de publication; ni la thèse ni de longs extraits de celle-ci ne doivent être imprimés ou autrement reproduits sans son autorisation écrite.

ISBN 0-315-45080-0

ABSTRACT

The cobalt(II) and nickel(II) coordination complexes of three potentially hexadentate phthalazine hydrazone ligands, obtained by reacting 1,4-dihydrazinophthalazine (DHPH) with an appropriate aldehyde or ketone, have been investigated, in which the variable terminal donor substituents include 6-methyl pyridine (PMP), pyridine (PPA) and N-methyl imidazole (PMI) groups. Studies on the analyt-



ical, spectral, X-ray, and magnetic data of the complexes reveal that the ligands are able to form double μ -bridged bimetallic complexes, in which two pseudo-octahedral metal centers are brought into close proximity by a common phthalazine diazine bridge as well as by the second either anionic [binuclear 2:1 (metal:ligand) species] or another diazine bridge [binuclear 1:1 derivatives]. In the binuclear 2:1 complexes three in-plane coordination sites of the pseudo-octahedral metal center are occupied

by ligand nitrogen donors and the rest of the sites involve coordinated anions and water/solvent molecules. Two binuclear 2:1 chloride complexes of the ligand PMP, $[\text{Co}_2(\text{PMP})\text{Cl}(\text{H}_2\text{O})_4]\text{Cl}_3 \cdot 4\text{H}_2\text{O}$ and $[\text{Ni}_2(\text{PMP})\text{Cl}(\text{H}_2\text{O})_4]\text{Cl}_3 \cdot 4.5\text{H}_2\text{O}$, have been characterized by single crystal X-ray diffraction. For the 1:1 compounds the six coordination sites are all occupied by the nitrogen atoms from two ligands. All the complexes exhibit very intense metal-to-ligand charge transfer absorption ($\epsilon > 9200 \text{ Lmol}^{-1}\text{cm}^{-1}$) in the visible region ($19000 - 21000 \text{ cm}^{-1}$). Variable-temperature magnetic susceptibility measurements on some complexes indicate antiferromagnetic exchange between the metal ion centers.

ACKNOWLEDGEMENTS

First of all, I wish to express my sincere gratitude to my supervisor Dr. L. K. Thompson, Professor of Chemistry at Memorial University, for his patience, valuable advice, and kind encouragement throughout the course of this study.

My special appreciation is extended to Dr. J. N. Bridson, Head of the Chemistry Department, for his enthusiastic support and recommendation for my graduate studies at Memorial. Helpful advice and assistance from Dr. S. K. Mandal are also highly appreciated.

Financial support from Memorial University, in the form of University Graduate Fellowships and Teaching Assistantships, and from Dr. Thompson's Grant (Natural Sciences and Engineering Research Council of Canada, Operating Grant No. A1031) are gratefully acknowledged.

Furthermore, many thanks also go to Dr. M. J. Newlands for his graphics assistance, to Mrs. M. Hooper for her assistance in the metal analyses, and to Mr. J. Sheng for assisting me in typing this work.

Finally, I am greatly indebted to my parents for their enthusiasm, help and encouragement.

Table of Contents

ABSTRACT	i
ACKNOWLEDGEMENTS	iii
TABLE OF CONTENTS	iv
LIST OF FIGURES	vii
LIST OF TABLES	x
 SECTION I INTRODUCTION	 1
Chapter 1 GENERAL SIGNIFICANCE AND PURPOSE	2
1.1. Binuclear complexes as models for metalloproteins	2
1.2. Binuclear complexes as mediators of ne^- redox processes	9
1.3. The objectives of the project	11
 Chapter 2 HISTORICAL BACKGROUND AND LITERATURE SURVEY	 13
2.1. Compartmental ligands	15
2.1.1. Macrocyclic compartmental ligands	15
2.1.2. Acyclic compartmental ligands	17
2.2. Isolated donor sets	18
2.2.1. Macrocyclic systems	18
2.2.2. Acyclic systems	19
 Chapter 3 ELECTRONIC SPECTRA AND MAGNETIC PROPERTIES OF COBALT COMPLEXES	 32
3.1. High-spin octahedral and tetrahedral complexes of $Co(II)$	34
3.2. Magnetic properties of high-spin $Co(II)$ complexes	36
3.3. Low-spin octahedral complexes of $Co(III)$	38
 Chapter 4 ELECTRONIC SPECTRA AND MAGNETIC PROPERTIES OF NICKEL(II) COMPLEXES	 39
4.1. Electronic spectra of $Ni(II)$ in an octahedral field	39
4.2. Electronic spectra of $Ni(II)$ in a tetrahedral field	41
4.3. Magnetic properties of $Ni(II)$ complexes	42

Chapter 5	MAGNETIC PROPERTIES OF BINUCLEAR CENTERS	43
5.1.	Antiferromagnetic behaviour	43
5.2.	Mechanisms of antiferromagnetic exchange interaction	44
5.3.	Antiferromagnetism in binuclear transition metal complexes	46
5.4.	Magnetic exchange in binuclear Ni(II) complexes	48
5.5.	Magnetic exchange in binuclear Co(II) complexes	54
Chapter 6	SOME BINUCLEATING SEXADENTATE PHTHALAZINE HYDRAZONE LIGANDS	58
6.1.	The binucleating ligand PMP	60
6.2.	The binucleating ligand PPA	61
6.3.	The binucleating ligand PMI	61
SECTION II	RESULTS AND DISCUSSION	63
Chapter 7	BINUCLEAR COBALT(II)/NICKEL(II) COMPLEXES OF THE LIGANDS PMP, PPA AND PMI	64
Chapter 8	CRYSTAL AND MOLECULAR STRUCTURES OF THE BINUCLEAR HALIDE COMPLEXES OF THE LIGAND PMP	70
8.1.	Crystal structure of $[\text{Co}_2(\text{PMP})\text{Cl}(\text{H}_2\text{O})_4]\text{Cl}_3 \cdot 4.0\text{H}_2\text{O}$ (36)	70
8.2.	Crystal structure of $[\text{Ni}_2(\text{PMP})\text{Cl}(\text{H}_2\text{O})_4]\text{Cl}_3 \cdot 4.5\text{H}_2\text{O}$ (50)	74
Chapter 9	SPECTROSCOPY AND STRUCTURES OF THE BINUCLEAR PMP, PPA AND PMI COMPLEXES	84
9.1.	The infrared spectra of the binuclear complexes	84
9.2.	The electronic spectra of the binuclear complexes	91
Chapter 10	MAGNETIC PROPERTIES OF THE BINUCLEAR PMP, PPA AND PMI COMPLEXES	98
10.1.	The room-temperature magnetic moment	98
10.2.	The variable-temperature magnetic susceptibility	104
Chapter 11	CONCLUDING REMARKS AND SUMMARY	117

SECTION III	EXPERIMENTAL AND MISCELLANEOUS	121
Chapter 12	EXPERIMENTAL	122
12.1.	Elemental analysis and physical measurements	122
12.2.	The syntheses of the ligands	123
12.3.	The syntheses of the complexes	125
REFERENCES	129
APPENDIX A	Some X-ray data for complexes 38 and 50	134
APPENDIX B	V-T magnetic susceptibility data of some complexes	136

LIST OF FIGURES

Fig. 1.1	Proposed iron site in oxyhemerythrin.	3
Fig. 1.2	(a) Proposed binuclear site in oxyhemocyanin. (b) The binuclear site in <i>Panulirus interruptus</i> hemocyanin.	4
Fig. 1.3	(a) Models for the bicopper-site met(resting) and oxy-tryosinase. (b) Proposed mechanism of phenol hydroxylation and oxidation to form <i>o</i> -quinones by tryosinase.	5
Fig. 1.4	Proposed active site in cytochrome <i>c</i> oxidase.	6
Fig. 1.5	Schematic representation of the bimetal site in Cu-Zn superoxide dismutase.	7
Fig. 1.6	Binuclear cation for $[\text{Co}_2(\text{TAPH})](\text{NO}_3)_4$.	11
Fig. 1.7	Binuclear cation for $[\text{Co}_2(\text{DPT})_2]\text{Cl}_2 \cdot 2\text{H}_2\text{O}$.	11
Fig. 2.1	Schematic representation of the dinitrogen trapping by binucleated metals.	13
Fig. 2.2	Diazine unit and its derivatives.	20
Fig. 3.1	Splitting of the 4F and 4P free ion terms of high spin Co(II) in various coordination geometries.	33
Fig. 3.2	Simplified Tanabe-Sugano diagram for d^7 , Co(II), ion in an octahedral crystal field and possible spin-allowed transitions (<i>B</i> represents the interelectronic repulsion or Racah parameter).	35

Fig. 4.1	The splitting of d orbitals in fields of different symmetries, and the resulting electronic configuration of d^8 , Ni(II), ion.	40
Fig. 4.2	Simplified Tanabe-Sugano diagram for d^8 , Ni(II), ion in an octahedral crystal field and possible spin-allowed transitions.	41
Fig. 5.1	A comparison of the characteristic variation of susceptibility with temperature for normal paramagnetic (1), antiferromagnetic (2) and ferromagnetic (3) materials.	45
Fig. 5.2	Superexchange in linear M-O-M system. An example of superexchange via (a) σ -bonding and (b) π -bonding.	46
Fig. 5.3	The relative energies and multiplicities of the possible spin state of a binuclear complex.	47
Fig. 5.4	Ni(II) with an internal axial field and an external magnetic field.	49
Fig. 6.1	The intermediate DHPH and its derivatives; binucleating ligands PMP, PPA and PMI.	59
Fig. 8.1	Structural representation of $[\text{Co}_2(\text{PMP})\text{Cl}(\text{H}_2\text{O})_4]^{3+}$, 38 , with hydrogen atoms omitted (40% probability thermal ellipsoids).	75
Fig. 8.2	Structural representation of $[\text{Ni}_2(\text{PMP})\text{Cl}(\text{H}_2\text{O})_4]^{3+}$, 50 , with hydrogen atoms omitted (40% probability thermal ellipsoids).	81
Fig. 9.1	Proposed structure for the binuclear cation $[\text{M}_2\text{L}_2]^{4+}$ in the binuclear 1:1 derivatives.	97

Fig. 10.1	Magnetic susceptibility data for the PMP Ni(II) chloride complex 50 . The solid line was calculated from equation (10-2) with $g = 2.227(3)$, $J = -12.99(6) \text{ cm}^{-1}$, $D = 7.60(2) \text{ cm}^{-1}$, $Z'J' = 0.040(2) \text{ cm}^{-1}$ (corrected for 4% paramagnetic impurity).	106
Fig. 10.2	Magnetic susceptibility data for the PMP Ni(II) bromide complex 51 . The solid line was calculated from equation (10-2) with $g = 2.248(8)$, $J = -10.60(1) \text{ cm}^{-1}$, $D = 10.3(1) \text{ cm}^{-1}$, $Z'J' = 0.0010(2) \text{ cm}^{-1}$ (corrected for 4.2% paramagnetic impurity).	107
Fig. 10.3	Magnetic susceptibility data for the PPA Ni(II) nitrate complex 57 . The solid line was calculated from equation (10-2) with $g = 2.148(2)$, $J = -0.35(1) \text{ cm}^{-1}$, $D = 20.22(2) \text{ cm}^{-1}$, $Z'J' = 0.41(1) \text{ cm}^{-1}$.	108
Fig. 10.4	Magnetic susceptibility data for the PPA Ni(II) tetrafluoroborate complex 59 . The solid line was calculated from equation (10-2) with $g = 2.127(2)$, $J = -0.34(1) \text{ cm}^{-1}$, $D = 20.50(1) \text{ cm}^{-1}$, $Z'J' = 0.30(1) \text{ cm}^{-1}$.	109
Fig. 10.5	Magnetic susceptibility data for the PMP Co(II) chloride complex 36 . The solid line was calculated from equation (5-27) with $g = 2.45$, $J = -3.18 \text{ cm}^{-1}$.	113
Fig. 10.6	Magnetic susceptibility data for the PMP Co(II) bromide complex 37 . The solid line was calculated from equation (5-27) with $g = 2.31$, $J = -3.16 \text{ cm}^{-1}$.	114
Fig. 10.7	Magnetic data for $[\text{Co}_2(\text{PMP})\text{Cl}(\text{H}_2\text{O})_4]\text{Cl}_3 \cdot 4\text{H}_2\text{O}$, 36 .	115
Fig. 10.8	Magnetic data for $[\text{Co}_2(\text{PMP})\text{Br}(\text{H}_2\text{O})_4]\text{Br}_3 \cdot 3\text{H}_2\text{O}$, 37 .	116
Fig. 11.1	The proposed binuclear structure for 47 and 62 .	118
Fig. 11.2	The proposed binuclear structure for 41 .	119

LIST OF TABLES

Table 2.1.	The major parameters of some binuclear complexes.	22
Table 2.2.	Magnetic and key structural parameters for binuclear μ -bridged Cu(II) complexes of the ligand 27 .	28
Table 3.1.	Typical values of room temperature effective magnetic moments of Co(II) and Ni(II) complexes in various coordination environments.	37
Table 7.1.	Analytical data for the binuclear Co(II) complexes of the ligands PMP, PPA and PMI.	65
Table 7.2.	Analytical data for the binuclear Ni(II) complexes of the ligands PMP, PPA and PMI.	66
Table 8.1.	Summary of crystal data and diffraction data collection.	72
Table 8.2.	Atomic parameters X, Y, Z and BISO for 36 . E.S.D's refer to the last digit printed.	73
Table 8.3.	Interatomic distances (\AA) and angles (deg.) relevant to the Co(II) coordination sphere in 36 .	76
Table 8.4.	Interatomic distances (\AA) and angles (deg.) relevant to the ligand in the complex 36 .	77

Table 8.5.	Atomic parameters X, Y, Z and BISO for 50 . E.S.D's refer to the last digit printed.	79
Table 8.6.	Interatomic distances (Å) and angles (deg.) relevant to the Ni(II) coordination sphere in 50 .	82
Table 8.7.	Interatomic distances (Å) and angles (deg.) relevant to the ligand in the complex 50 .	83
Table 9.1.	Infrared spectral data for the binuclear Co(II) complexes.	85
Table 9.2.	Infrared spectral data for the binuclear Ni(II) complexes.	86
Table 9.3.	Electronic spectral data for the binuclear Co(II) complexes.	92
Table 9.4.	Electronic spectral data for the binuclear Ni(II) complexes.	93
Table 10.1.	Magnetic data for the binuclear Co(II) complexes.	99
Table 10.2.	Magnetic data for the binuclear Ni(II) complexes.	103

SECTION I INTRODUCTION

CHAPTER 1

GENERAL SIGNIFICANCE AND PURPOSE

An important new development in the field of coordination chemistry is the design and synthesis of ligands capable of binding two transition metal ions. Such systems include saturated monocyclic¹ and bicyclic² hexamines and related ligands³, cyclic⁴ and acyclic⁵ Schiff bases, polycyclic cryptands⁶, "earmuffs"⁷, "wishbones"⁸, and "face-to-face"⁹, "capped"¹⁰, and "crowned"¹¹ porphyrins. Of particular interest to us is the use of binucleating ligands to fix two interacting metal atoms within a ligand cavity. The resulting bimetallic center may be capable of binding substrates or incorporating bridging ligands. Systems of this type may have value (a) as models for metalloproteins and (b) as mediators of multi-electron redox processes.

1. 1. Binuclear Complexes as Models for Metalloproteins

There are many metalloproteins, or metalloenzymes, which possess functional centers containing two metal atoms held close together, less than 10 Å apart and often less than 5 Å apart¹². The metal atoms often share a bridging ligand, or ligands, and the pairing of metals may be homobimetallic or heterobimetallic. The desire to understand the nature of these sites has led to the use of bimetallic complexes of binucleating ligands as speculative models for the metal

environment. With time and the availability of more precise information from X-ray studies these have, in certain cases, approached corroborative status.

A brief description of the sites in selected bimetallobiomolecules is given below. The molecules under discussion herein are the homobimetallo-systems hemerythrin, hemocyanin and tyrosinase, and the heterobimetallo-species cytochrome c oxidase and superoxide dismutase.

A. Hemerythrin (Fe, Fe)¹³

Hemerythrin has been designated an "alternative dioxygen carrier". It is present in the red blood cells of some marine invertebrate phyla notably siphunculid worms. The active center is a pair of iron atoms about 3.5 Å apart and contained within a single polypeptide chain.

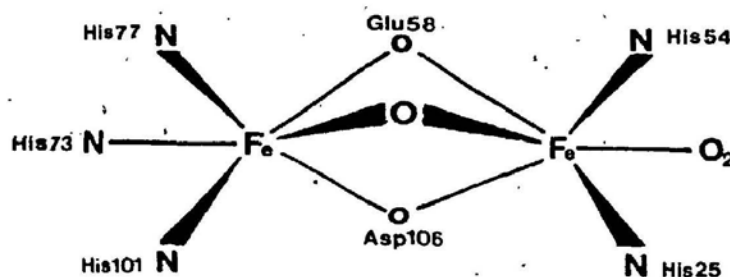


Fig. 1.1 Proposed iron site in oxyhemerythrin.

For the oxy form the structure in Fig. 1.1 has been suggested, in which the binuclear iron center contains a μ -oxo bridge similar to that in μ -oxo diiron(III) complexes.

B. Hemocyanin (Cu, Cu)^{14,a,b,c}

Dioxygen, for the metabolism of arthropods and molluscs, is bound and transported by hemocyanin. The active center is a pair of copper atoms capable of binding one dioxygen molecule. A variety of studies indicate that the Cu(II) ions in oxyhemocyanin reside in a ligand environment composed of two or three nitrogen donors, a bridging dioxygen ligand, and an endogenous protein bridge. The Cu-Cu distance is 3.55 Å and each Cu is square planar or square-pyramidal (Fig. 1.2, a). The bridge (X) is believed to mediate the very strong ($-2J > 1000 \text{ cm}^{-1}$) antiferromagnetic spin exchange interaction between the metals which results in an essentially diamagnetic pair of Cu(II) atoms^{14,b}.

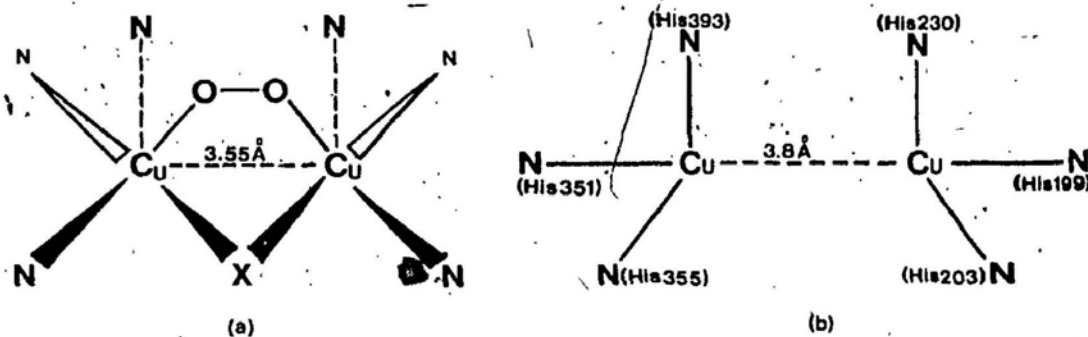


Fig. 1.2 (a) Proposed binuclear site in oxyhemocyanin. (b) The binuclear site in *Panulirus interruptus* hemocyanin.

Recently, the three-dimensional structure of *Panulirus interruptus* deoxyhemocyanin, as the first member of the copper-containing class of oxygen-carrying proteins, has been determined by X-ray crystallography^{14,c}. The structure at 3.2 Å resolution shows that the six histidines in the second domain of the subunit ligate the two oxygen-binding copper atoms which are separated by a distance of 3.8(0.4) Å (Fig. 1.2, b). The availability of binuclear copper model com-

pounds will help to identify the active site geometry and nature of this endogenous bridge. Even when the structures of the binuclear copper proteins are known from X-ray crystallography, however, well designed model compounds will be useful to probe the fundamental differences in their functions.

C. Tyrosinase (Cu, Cu)^{14,a,d}

Tyrosinase is a Cu-containing mono-oxygenase found in many different micro-organisms, plants, and animals, and is capable of catalysing the *o*-hydroxylation of monophenols and oxidation of *o*-diphenols to *o*-quinones. The binuclear site contains antiferromagnetically coupled Cu(II) pairs. The structure representative of the metal centers has been proposed as shown in Fig. 1.3, a.

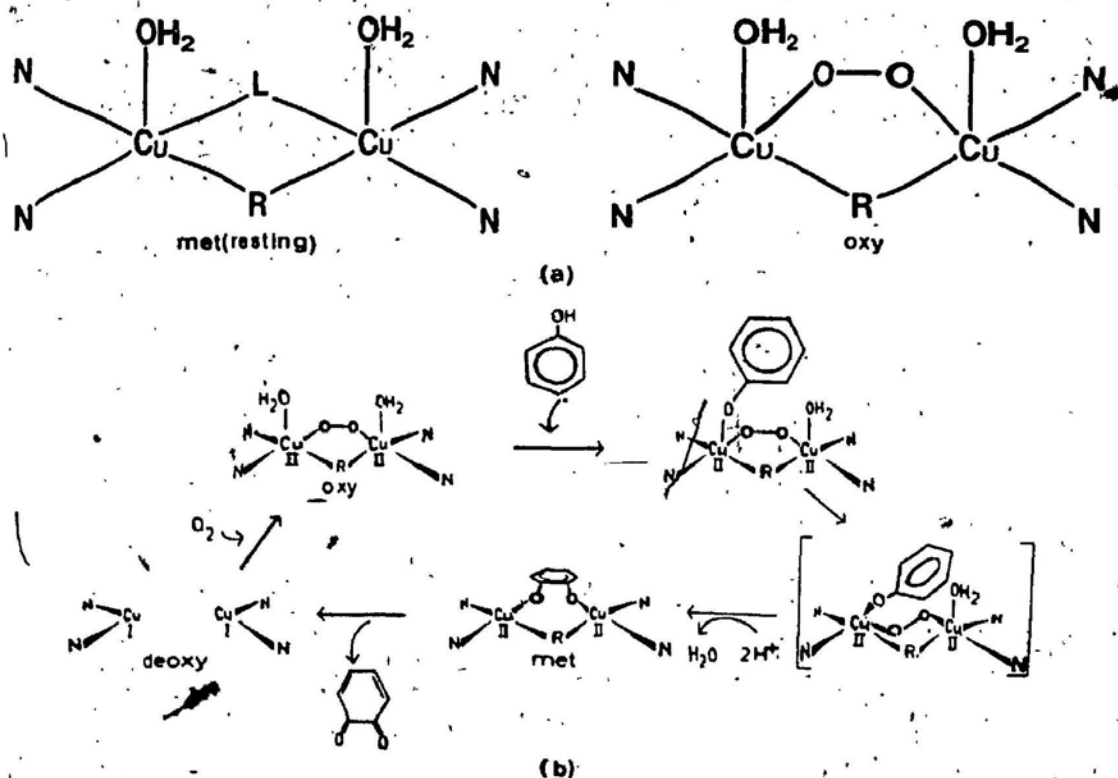


Fig. 1.3 (a) Models for the bicopper-site met(resting) and oxy-tyrosinase. (b) Proposed mechanism of phenol hydroxylation and oxidation to form *o*-quinones by tyrosinase.

A detailed study on competitive inhibitor binding to tyrosinase^{14,4} has led to a structural mechanism for the functions of the coupled binuclear Cu(II) active site in monophenol hydroxylation reactions (Fig. 1.3, b).

D. Cytochrome c Oxidase (Fe, Cu)¹⁵

Cytochrome c oxidase is a complex enzyme which contains two heme units, low spin heme_a and high spin heme_{a3}, and two Cu(II) atoms. It is located as the terminal component of the mitochondrial respiratory chain and has the important role of catalysing the rapid, four-electron reduction of molecular oxygen to water.

In the oxidised form heme_{a3} and Cu_{a3} exhibit properties which indicate that the two metal centers are strongly antiferromagnetically coupled, making the two metals EPR invisible, and reducing their magnetic susceptibilities (the exchange coupling constant, $-2J$, of $> 400 \text{ cm}^{-1}$ for the oxidase). The heme_{a3} and Cu_{a3} were therefore assumed to be in close proximity and linked by a ligand which

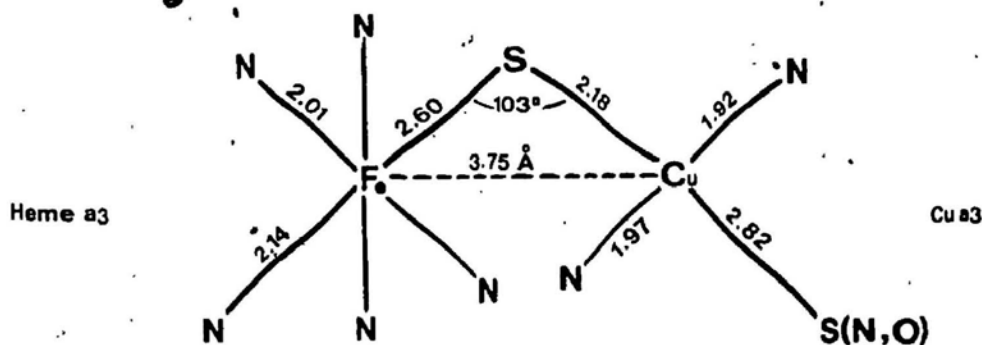


Fig. 1.4 Proposed active site in cytochrome c oxidase.

could mediate any magnetic exchange. Several potential links have been proposed (e.g., imidazolate, carboxylate, and oxo-bridge), but an oxo-bridge was preferred

as a working hypothesis for the site¹⁶. A detailed investigation was concerned with both metal centers and led to a proposal for the fully oxidised heterobimetallic site¹⁷ (Fig. 1.4).

E. Cu-Zn Superoxide Dismutase [Cu(II), Zn(II)]¹⁸

Superoxide dismutases are metalloenzymes which combat the potentially toxic effects of superoxide ions, formed in one-electron oxidation reactions involving molecular oxygen, by catalysing the dismutation of the anion to dioxygen and hydrogen peroxide. The protein consists of two identical, non-covalently associated subunits in each of which the metal binding sites are near the ends of a cylindrical arrangement. The essential features of the metal binding region are shown in Fig. 1.5.

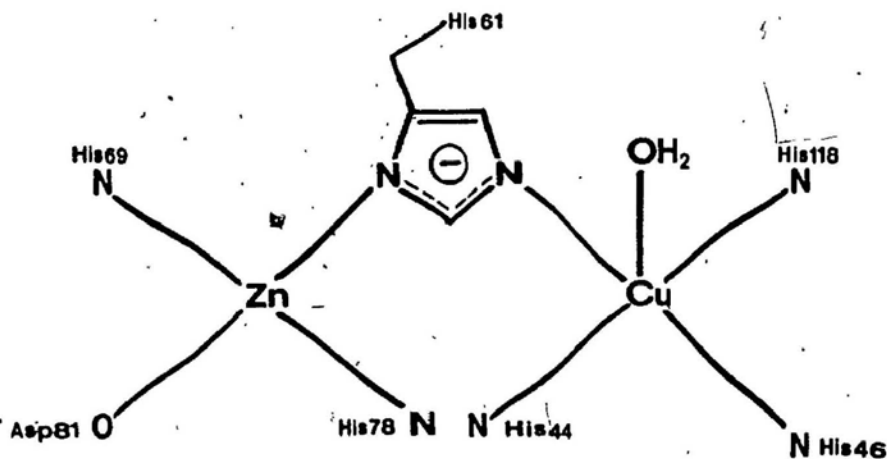


Fig. 1.5 Schematic representation of the bimetal site in Cu-Zn superoxide dismutase.

The Zn atom plays a structural role in which it helps the protein to preform the coordination environment around the copper, and the copper is the active catalytic center. Zn can be replaced by Cu to give the active "four-copper" form,

$\text{Cu}_2\text{Cu}_2\text{SOD}$, which has also been studied in some detail¹⁰.

The upshot of these brief discussions above all is that synthetic binuclear metal complexes act as appropriate models for natural binuclear metal centers when they mimic some chemical/physical property of the biosite, thus improving our knowledge of it. While it is a truism that synthetic systems are unlikely to replicate all the properties, physical and chemical, of the metalloproteins, it is also true that much can be learned about the chemistry of the active sites from a study of model compounds.

A considerable effort has been directed in recent years toward the synthesis of ligands capable of holding two metal ions, either the same or different, at separations (typically about 2.5 - 6 Å) which are subject to control by appropriate modification of the molecular topology. Although the imitation of the functional roles of the biosites is currently not at a very well-advanced stage, the first steps have been taken along the path, especially in the area of homobinuclear Cu(II) chemistry.

Ligand modification to alter the properties of the binuclear site, and preparation of new mixed-metal complexes, are expected to open new areas of modern chemistry. An apposite concluding remark can be found in Jean-Marie Lehn's review⁶; "how promising the future of the chemistry of these systems appear and how much it gives room to the creative imagination and experimental skill of the chemist".

1. 2. Binuclear Complexes as Mediators of Multi-electron Redox Processes

The second area in which binuclear complexes may prove to be useful is the mediation of redox reactions, in particular multi-electron processes. Reactions involving an n -electron reduction or oxidation could be accomplished in theory using n 1-electron steps or one n -electron step. In practice, substrates such as O_2 and N_2 are difficult to reduce in single-electron steps since the intermediate species are high in energy. The reactions would be thermodynamically favourable, however, if the required electrons could be transferred in a concerted process.

Electrochemical studies on a dicopper cryptate have shown that weakly-interacting metals in a binuclear complex can act independently to transfer two electrons at the same potential²⁰. The reduction of dioxygen by a binuclear "face-to-face" porphyrin at an electrode surface has been reported⁹. Particularly, it is well worth singling out the latter work for recognition.

In designing possible O_2 reduction catalysts, chemists have been looking for materials capable of delivering $4e$, more or less simultaneously, to the O_2 substrate at as positive a potential as possible. A mononuclear complex is highly unlikely to effect such a process, which has thus led to the preparation of binuclear ligands, capable of holding two metal centers in a suitable geometry so that they may jointly bind O_2 and, each metal center transferring $2e$, carry out a $4e$ process.

To this end, Collman *et al.*²¹ looked to biology and inorganic reaction mechanisms for their initial catalyst design. It is well understood that

Cytochrome c oxidase employs four metals, two at the oxygen-binding site (a heme and a copper) to reduce O_2 to H_2O . Furthermore, iron(II) porphyrins decompose O_2 through a mechanism involving two porphyrins acting on one O_2 . So they prepared a variety of porphyrin dimers linked so that the planar macrocycles and their metals are held in a "face-to-face" orientation.

After a series of preparations of porphyrins bearing functionalized α , γ -meso alkyl groups, Collman *et al*⁹, in 1980, found that when the Co-Co distance is such (4 Å) as to permit formation of an -O-O- bridge between the Co-Co centers, the face-to-face porphyrin bound on a graphite substrate catalyzes the 4e reduction of oxygen in acid electrolytes. Since then, 3d transition metal chelates have been widely studied as electroncatalysts for the cathodic reduction of O_2 . Clearly, the bridging association of O_2 , requiring the presence of two Co centers at the appropriate distance, is a crucial condition for the occurrence of 4e reduction.

In principle, this condition can also be fulfilled by planar chelates, containing two Co-ions. Indeed, 4e reduction of O_2 in a planar cobalt complex (Fig. 1.6), $[Co_2(TAPH)](NO_3)_4$, adsorptively attached to graphite in alkaline solution, was reported by Yeager²² in 1984. Recently, van der Putten *et al*²³ reported that $[Co_2(DPT)_2]Cl_2$ is also able to reduce O_2 to H_2O in alkaline solution (Fig. 1.7).

All these studies demonstrate that concerted multi-electron processes at binuclear centers are feasible. Notable goals for future work may be the electrochemical decomposition of H_2O to O_2 (a terminal step in photosynthesis), and the electro-catalytic reduction of N_2 to ammonia or hydrazine.

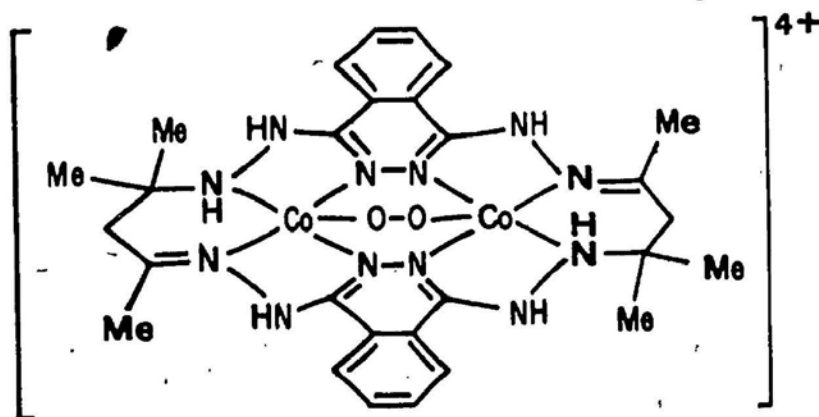


Fig. 1.6 Binuclear cation for $[\text{Co}_2(\text{TAPH})](\text{NO}_3)_4$.

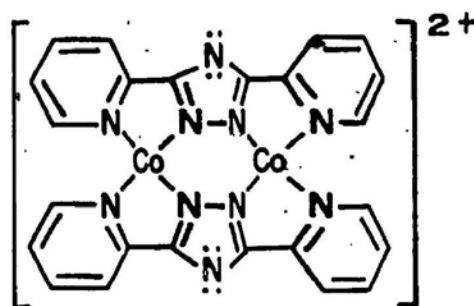


Fig. 1.7 Binuclear cation for $[\text{Co}_2(\text{DPT})_2]\text{Cl}_2 \cdot 2\text{H}_2\text{O}$.

1. 3. The Objectives of the Project

The principal purposes of this present study are:

- [1] to synthesize coordination complexes of disubstituted hydrazinophthalazine ligands involving Co and Ni salts, since previous studies on the dicopper complexes of such ligands have proved to be very interesting from the stand-

point of their structural, magnetic and electrochemical properties;

- [2] to characterize the resulting complexes by X-ray crystallography;
- [3] to characterize the complexes by conventional physical methods, including UV/VIS. Infrared spectroscopy and magnetic measurements (room temperature);
- [4] to investigate the spin exchange situation in the binuclear species using variable temperature magnetic measurements and relate the exchange to structural parameters, e.g., geometry, bridge group etc., and compare such a study with similar studies on related copper complexes;

CHAPTER 2

HISTORICAL BACKGROUND AND LITERATURE SURVEY

In 1970 Robson introduced the term "binucleating ligands"²⁴ to describe a group of compounds which were synthesized to be capable of binding and possibly activating molecular nitrogen. The concept was that two metal ions should be fixed at an appropriate distance, leaving a bridging position, to allow for the entry of the dinitrogen (Fig. 2.1). The complexes could then be regarded as geometrical models for potential nitrogen-fixing systems²⁵.

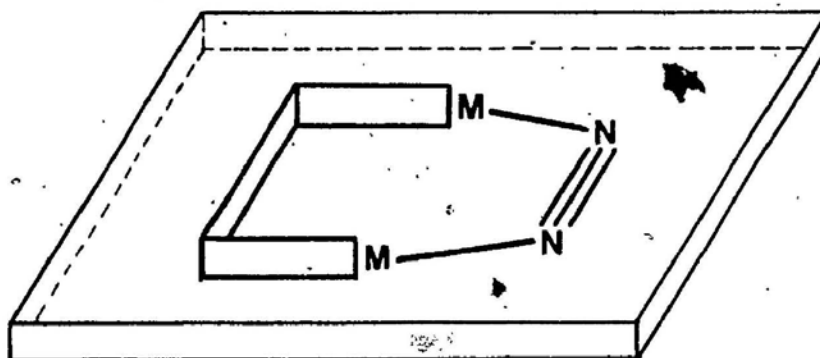


Fig. 2.1 Schematic representation of the dinitrogen trapping by binucleated metals.

The study of nitrogen fixation, however, has evolved into a fascinating area of chemistry involving studies on multicentred metalloproteins and a plethora of synthetic simulations²⁶. Binucleating ligands and their metal complexes have therefore developed into an extremely important research area. Although it is now dioxygen that is at the focal point, the original thesis of the activation of

small molecules persists as a central theme.

The following review will briefly discuss the evolution of binucleating ligands and some physical/chemical properties of their transition metal complexes.

The term binucleating ligand was defined as "a polydentate chelating ligand capable of simultaneously binding two metal ions" ²⁴. Later, the definition was refined to present macrocyclic binucleating ligands as macrocyclic ligands capable of securing two metals ions in close proximity²⁷. Since Robson introduced this term, there has been a steady increase in the number and type of such ligands synthesized. Their complexes fall, usually, into two general categories²⁸:

- [1] The first group consists of those complexes in which the metals share at least one donor atom in species containing adjacent sites, in which the central donor atom/atoms provide a bridge. The ligands giving these complexes have been collectively termed "COMPARTMENTAL LIGANDS".
- [2] The second class is composed of those complexes in which donor atoms are not shared and therefore designated as "ISOLATED DONOR SETS".

Selected examples of these two types of ligands will be given below to illustrate the number and variety of binucleating ligands. It should be noted here that the discussion will be restricted to the binucleating Schiff base ligands, both macrocyclic and acyclic but with emphasis on the latter.

2. 1. Compartmental Ligands

The ligands in this category are mainly Schiff bases derived from 2,6- disubstituted phenols, β -ketophenols, and 2,6-diacetylpyridine in which the central phenolic, keto-oxygen or pyridine nitrogen atoms can act as the bridging donor atoms. These ligands can be divided into two types:

- [A] a macrocyclic form, derived from a "2+2" condensation reaction.
- [B] an acyclic form, in which one donor bridge is removed.

Selected examples of each type of the ligands will be given as follows.

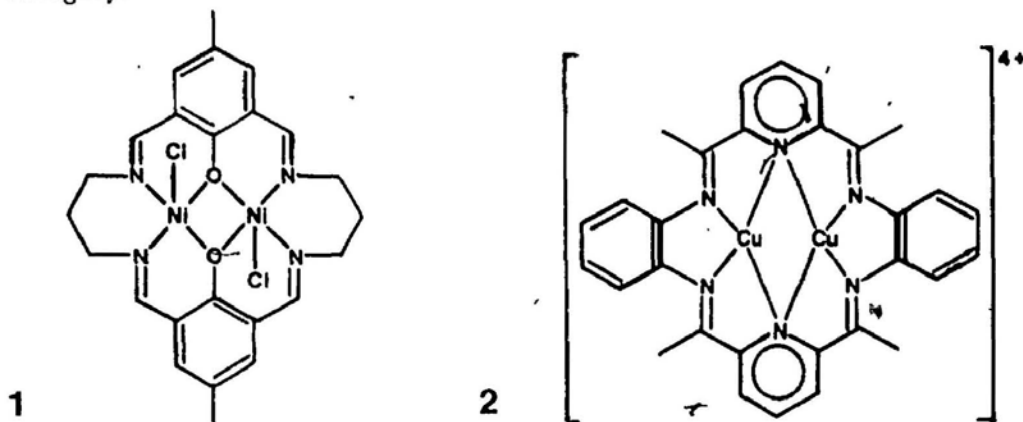
2. 1. 1. Macrocyclic Compartmental Ligands

Generally, the macrocycles, such as **1**²⁷ and **2**²⁹, and their complexes are prepared by three different strategies:

- [1] A direct complexation reaction between a presynthesized macrocyclic ligand and the metal ion in solution. Advantages of this approach are that the macrocyclic ligands may be isolated, purified, and characterized before the synthesis of the complex, since the purification and characterization of an organic ligand is often more easily accomplished than those of a metal complex ²⁹;
- [2] " *in situ* " syntheses, i.e., a template reaction involving condensation of the precursors in the presence of the required metal salt²⁷;
- [3] The synthesis of the macrocyclic complex involves the modification of the ligand and/or the metal ion in the macrocyclic complex. This third approach

is appropriate to the synthesis of non-symmetric species, and heterobinuclear metal complexes.

Certainly, many compounds may be synthesized by procedures from more than one category.



For the complex **1** with the counter ions Cl^- , high-spin behavior ($\mu = 3.15$ BM) was observed at room temperature but deviations from Curie-Weiss behavior below 120 K were interpreted as resulting from an antiferromagnetic interaction²⁷. From spectral evidence Robson *et al* concluded that the two Ni(II) ions were square pyramidal with an apical coordinated chloride.

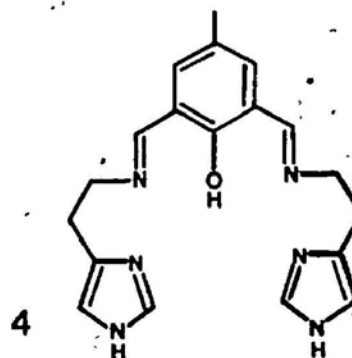
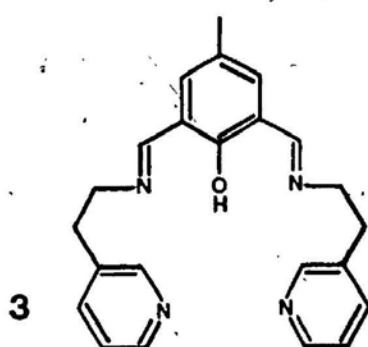
Robson's macrocycle **1** has also been used to generate mixed-valence metal complexes Co(III)-Co(II)³⁰, complexes of metals in low oxidation states Cu(I)-Cu(I)³¹, and a range of heterobinuclear metal complexes Cu-M, M = Co(II), Ni(II), Fe(II), and Zn(II)^{32,33}. X-ray crystallographic studies have confirmed the binuclear nature of the homobinuclear species derived from **1**. Interest in the potential role of these complexes in modelling biometallosites has led to extensive electrochemical, spectral and magnetic studies being carried out³¹⁻³⁴.

The binuclear Cu(II) complex **2** was prepared both by direct reaction of hydrated Cu(II) nitrate with the free ligand in ethanol and by an *in situ* pro-

cedure involving 2,6-diacetylpyridine and *o*-phenylenediamine in the presence of Cu(II) ions²⁹. Studies of the magnetic properties of this compound indicate a weak Cu(II)-Cu(II) interaction.

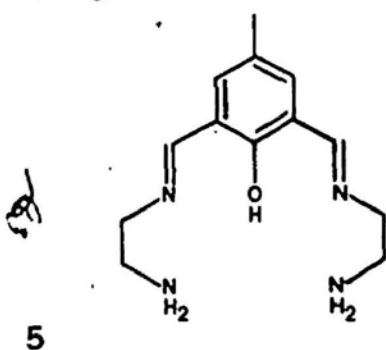
2. 1. 2. Acyclic Compartmental Ligands

The ligands provide only one endogeneous bridging donor and so have a labile bridging site available between the metal sites into which a variety of anions (X^-) can be introduced as exogeneous bridges. In principle, this subclass has the potential to bind molecules such as dioxygen, or dinitrogen, at the exogeneous bridging site. The complexes are generally prepared by template procedures, or by prior formation of the ligand followed by metal incorporation.

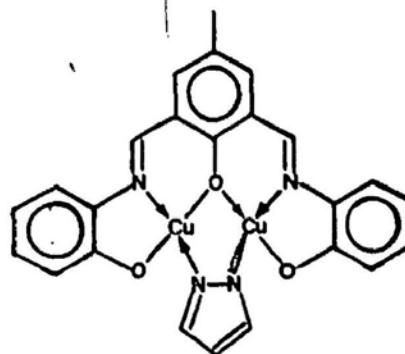


Mixed valence state Cu(II)-Cu(I) and low oxidation state Cu(I)-Cu(I) complexes of **3** and **4** have been prepared³⁵. The two Cu ions in complex $[Cu_2(L5)Br_2(MeOH)](ClO_4)$ are five-coordinated but in different environments; there is a bridging bromide anion and one copper has bromide as its fifth ligand, whereas the other has methanol^{36,37}. The viability of adding small molecules across the exogeneous bridging site has been demonstrated by using pyrazole as ligand, which has been confirmed by X-ray crystal structure analysis of the bis-

Cu(II) complex **6**³⁵



6



2. 2. Isolated Donor Sets

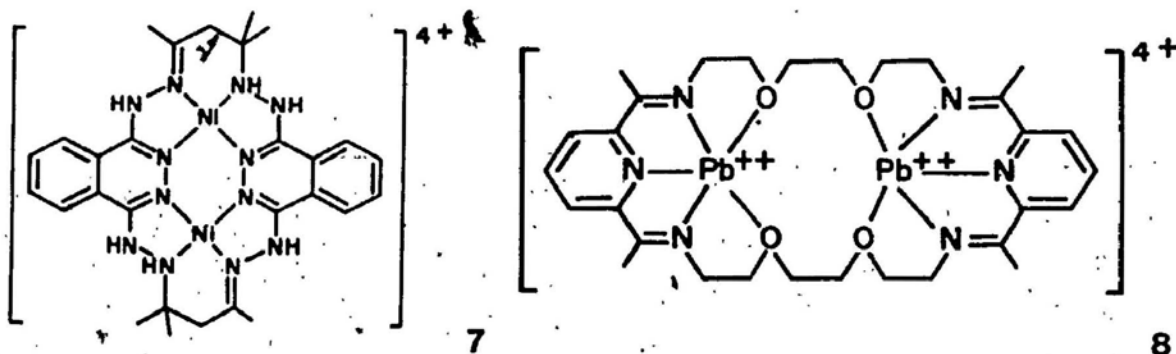
There now exists a wide variety of ligands in this class. In contrast to the compartmental ligands the isolated donor sets are variations not only on a single theme but also on different structural frameworks. Similarly, there are two types of these ligands: [A] Macrocyclic Systems, and [B] Acyclic Systems.

Selected examples of each type of ligand will be illustrated as follows.

2. 2. 1. Macrocyclic Systems

Rosen³⁸ synthesized the Ni(II) complex ion, **7**, as a fluoroborate derivative, from the reaction of 1,4-dihydrazinophthalazine with 2,2-dimethoxypropane in the presence of $\text{Ni}(\text{BF}_4)_2 \cdot 6\text{H}_2\text{O}$ in methanol containing a few drops of concentrated HBF_4 . The 2,2-dimethoxypropane is used as a dehydrating agent and is, in fact, the source of acetone for the acid-catalyzed condensation reaction with the hydrazine group.

The fluoroborate complex is paramagnetic with a magnetic moment slightly below the usual values for six-coordinate Ni(II) ions. This lowering of the magnetic moment is attributed to a weak antiferromagnetic interaction between the Ni(II) ions. The six-coordination of the fluoroborate derivative is explained by stacking the macrocyclic complexes in a staggered configuration such that uncoordinated hydrazine nitrogen atoms of adjacent molecules occupy the fifth and sixth positions of Ni(II) ions within the macrocyclic ligand.



Macrocyclic tetra-imines, or "2+2" Schiff bases, **8**, have been isolated and studied by Nelson⁴. The studies showed that the transmetalation route could be used to synthesize the otherwise inaccessible dicopper(II) species. By utilizing this technique with Sr^{2+} and Ba^{2+} , as the large radius templates, a wide range of macrocycles have been constructed³⁹.

2. 2. 2. Acyclic Systems

This subclass covers a somewhat miscellaneous group of compounds, some of which indicate that even the simplest of systems should not be discounted as potential binucleating ligands.

Binucleating ligands containing just nitrogen donor atoms have received increasing attention in recent years and have been based largely on substituted "DIAZINE" ($=N-N=$) type units. The transition metal complexes of polyfunctional diazine ligands, derived from [1] Hydrazine⁴⁰⁻⁴⁴, [2] Triazole^{23,45,46}, [3] Pyrazole⁴⁷, [4] Pyridazine⁴⁷⁻⁶¹, and [5] Phthalazine^{37,47,48,62-74}, have binuclear centers, in which the metals are brought into close proximity due to the presence of the diazine fragments in these systems (See Fig. 2.2) and the metal atoms are almost invariably antiferromagnetically coupled via a superexchange mechanism.

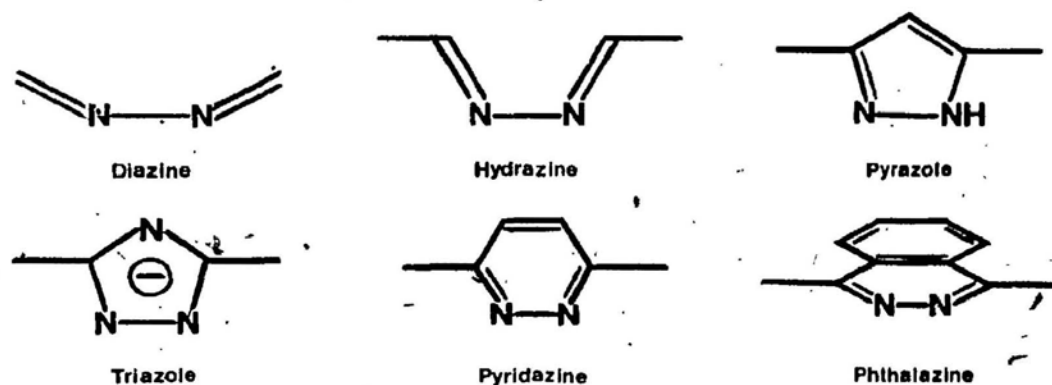
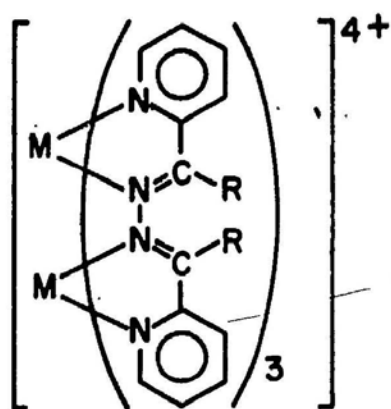


Fig. 2.2 Diazine unit and its derivatives.

Pyridine-2-aldazine(PAA), derived from the condensation of pyridine-2-aldehyde and hydrazine, has been shown to produce metal complexes with a variety of different stereochemistries⁴⁰⁻⁴², which arise largely as a result of free rotation about the N-N bond. Stratton and Busch⁴⁰ reported the systems $[M_2(L)_3]^4$ (where $M = Fe(II), Co(II), Ni(II)$; $L = PAA, PMK$, i.e., 2-pyridyl-methyl-ketazine) where the ligand was predicted to adopt configuration **9**.

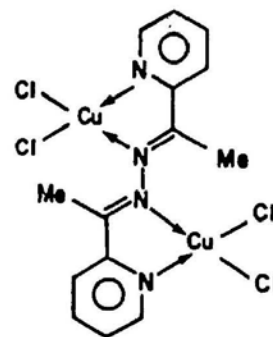
Later studies^{43,44} on binuclear $Cu(II)$ complex of PMK have confirmed some of the earlier predictions concerning the bridging tetradentate coordination of



$R = H$ (PAA)

$R = CH_3$ (PMK)

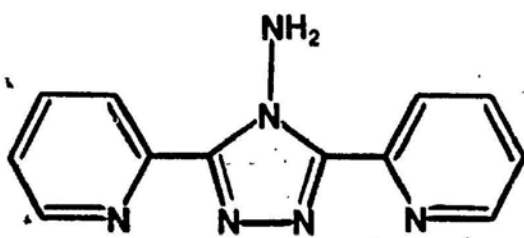
9



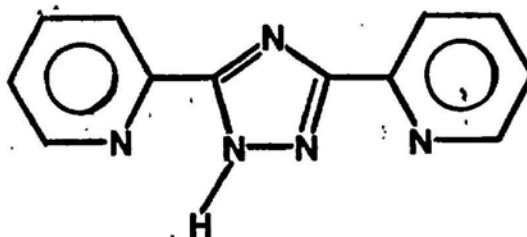
10

PMK and PAA. However, the X-ray crystal structure further shows that the ligand PMK, **10**, in the binuclear complex $Cu_2(PMK)Cl_4$ has a trans-trans conformation. Though the ligand is conjugated, it is not planar due to a rotation about the N-N bond. The bridge connecting the two metal centers consists of an diazine linkage. The complex exhibits antiferromagnetic exchange ($-2J = 52 \text{ cm}^{-1}$), which is assumed to occur solely via this bridging N-N linkage.

The compounds of both 3,5-disubstituted -1,2,4-triazoles **11**, [ABPT = 4-amino-3,5-bis(pyridin-2-yl)-1,2,4-triazole]⁴⁵, and **12**, [BPTH = 3,5-bis(pyridine-2-yl)-1H-triazole]⁴⁶, are interesting binucleating chelating ligands and suitable for studying magnetic exchange between transition-metal ions.



11



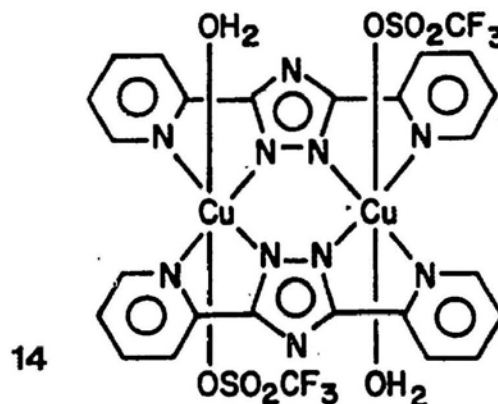
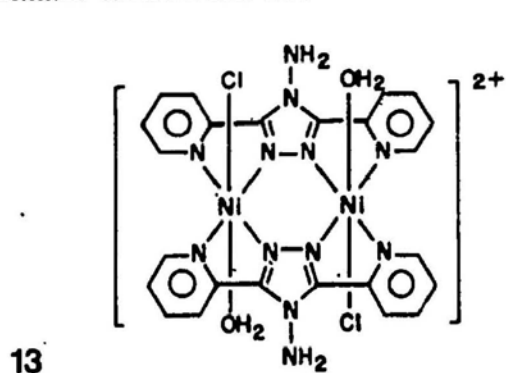
12

The binuclear complexes $[Ni_2(ABPT)_2Cl_2(H_2O)_2]Cl_2 \cdot 4H_2O$ (**13**) and $[Cu(BPT)(CF_3SO_3)(H_2O)]_2$ (**14**) were identified by X-ray analysis^{45,46} (See Table 2.1). The binuclear unit $[M_2L_2]$ is nearly planar. The metal atoms in the dimer

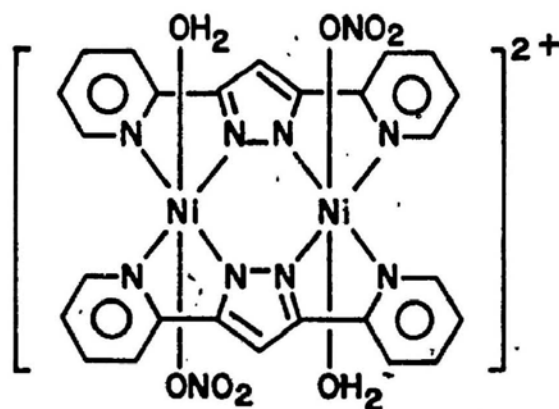
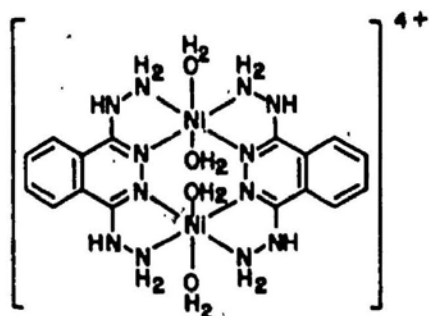
Table 2.1 The major parameters of some binuclear complexes.

Complex	M-M (Å)	M-O-M (deg.)	θ	$-2J$ (cm ⁻¹)	μ_{eff} (BM)	Ref.
[Ni ₂ (ABPT) ₂ Cl ₂ (H ₂ O) ₂]Cl ₂ ·4H ₂ O	4.135	-	2.15	12.5	-	45
[Cu(BPT)(CF ₃ SO ₃)(H ₂ O)] ₂	4.085	-	2.19	118	-	46
[Cu ₂ (DPPN)(OH)Cl ₃ (H ₂ O)]	3.376	126.5	-	-	-	50
[Cu ₂ (PPDMe)(OH)(NO ₃) ₂ (H ₂ O) ₂]NO ₃ ·H ₂ O	3.338	119.3	2.07	770	0.55	54
[Cu ₂ (PPDMe)(OH)Cl ₂][CuCl ₃ (H ₂ O)]H ₂ O	3.384	126.0	-	-	1.03	54
[Ni ₂ (PPD) ₂ (H ₂ O) ₄]Cl ₄ ·2H ₂ O	3.920	-	2.11	29.6	2.95	55
[Cu ₂ (PPD)(OH)Cl ₃ (H ₂ O)]0.8H ₂ O	3.454	116.4	2.16	898	-	57
[Cu ₂ (PPD)(OH)Br ₃ (H ₂ O)]0.6H ₂ O	3.413	118.9	2.08	1304	~diamag.	57
[Cu ₂ (MIP)(OH)Br ₃ (H ₂ O)]H ₂ O	3.420	124.9	2.17	992	0.35	57
[Cu ₂ (PTP)Cl ₄]EtOH	3.198	-	2.03	131	1.61	59
[Cu ₂ (PTP) ₂](ClO ₄) ₂	3.422	-	-	-	diamag.	60
[Cu ₂ (EtBITP)(OH)Cl ₃]DMF	3.017	104.7	2.01	260	1.38	61
[Ni ₂ (DHPHPY)Cl(H ₂ O) ₄]Cl ₃ ·2H ₂ O	3.603	-	-	-	2.74	66
[Cu ₂ (MIP)(OH)Cl ₃ (H ₂ O)]H ₂ O	3.425	126.3	2.00	800	0.62	76
[Cu ₂ (FPA-H)(OH)(H ₂ O) ₂](ClO ₄) ₂ ·H ₂ O	3.295	117.3	2.11	990	0.34	83

are bridged by two triazole rings. The structure may be compared to that of $[\text{Ni}(\text{DHPH})(\text{H}_2\text{O})_2]_2\text{Cl}_4 \cdot 2\text{H}_2\text{O}$ ⁶², DHPH = 1,4-dihydrazinophthalazine, which has a similar framework **15**.

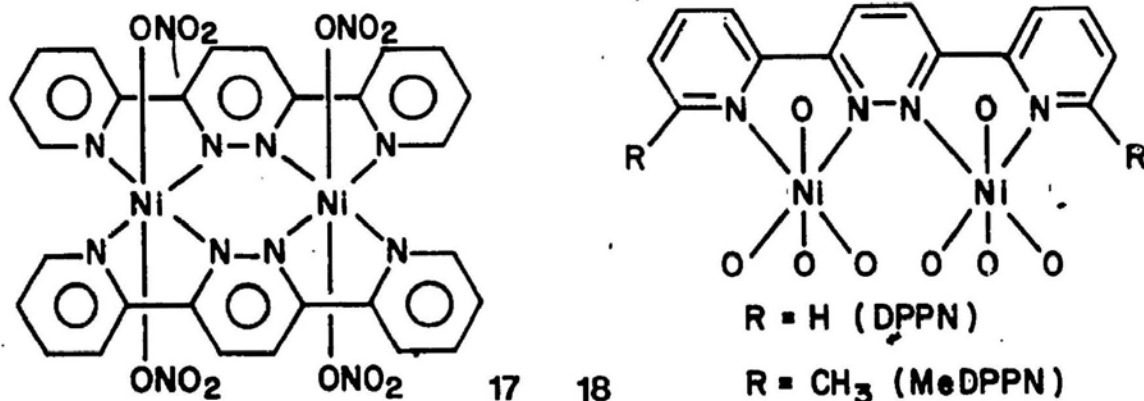


The essential difference between the two structures, however, is that the central part is a five-membered ring in the triazole compound and a six-membered ring in the phthalazine one. Magnetic susceptibility measurements on **13** and **14** revealed that a relatively weak antiferromagnetic exchange is present in the former complex and a quite large antiferromagnetic interaction between the Cu(II) centers in the latter one.



The Ni(II) complexes of 3,5-di(pyrid-2-yl)pyrazole (DPPH) and 3,6-di(pyrid-2-yl)pyridazine (DPPN) ligands, $[\text{Ni}(\text{DPP})(\text{NO}_3)(\text{H}_2\text{O})]_2$ and $[\text{Ni}(\text{DPPN})(\text{NO}_3)_2]_2 \cdot 4\text{H}_2\text{O}$, were synthesized and the structures were proposed as binuclear complexes (**16** and **17** respectively) as a consequence of their magnetic

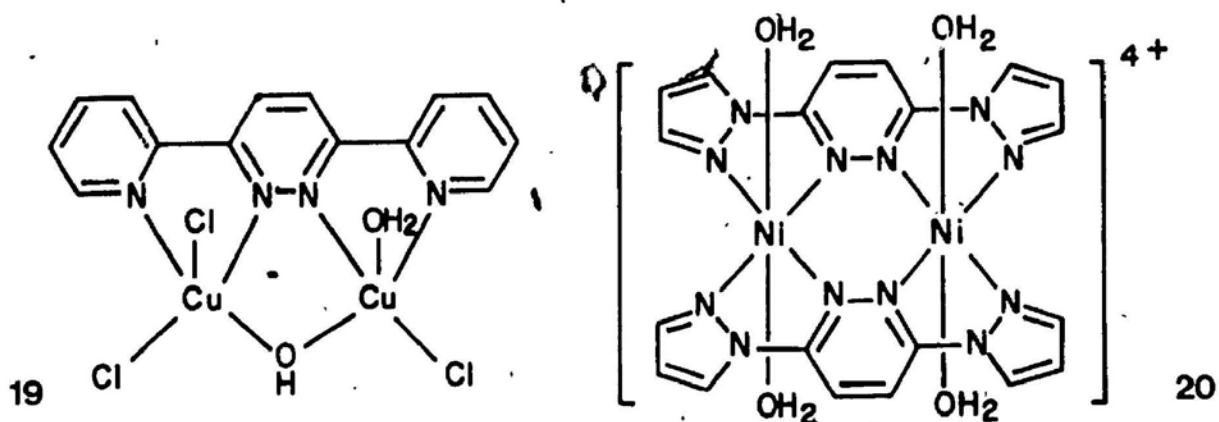
properties⁴⁷, i.e., analogous to the crystal structure **15**, but no further reports of the X-ray structures confirm them. Nevertheless, Ball and Blake's other structural suggestion **18** has been confirmed by later X-ray studies on the complexes, formed with Cu(II) halides⁵⁰⁻⁵³.



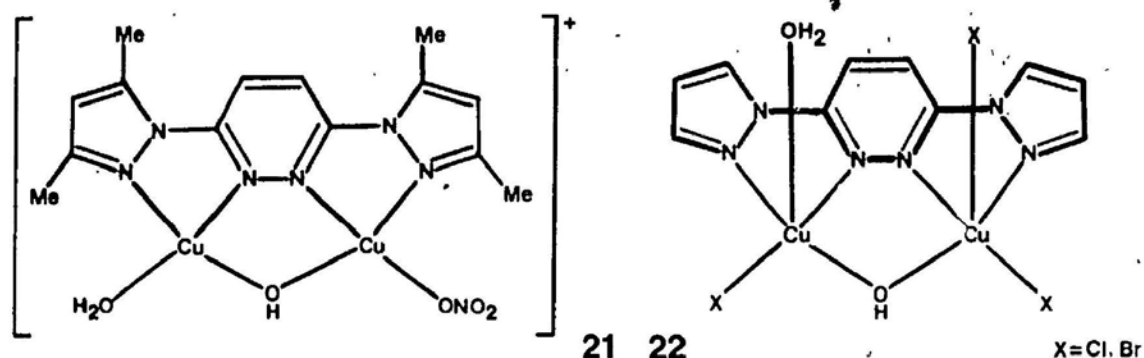
The crystal structures of the isolated complexes $[\text{Cu}_2(\text{DPPN})\text{Cl}_3(\text{OH})(\text{H}_2\text{O})]$, $[\text{Cu}_2(\text{DPPN})\text{Cl}_4(\text{H}_2\text{O})]$ and $[\text{Cu}_2(\text{DPPN})\text{Cl}_2(\text{OH})(\text{NO}_3)(\text{H}_2\text{O})]$ verify the presence of the binuclear complexes, in which the two Cu(II) atoms, bridged by the hydroxyl group (or chlorine atom) and the pair of nitrogen atoms of pyridazine moiety, are in different coordination environments, **19** (See Table 2.1).

Recently, Thompson *et al* reported the crystal structures of binuclear complexes $[\text{Ni}_2(\text{PPD})_2(\text{H}_2\text{O})_4]\text{Cl}_4 \cdot 2\text{H}_2\text{O}$, **20**, [PPD = 3,6-bis(1-pyrazolyl)pyridazine]⁵⁵ and $[\text{Cu}_2(\text{PPDMe})(\text{OH})(\text{NO}_3)_2(\text{H}_2\text{O})_2](\text{NO}_3) \cdot \text{H}_2\text{O}$, **21**, [PPDMe = 3,6-bis(3,5-dimethyl-1-pyrazolyl)pyridazine]⁵⁴. Structurally, these two complexes are very close to the compounds **17** and **18** respectively, thus supporting Ball and Blake's predictions. Variable-temperature magnetic measurements on both complexes indicate significant antiferromagnetic exchange between the metal centers.

Analogous Cu(II) complexes, $[\text{Cu}_2(\text{PPD})(\text{OH})\text{X}_3(\text{H}_2\text{O})]n\text{H}_2\text{O}$ (X = Cl, n = 0.8; X = Br, n = 0.6), **22**, have also been determined by single-crystal X-ray diffractometry, and characterized by exhibiting positive redox potentials (0.41 ~



0.47 V vs. SCE) associated with two-electron reduction as well as very strong spin exchange ($-2J = 898$, and 915 cm^{-1} , respectively.)⁵⁷. These two binuclear, spin coupled Cu(II) complexes have square-pyramidal, hydroxide-bridged Cu(II) centers separated by $3.4 \sim 3.5 \text{ \AA}$, with Cu-O-Cu angles of $116 - 125^\circ$, and are considered to be useful models for oxyhemocyanin^{14,a,b,c,58}.

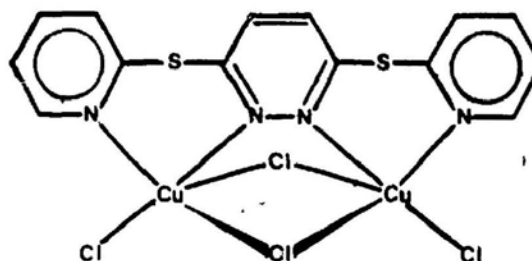
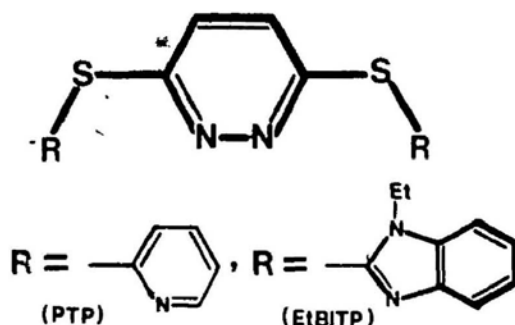


Binuclear Cu(II) and Cu(I) complexes of a series of quadridentate pyridazine thioether ligands involving nitrogen donor groups (derived from pyridine, benzimidazole) (23) have been described by Thompson *et al*^{56,59-61}. All of copper(II) complexes exhibit positive redox potentials ($0.4 \sim 0.6 \text{ V vs. SCE}$) associated with two-electron reduction and moderate antiferromagnetic exchange ($\mu_{eff} = 1.1 \sim 1.7 \text{ BM}$ at room temperature). The complexes $[\text{Cu}_2(\text{PTP})\text{Cl}_4]\text{C}_2\text{H}_5\text{OH}$, **24**, $[\text{Cu}_2(\text{PTP})_2](\text{ClO}_4)_2$, **25**, and $[\text{Cu}_2(\text{EtBITP})(\text{OH})\text{Cl}_3]\text{DMF}$, **26**, have been characterized by the X-ray crystallog-

raphy (Table 2.1).

23

24

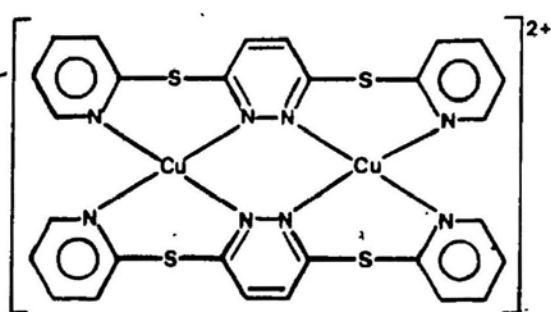


In the complex **25**, the binuclear cation consists of two pseudo-tetrahedral Cu(I) centers, separated by 3.422 Å and bridged by two pyridazine groups with terminal pyridine donors completing the four-coordination. The compound **24**, in which the two square pyramidal Cu(II) centers are triply bridged by two Cl atoms and the pyridazine nitrogen pair with a Cu-Cu separation of 3.198 Å reacts rapidly with appropriate reducing agents (e.g., I⁻, SO₃²⁻) to produce derivatives containing the very stable binuclear Cu(I) cation [Cu₂(PTP)₂]²⁺, which is identical to the cation found in **25**⁶¹.

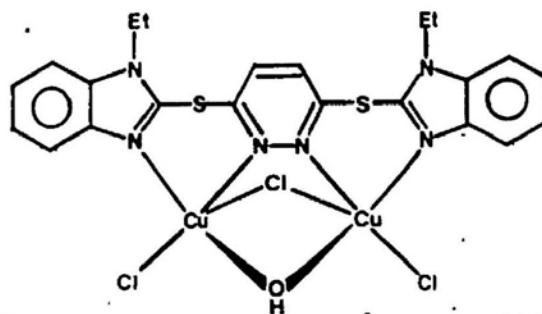
The five-coordinate Cu(II) centers in **26**, which contains a triply bridged binuclear structure involving hydroxo- and chloro- bridges in addition to the diazine, have stereochemistries that can best be described as distorted trigonal bipyramidal. This feature distinguishes this system from other analogous five-coordinate derivatives where the five-coordination most closely approached that of a square pyramid⁶¹ (See Table 2.1).

The high, positive redox potentials for these systems, which parallel those of some copper oxidase/oxygenase enzymes, suggest their possible catalytic activity in oxidase and oxygenase function. Preliminary initial velocity kinetic studies on the hydroxo-bridged complex [Cu₂(PTP)(OH)Cl₃]EtOH indicate significant

catecholase activity involving the aerobic oxidation of 3,5-di-*t*-butylbenzene-1,2-diol, in which a Michaelis-Menten kinetic treatment gave the binding constant $K_m = 3.4 \times 10^{-4} \text{ mol dm}^{-3}$ and a value of $k_p = 2.1 \times 10^{-2} \text{ S}^{-1}$ for the dissociation of the catechol-complex intermediate⁵⁶.



25



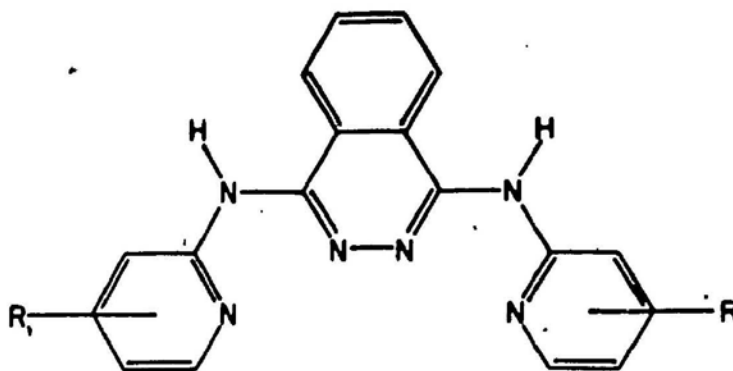
26

Another representative group of binucleating ligands of this subclass are **27**^{63-65,67-73,75,77-80}. Two decades ago the ligand PAP was prepared by Thompson⁸¹. Since then, a series of studies on the coordination chemistry of this ligand have been carried out, and extended to its derivatized analogues as well. X-ray structural studies on the systems reveal that the ligands **27** are capable of forming μ -bridged bimetallic complexes involving a variety of exogeneous bridge groups, e.g., $[\text{Cu}_2(\text{PAP})(\text{OH})(\text{SO}_4)\text{Cl}]2\text{H}_2\text{O}$, **28**, and $[\text{Cu}_2(\text{PAP46Me})\text{Cl}_4]$, **29** (See Table 2.2).

A common structural feature in this series includes the hydroxide bridge and the phthalazine diazine bridge, and a systematic structural variation is developed by varying the third anionic bridge. The order of increasing oxygen bridge angle ($\text{Cl}^- \sim \text{Br}^- < \text{IO}_3^- < \text{NO}_3^- < \text{SO}_4^{2-}$) is matched by the trend in increasing anti-ferromagnetic exchange. A linear relationship is demonstrated between the exchange and the oxygen bridge angle for systems in which the Cu(II) centers have $d_{x^2-y^2}$ ground states⁷⁵ (Table 2.2).

Table 2.2 Magnetic and key structural parameters for the binuclear μ -bridged Cu(II) complexes of the ligands **27**.

Complex	Cu-Cu (Å)	Cu-O-Cu (deg.)	g	$-2J$ (cm ⁻¹)	μ_{eff} (BM)	Ref.
[Cu ₂ (PAP)(OH)Cl ₃]·1.5H ₂ O	3.001	101.8	2.28	201	1.60	63
[Cu ₂ (PAP)(OH)Br ₃]·1.5H ₂ O	3.010	100.1	2.20	191	1.66	63
[Cu ₂ (PAP)(OH)(IO ₃) ₃]·4H ₂ O	3.165	113.8	2.15	283	1.34	72
[Cu ₂ (PAP)(OH)(SO ₄)Cl]·2H ₂ O	3.211	115.5	2.20	532	1.01	75
[Cu ₂ (PAP4Me)(OH)(NO ₃) ₂ (H ₂ O) ₂]NO ₃	3.138	115.3	2.10	497	1.02	75
[Cu ₂ (PAP6Me)(OH)Cl ₃]·3H ₂ O	3.137	112.2	2.11	432	1.0	78
[Cu ₂ (PAP6Me)(OH)(NO ₃) ₃]·0.5H ₂ O	3.134	114.1	2.04	501		80
[Cu ₂ (PAP46Me)(OH)(NO ₃) ₂ (H ₂ O)]NO ₃	3.156	113.7	2.05	597	0.9	79
[Cu ₂ (PAP46Me)Cl ₄]	3.251	-	2.05	55.2	1.73	59

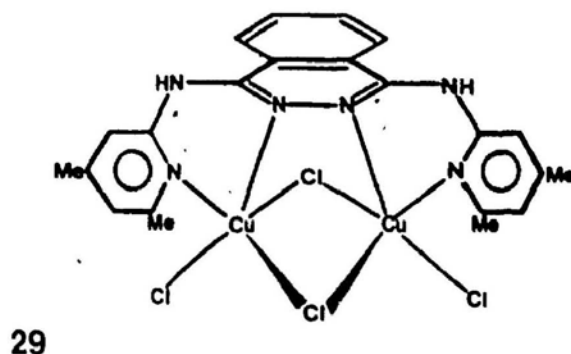
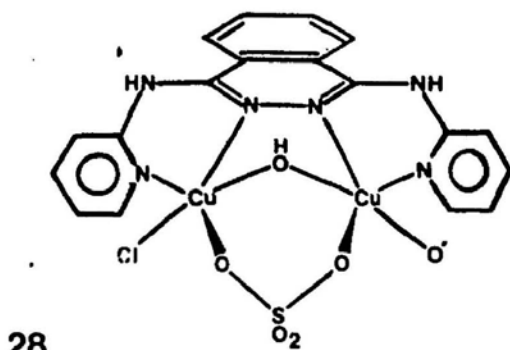


Ligands 27

PAP	R = H
PAP4Me	R = 4 Me
PAP6Me	R = 6 Me
PAP46Me	R = 4,6 DiMe

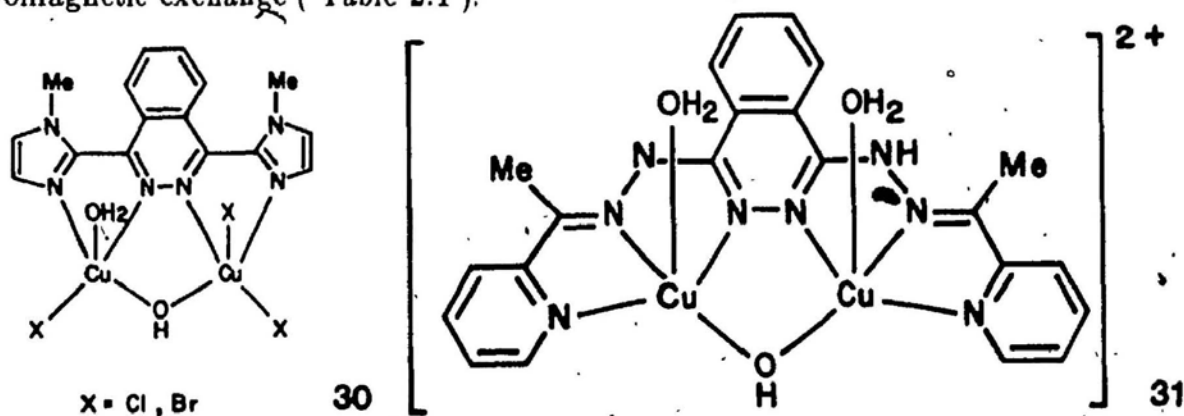
Structurally, all of the hydroxo-bridged complexes involve "magnetically symmetric" binuclear centers with distorted, five-coordinate copper ion stereochemistries. In most cases the distortion approximates a square pyramidal situation with nominally $d_{x^2-y^2}$ ground state copper centers. In these cases each Cu atom is bound via an equatorial interaction to both the hydroxide bridge and the diazine bridge, which results in a situation where magnetic interactions via these group are the most relevant, while any axial bridge interaction will be regarded as "non-magnetic". Two complexes, $[\text{Cu}_2(\text{PTP})\text{Cl}_4]\text{EtOH}$, **24**, and $[\text{Cu}_2(\text{PAP46Me})\text{Cl}_4]$, **29**, have been shown to have triple bridged structures involving two chlorine bridges, in an asymmetric binuclear center^{59,60}. The essentially square-pyramidal Cu centers are each bound via an axial and an equatorial interaction to each Cl bridge, thus creating an effectively "non-magnetic" superexchange pathway via these bridge groups. An equatorial interaction from each Cu atom to the diazine bridge, in each case, generates a viable superexchange pathway.

The complex $[\text{Cu}_2(\text{PAP})(\text{OH})\text{Cl}_3] \cdot 1.5\text{H}_2\text{O}$ has been used in studies on catecholase activity⁸². The preliminary kinetic data for the catalytic oxidation of 3,5-di-tert-butylcatechol ("catechol") to 3,5-di-tert-butylquinone reveal that the reaction shows a first order dependence on the initial copper complex, but no



dependence upon "catechol", when the latter is in reasonable excess. In excess oxygen and catechol the rate constant, k , is $ca. 5 \times 10^{-4} \text{ atm}^{-1} \text{ sec}^{-1}$ at room temperature in 70% (v/v) acetonitrile/water.

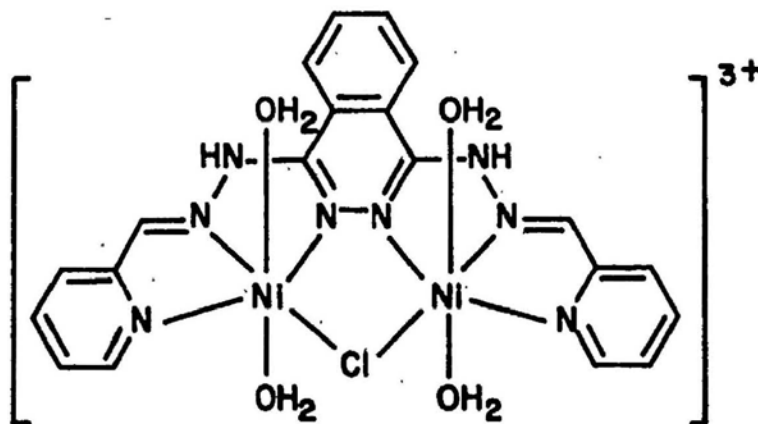
Another phthalazine derivative 1,4-bis(1-methyl-2-imidazolyl)phthalazine (MIP) and its binuclear Cu(II) complexes **30**, $[\text{Cu}_2(\text{MIP})(\text{OH})\text{X}_3(\text{H}_2\text{O})]\text{H}_2\text{O}$ ($\text{X} = \text{Cl}$, and Br), are also described by Thompson *et al*^{57,76}. The crystal and molecular structures show that the square-pyramidal Cu(II) centers are bridged by two groups; phthalazine and hydroxide. The complexes exhibit very low room-temperature magnetic moments indicative of strong spin exchange. Large Cu-Cu separations (3.420 and 3.425 Å) and Cu-O(H)-Cu bridge angles (125 and 126 °) are considered to be a dominant factor responsible for this very large antiferromagnetic exchange (Table 2.1).



Recently, Thompson *et al*⁸³ reported an interesting binucleating hexaden-

tate ligand(PPA), synthesized by condensation of 2-acetylpyridine and DHPH, and the corresponding μ -hydroxo-bridged Cu(II) complex, **(31)**, $[\text{Cu}_2(\text{PPA-H})(\text{OH})(\text{H}_2\text{O})_2](\text{ClO}_4)_2 \cdot 2\text{H}_2\text{O}$, which exhibits very strong antiferromagnetic exchange ($-2J \Rightarrow 990 \pm 50 \text{ cm}^{-1}$) as well as very intense visible absorption (610 nm , $\epsilon = 18400 \text{ l mol}^{-1} \text{ cm}^{-1}$) and undergoes, unlike comparable (N_4) diazine complexes, oxidation in a single two-electron step at 0.50 V (vs. SCE) to form a stable binuclear Cu(III) species (Table 2.1).

The molecular structure of **31** consists of an almost planar ligand binding two five-coordinate (distorted square-pyramidal) Cu(II) ions separated by 3.295 \AA and bridged by a hydroxide with a Cu-O-Cu bridge angle of 117.3° . Two axially bound water molecules complete the square pyramidal coordination. The unusual stoichiometry of the complex indicates that the ligand has lost a proton. The only other structurally documented, related complex is $[\text{Ni}_2(\text{DHPHPY})\text{Cl}(\text{H}_2\text{O})_4]\text{Cl}_3 \cdot 2\text{H}_2\text{O}$ (**32**), formed by the reaction of pyridinecarboxaldehyde with DHPH in the presence of the Ni(II) ion, in which the Ni(II) centers are remarkably planar with a μ -chloro-bridging angle of 98.4° and a Ni-Ni separation of 3.603 \AA (Table 2.1).



CHAPTER 3

ELECTRONIC SPECTRA AND MAGNETIC PROPERTIES OF COBALT COMPLEXES

The spectral and magnetic properties of high spin cobalt(II) complexes are briefly reviewed with the aim of showing how it is possible to relate the experimental data to the electronic structure and the coordination geometry of the complexes. It is hoped that this may be of help to characterize Co(II) complexes or use Co(II) as a spectroscopic probe. The high spin Co(II) ion, which has three unpaired electrons, is the only common d^7 ion and its spectra have been widely studied^{84,87}. It shows a variety of coordination numbers and coordination geometries, and is able to bind to a large number of different ligands. It is also largely used as a tool for determining the coordination environment of the metal site in metallo-enzymes and metalloproteins^{85,86}. In fact, Co(II) is often able to substitute Zn(II) which is present in naturally occurring zinc enzymes, and several cases are known where cobalt enzymes remain active. It is therefore necessary to have a clear knowledge of the spectral properties of Co(II) in various coordination environments so as to be able to obtain the required structural information.

Every attempt to understand the spectral and magnetic properties of Co(II) complexes must start from the ligand field energy levels. High spin Co(II) ions have the ground level characterized by the $s = 3/2$ quantum number. The free ion terms of interest are the 4F and 4P terms, they undergo splitting upon metal

coordination depending on the symmetry of the coordination polyhedron (Fig. 3.1). It is useful to refer to octahedral symmetry (O_h point group) if the ion is six coordinate, to square pyramidal (C_{4v}) or to trigonal bipyramidal (D_{3h}), if the ion is five coordinate and, if the ion is four coordinate, to tetrahedral symmetry (T_d). It should be noted that octahedral symmetry provides an orbitally triply-degenerate ground level ($^4T_{1g}$). Five-coordinate chromophores have either orbitally non-degenerate (trigonal bipyramidal) or doubly degenerate (square pyramidal) ground levels. In the case of tetrahedral symmetry the ground level is orbitally non-degenerate (4A_2). These properties will account for the magnetic susceptibility values of high spin Co(II) complexes in the various coordination geometries.

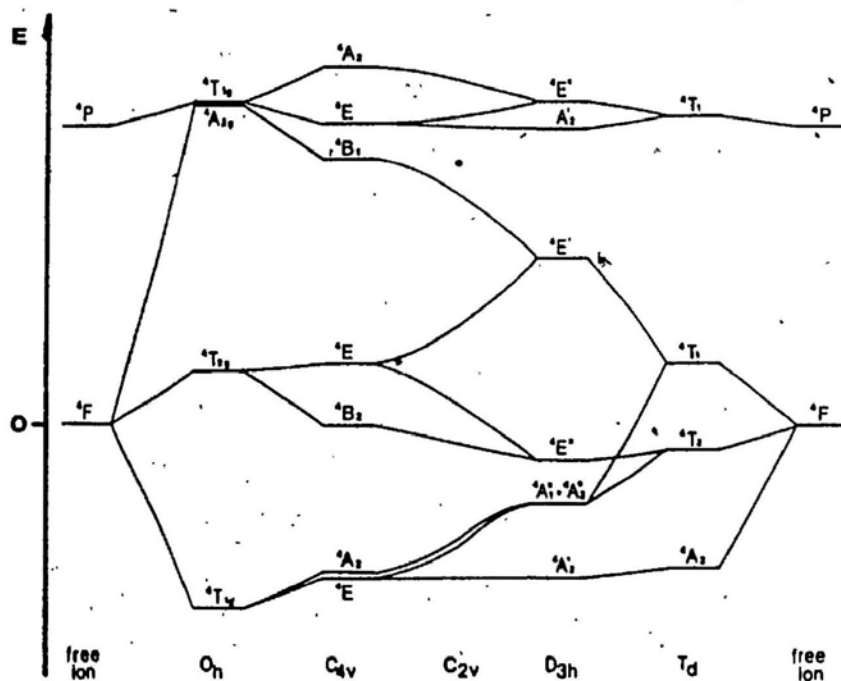


Fig. 3.1 Splitting of the 4F and 4P free ion terms of high spin Co(II) in various coordination geometries.

3. 1. High-Spin Octahedral and Tetrahedral Complexes of Co(II)⁸⁷

In an octahedral crystal field, three spin-allowed transitions are anticipated because of the splitting of the free-ion, ground 4F term, and the accompanying 4P term. The spectra, which can be interpreted by using the Tanabe-Sugano diagram (Fig. 3.2), usually consist of a band in the near infrared, which may be assigned as

$$\nu_1 = {}^4T_{2g}(F) \leftarrow {}^4T_{1g}(F) \quad (7\,000 \sim 9\,000 \text{ cm}^{-1})$$

and another in the visible (ν_3), often with a shoulder (ν_2) on the low-energy side. Since the transition ${}^4A_{2g}(F) \leftarrow {}^4T_{1g}(F)$ is essentially a 2-electron transition from $t_{2g}^5 e_g^2$ to $t_{2g}^3 e_g^4$ it is expected to be weak, and the usual assignment is

$$\nu_2 = {}^4A_{2g}(F) \leftarrow {}^4T_{1g}(F) \quad (\text{shoulder, weak}) (12\,000 \sim 14\,000 \text{ cm}^{-1})$$

$$\nu_3 = {}^4T_{1g}(P) \leftarrow {}^4T_{1g}(F) \quad (\text{main}) (17\,000 \sim 20\,000 \text{ cm}^{-1})$$

Indeed, in some cases it is probable that ν_2 is not observed at all, but that the fine structure arises from term splitting due to spin-orbit coupling or distortion from regular octahedral symmetry.

For d^7 ions in tetrahedral crystal fields, the splitting of the free-ion, ground F term is the reverse of that in octahedral fields so that ${}^4A_2(F)$ lies lowest. In fact, the observed spectra usually consist of a broad, intense band in the visible region (responsible for the colour and often about 10 times as intense as in octahedral compounds) with a weaker one in the infrared. The only satisfactory interpretation is to assign these, respectively, as

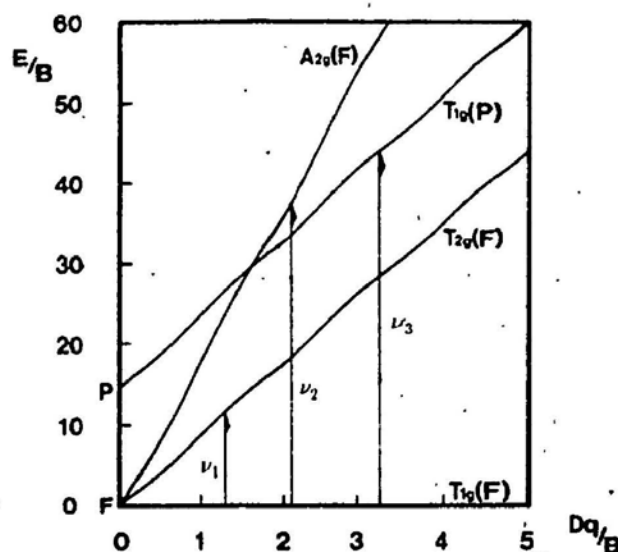


Fig. 3.2 Simplified Tanabe-Sugano diagram for d^7 , Co(II) , ion in an octahedral crystal field and possible spin-allowed transitions. (B represents the interelectronic repulsion or Racah parameter.)

$$\nu_3 = {}^4T_1(P) \leftarrow {}^4A_2(F) \quad (14\,000 \sim 16\,000 \text{ cm}^{-1})$$

$$\nu_2 = {}^4T_1(F) \leftarrow {}^4A_2(F) \quad (5\,000 \sim 8\,000 \text{ cm}^{-1})$$

in which case $\nu_1 \equiv {}^4T_2(F) \leftarrow {}^4A_2(F)$ should be in the region $3000 \sim 5000 \text{ cm}^{-1}$. Examination of this part of the infrared has sometimes indicated the presence of a band, though overlying vibrational bands make interpretation difficult. The ability to assign the absorption bands reasonably in this manner, keeping in mind the greater intensity expected in the tetrahedral case, is a more reliable guide to stereochemistry than simple colour. The most obvious distinction between the octahedral and tetrahedral compounds is that in general the former are pink to violet in colour whereas the latter are green or blue. Certainly, this is not an infallible distinction but is a useful empirical guide whose reliability is improved by a more careful analysis of the electronic spectra mentioned above.

3. 2. Magnetic Properties of High-Spin Co(II) Complexes

Magnetic properties provide a complementary means of distinguishing stereochemistry. The T ground term of the octahedral ion is expected to give rise to a temperature-dependent orbital contribution to the magnetic moment whereas the A ground term of the tetrahedral ion is not. As a matter of fact, in a tetrahedral field the excited ${}^4T_2(F)$ term is "mixed into" the ground 4A_2 term because of spin-orbit coupling and tetrahedral complexes of Co(II) are expected to have magnetic moments given by

$$\mu_e = \mu_{spin-only} \left(1 - 4 \frac{\lambda}{10Dq} \right) \quad (3-1)$$

where $\lambda = -170 \text{ cm}^{-1}$ and $\mu_{spin-only} = n \sqrt{n+2} = 3.87 \text{ BM}$ for the high spin Co(II). Deviations are caused by unquenched orbital contributions (See Chapter 5). Thus the magnetic moments of the tetrahedral complexes lie in the range $4.0 \sim 4.6 \text{ BM}$; whereas those of octahedral complexes are around $4.8 \sim 5.2 \text{ BM}$ at room temperature, falling off appreciably as the temperature is reduced.

Square planar complexes are also well authenticated. They are primarily of interest because of their oxygen-carrying properties, and are invariably low-spin with magnetic moments at room temperature in the range $2.1 \sim 2.9 \text{ BM}$, indicating 1 unpaired electron.

Typical values of the magnetic moments of Co(II) complexes at room temperature are shown in Table 3.1. Certainly, there is no definite criterion for assigning the coordination number. The highest values are observed for octahedral and square pyramidal complexes, in agreement with the (quasi)

degenerate nature of the ground state. However, relatively large orbital contributions are observed also for trigonal bipyramidal and tetrahedral complexes. For the (quasi) degenerate ground states the values of the magnetic moments depend largely on the splitting of the $^4T_{1g}$ level, a larger splitting yielding lower μ values. The sign of the splitting determines the sign of the magnetic anisotropy.

Table 3.1 Typical values of room temperature effective magnetic moments of Co(II) and Ni(II) complexes in various coordination environments.

Coordination	μ_{eff} (BM)	
	Co(II)	Ni(II)
Octahedral	4.8 - 5.2	2.9 - 3.3
Square pyramidal	4.3 - 5.0	-
Trigonal Bipyramidal	4.2 - 4.9	-
Tetrahedral	4.0 - 4.6	3.2 - 4.1
Square planar	2.1 - 2.9	diamag.

The temperature-dependence of the magnetic moment in magnetically dilute complexes can be used as a tool for identifying the stereochemistry of the complexes since for square pyramidal and octahedral complexes, the thermal population of the excited levels decreases markedly with temperature and generally a decrease of the magnetic moment is observed in the range 5 - 300 K. It seems to be a general rule that a large temperature-dependence is observed for those compounds which have the highest room temperature moments.

3. 3. Low-Spin Octahedral Complexes of Co(III)

Most octahedral complexes of Co(III) are low-spin and hence diamagnetic. Their magnetic properties are therefore of little interest but their electronic spectra have received a lot of attention.

It is possible to observe spin-allowed, d-d bands in the visible region of the spectra of low-spin Co(III) complexes, which have large values of $10Dq$, the crystal-field splitting, required to induce spin-pairing in the Co(III) ion. This means that the low-spin configuration occurs in complexes with ligands that do not cause the low-energy charge transfer bands which so often dominate the spectra of other low-spin complexes. In practice, two bands are generally observed and assigned to the transition:

$$\nu_1 = {}^1T_{1g} \leftarrow {}^1A_{1g} \quad (19\,000 \sim 22\,000 \text{ cm}^{-1})$$

$$\nu_2 = {}^1T_{2g} \leftarrow {}^1A_{1g} \quad (28\,000 \sim 30\,000 \text{ cm}^{-1})$$

These transitions correspond to the electronic promotion $t_{2g}^6 \rightarrow t_{2g}^5 e_g^1$ with the promoted electron maintaining its spin unaltered. The orbital multiplicity of the $t_{2g}^5 e_g^1$ configuration is 6 and so corresponds to two orbital triplet terms ${}^1T_{1g}$ and ${}^1T_{2g}$.

CHAPTER 4

ELECTRONIC SPECTRA AND MAGNETIC PROPERTIES OF NICKEL (II) COMPLEXES⁸⁸

The nickel (II) ion is a common d^8 ion and its spectroscopic and magnetic properties have been extensively studied. The coordination number of Ni(II) rarely exceeds 6 and its principal stereochemistries are octahedral and square planar (4-coordinate) with rather fewer examples of square pyramidal, trigonal bipyramidal, and tetrahedral. The square-planar compounds are diamagnetic and commonly red to yellow, whereas the octahedral and tetrahedral are paramagnetic because of the two unpaired electrons in the $t_{2g}^6 e_g^2$ and $e^4 t_2^4$ configurations respectively (See Fig. 4.1), and are generally green to blue.

In the absence of an X-ray analysis, satisfactory assignment of the electronic spectrum and confirmation of the expected magnetic properties may be used as a means of distinguishing these stereochemistries.

4.1. Electronic Spectra of Ni(II) in an Octahedral Field

In an octahedral crystal field three spin-allowed transitions are expected owing to the splitting of the free-ion, ground 3F term and the presence of the 3P term (Fig. 4.2). These bands are accordingly assigned as:

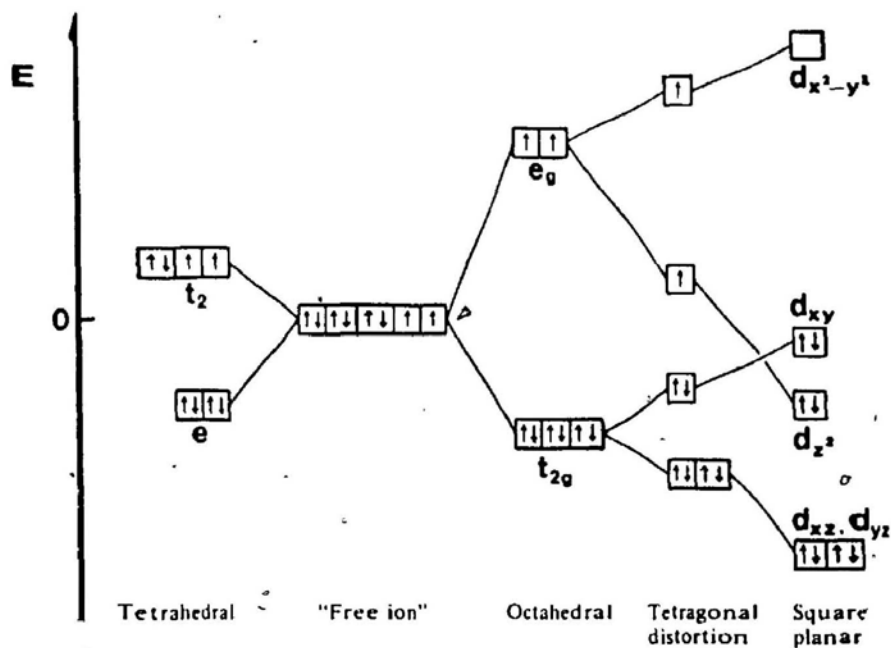


Fig. 4.1 The splitting of d orbitals in fields of different symmetries, and the resulting electronic configurations of d^8 , $Ni(II)$, ion.

$$\nu_1 = {}^3T_{2g}(F) \leftarrow {}^3A_{2g}(F) = 10Dq \quad (8\,000 \sim 12\,000 \text{ cm}^{-1})$$

$$\nu_2 = {}^3T_{1g}(F) \leftarrow {}^3A_{2g}(F) \quad (13\,000 \sim 17\,000 \text{ cm}^{-1})$$

$$\nu_3 = {}^3T_{1g}(P) \leftarrow {}^3A_{2g}(F) \quad (24\,000 \sim 29\,000 \text{ cm}^{-1})$$

where ν_1 gives the value of $10Dq$ directly. Often there is also evidence of weak spin-forbidden (i.e., spin triplet \rightarrow singlet) transitions and the ν_2 absorption has a strong shoulder on it. This has been ascribed to the influence of spin-orbit coupling in "mixing" a spin singlet (1E_g) with the spin triplet, ${}^3T_{1g}(F)$, thereby allowing the spin-forbidden transition to gain intensity from the spin-allowed transition.

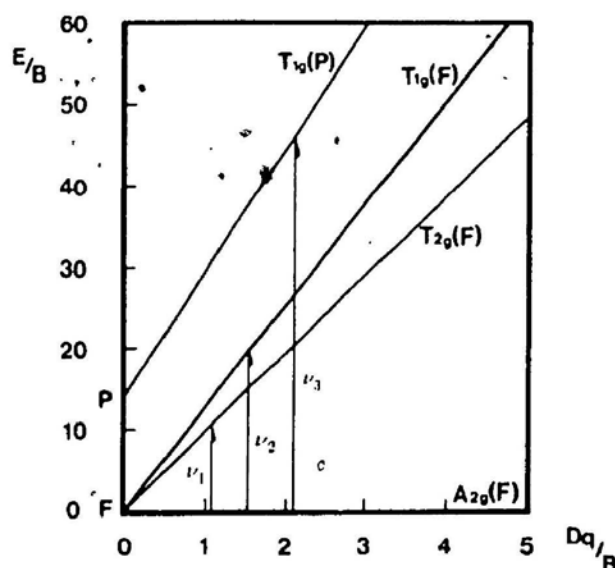


Fig. 4.2 Simplified Tanabe-Sugano diagram for d⁸, Ni(II), ion in an octahedral crystal field and possible spin-allowed transitions.

4. 2. Electronic Spectra of Ni(II) in the Tetrahedral Field

For d⁸ ions in tetrahedral fields the splitting of the free-ion ground term is the reverse of its splitting in an octahedral field, so that ${}^3T_1(F)$ lies lowest. The spectra of the tetrahedral Ni(II) include three bands arising from the transitions:

$$\nu_1 = {}^3T_2(F) \leftarrow {}^3T_1(F)$$

$$\nu_2 = {}^3A_2(F) \leftarrow {}^3T_1(F) \quad (7\,000 \sim 10\,000 \text{ cm}^{-1})$$

$$\nu_3 = {}^3T_1(P) \leftarrow {}^3T_1(F) \quad (13\,000 \sim 16\,000 \text{ cm}^{-1})$$

In practice the spectra are much more intense than those of octahedral complexes and bands are often split by spin-orbit coupling to an extent which can make unambiguous assignments difficult. The broad band around 15000 cm^{-1} is normally assumed to represent one (ν_3) rather than two transitions, with the

corollary that ν_1 must often be assumed to be beyond the lowest energies scanned in the spectrum.

4. 3. Magnetic Properties of Ni(II) Complexes

The T ground term of the tetrahedral ion is expected to lead to a temperature-dependent orbital contribution to the magnetic moment, whereas the A ground term of the octahedral ion is not, though "mixing" of the excited ${}^3T_{2g}(F)$ term into the ${}^3A_{2g}(F)$ ground term is expected to raise its moment according to Eq. (3-1), where $\lambda = -315 \text{ cm}^{-1}$ and $\mu_{\text{spin-only}} = 2.83 \text{ BM}$ (This is the exact reverse of the situations found for Co(II)). The upshot is that the magnetic moments of octahedral compounds are found to lie in the range $2.9 \sim 3.3 \text{ BM}$, whereas those of tetrahedral compounds lie in the range $3.2 \sim 4.1 \text{ BM}$ and are dependent on temperature and, in addition, are reduced towards $\mu_{\text{spin-only}}$ by electron delocalization on to the ligands as well as by distortions from ideal tetrahedral symmetry (See Table 3.1).

Although a square-planar d^8 complex could be, in principle, high-spin with unpaired electrons in the $d_{x^2-y^2}$ and d_{xy} orbitals this is not found to be the case. The separation of these two orbitals evidently always being sufficient to force spin-pairing and consequent diamagnetism. Their spectra are usually characterized by a fairly strong band in the yellow to blue ($17000 \sim 22000 \text{ cm}^{-1}$) region which is responsible for the reddish color, and another band near the ultraviolet. The likelihood of π -bonding and attendant charge transfer makes simple crystal-field treatment inappropriate, and unambiguous assignments are difficult.

CHAPTER 5

MAGNETIC PROPERTIES OF BINUCLEAR CENTERS

Polydentate ligands which incorporate two metal atoms are valuable to study the physical properties of model compounds. In order for "model" compounds to be considered as realistic mimics of protein active sites they should combine as many of the relevant physical properties (e.g., magnetic susceptibilities, spectral parameters, redox properties, etc.) as possible. The binuclear biosites in hemerythrin, cytochrome c oxidase, oxyhemocyanin, tyrosinase and the blue oxidase Type III all contain strongly antiferromagnetically coupled pairs of metal ions. The reproduction of such coupling has stimulated a large number of studies on the magnetic properties of a variety of binuclear compounds. The greater proportion of the work has centred on Cu(II) because the diamagnetism of the last three biosites has given an especial challenge. This chapter will briefly discuss the magnetic properties of the binuclear centers so as to interpret the significance of studying them in the binuclear model compounds.

5. 1. Antiferromagnetic Behaviour

There is a large number of systems which are said to be magnetically concentrated, where the electron spins on adjacent paramagnetic centers are strongly coupled to each other. This coupling between the electron spins leads to

antiferromagnetism when the spins are aligned anti-parallel and to ferromagnetism when the spins are aligned parallel. Broadly speaking, antiferromagnetic systems may be divided into two main types: those in which the magnetic exchange occurs between centers in the same molecules (intramolecular antiferromagnets), and those in which the exchange interaction extends over a large number of centers throughout a crystal lattice (intermolecular antiferromagnets). Binuclear transition metal complexes generally fall into the first group.

An intermolecular antiferromagnetic system normally exhibits the characteristic variation of magnetic susceptibility(χ) with temperature (T) shown in Fig. 5.1. Starting at high temperature, the magnetic susceptibility increases as the temperature is lowered. This variation of the χ with T often leads to a Curie-Weiss law [$\chi = C/(T - \theta)$] behaviour with appreciable positive values of θ (Weiss constant). However, if the temperature is lowered sufficiently, a fairly sharp maximum in the magnetic susceptibility is reached at a temperature, T_N (the *Néel* point), below which the susceptibility decreases rapidly with temperature, and will be dependent on the strength of the applied magnetic field. Intramolecular antiferromagnetic systems exhibit many of the general features of intermolecular antiferromagnetics, the major differences between them are that the maximum in the susceptibility is normally much broader, and the susceptibilities are not usually dependent on the strength of the applied field.

5. 2. Mechanisms of Antiferromagnetic Exchange Interaction

The antiferromagnetism involves the interaction between electronic spin on

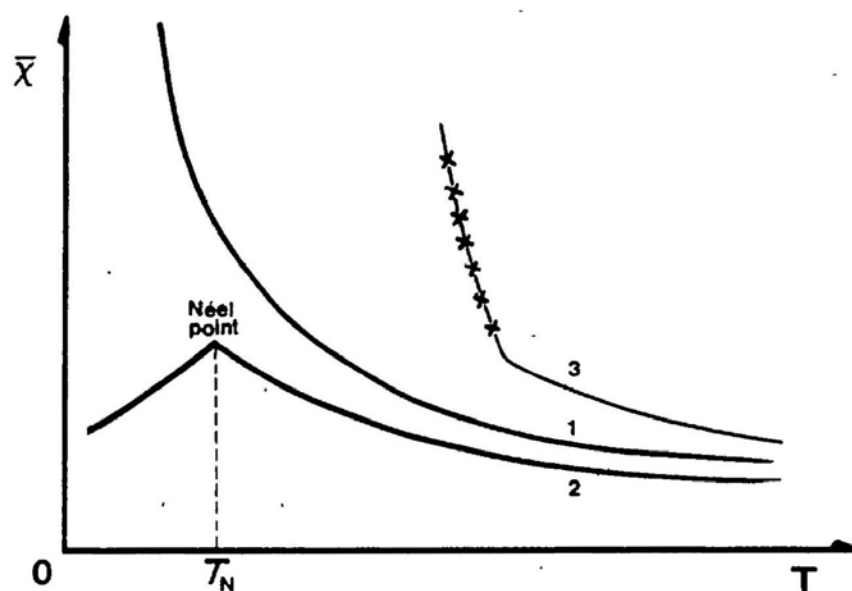


Fig. 5.1 A comparison of the characteristic variation of susceptibility with temperature for normal paramagnetic (1), antiferromagnetic (2) and ferromagnetic (3) materials.

neighbouring metal atoms. The following two mechanisms are usually used to account for antiferromagnetic exchange: (a) direct interaction, and (b) superexchange;

- [a] **Direct Interaction** This mechanism involves direct overlap between the orbitals containing the unpaired electrons, leading to mutual pairing in the ground state.
- [b] **Superexchange** This mechanism for antiferromagnetism involves the interaction of electrons with opposite spins on the two interacting ions *via* an intermediate diamagnetic anion. The mechanism again involves orbital overlap, but instead of only the metal d-orbitals being involved, the participation of filled orbitals on the intervening anion must also be considered, e.g., in a linear oxide system M_2O the interaction may occur in two ways, either *via* a σ -bonding or a π -bonding mechanism (See Fig. 5.2). The

superexchange mechanism may be extended to systems in which more than one anion intervenes between the paramagnetic ions.

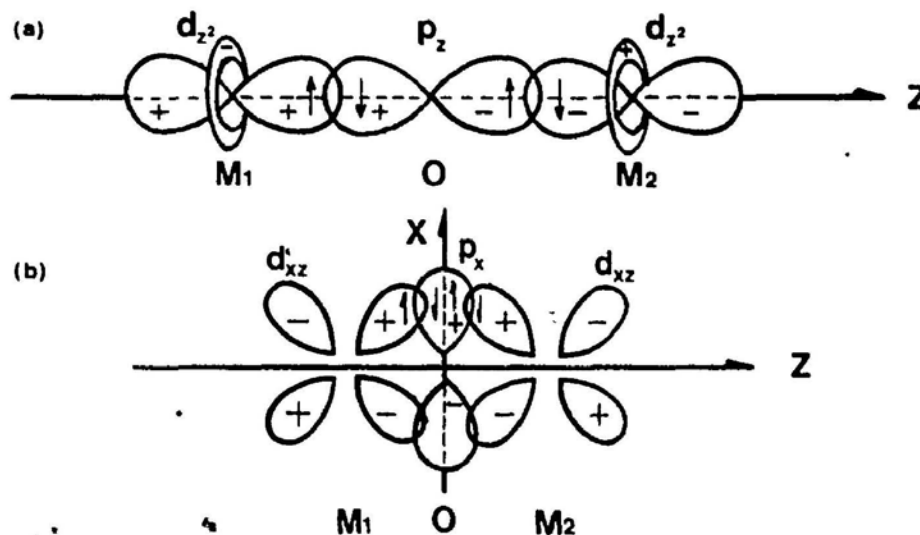


Fig. 5.2 Superexchange in a linear M-O-M system. An example of superexchange via (a) σ -bonding, and (b) π -bonding.

5. 3. Antiferromagnetism in Binuclear Transition Metal Complexes

The magnetic susceptibilities of binuclear transition metal complexes are generally interpreted by the dipolar coupling approach of Van Vleck⁸⁹ which can quantitatively treat the spin-spin interaction. The magnetic exchange between two metal ions of a binuclear complex may be represented by the isotropic spin-coupling Hamiltonian

$$H = -2J\hat{s}_1 \cdot \hat{s}_2 \quad (5-1)$$

where \hat{s}_1 and \hat{s}_2 are the spins of the ions and J , which is given the energy units K (Kelvin's) or cm^{-1} , is the exchange integral between two centers and measures the strength of the intradimer interaction. A negative value of J represents

antiferromagnetic exchange and a positive value refers to ferromagnetic exchange. Assuming each interacting ion to be identical with spin s , the possible new spin quantum numbers S for the dimer are:

$$S = 2s, 2s-1, \dots, 0 \quad (5-2)$$

The energy of each of these states is given by

$$E(S) = -J[S(S+1) - 2s(s+1)] \quad (5-3)$$

The state with the smallest value of S lies lowest, as has been shown in Fig. 5.3.

Energy	Multiplicity	Value of S
$ 20J $	<u>9</u>	4
$ 12J $	<u>7</u>	3
$ 6J $	<u>5</u>	2
$ 2J $	<u>3</u>	1
0	<u>1</u>	0

Fig. 5.3 The relative energies and multiplicities of the possible spin state of a binuclear complex.

The simplest example is an antiferromagnetic interaction between two $s = 1/2$ ions [e.g., Cu(II)]. There are two possible values of S , i.e., 1 and 0, with the spin-triplet ($S = 1$) at $-2J$ above the spin-singlet ground state. The magnetic susceptibility per mole of dimers for an $s = 1/2$ pair is given by the modified Van Vleck equation⁸⁹:

$$\chi = \frac{2Ng^2\beta^2}{3kT} \left[1 + \frac{1}{3} e^{-2J/kT} \right]^{-1} \quad (5-4)$$

The strong antiferromagnetic interactions in the bimetallobiomolecules containing two Cu(II) ions are most likely the consequence of a superexchange mechanism operating through bridging ligands¹⁸. One or more bridges may be present at the site, and, for example in oxyhemocyanin¹⁴, a bound peroxide provides an exogeneous bridge and there is support for the presence of a μ -hydroxy, or μ -phenoxy, endogeneous bridge. Also it has, from the Chapter 2, been clear that hydroxide and phenoxide bridges provide very efficient superexchange pathways in binuclear Cu(II) complexes, with the oxygen bridge angle playing a dominant role with respect to the sign and magnitude of the exchange.

5. 4. Magnetic Exchange in Binuclear Ni(II) Complexes

The electronic structure of Ni(II), d^8 , has been dealt with at length in Chapter 4. The reasons for this should be clear: Ni(II) forms complexes with a variety of ligands, as well as the fact that several stereochemistries are common. The spin of this ion is large enough to make it a sensitive probe of a variety of phenomena. Spin-orbit coupling is also important enough to cause the g values to deviate measurably from the free ion values, to values typically in the neighbourhood of 2.25. Yet, the g values are commonly found to be isotropic or near so. The lowest-lying excited states are far enough away (usually at least 800 cm^{-1}) so as to be unimportant magnetically. Furthermore, Ni(II) is a non-Kramers ion, and the resolution of degeneracies thereby allowed is occasionally observed. Thus, the zero-field splitting is large enough so that paramagnetic

resonance absorption is prevented at X-band.

The dominant feature of the magnetochemistry of octahedral Ni(II) is the zero-field splitting of the ground state (3A_2), as is shown in Fig. 5.4. The name "zero-field splitting" (ZFS) arises from the fact that the splitting occurs in the absence of a magnetic field, and it can be ascribed to the electrostatic field of the ligands. The ZFSs are often responsible for deviations from Curie law behaviour, and give rise to a characteristic specific heat behaviour. Furthermore, the ZFSs cause a single-ion anisotropy which is important in characterizing anisotropic exchange, and are one of the most important sources of paramagnetic anisotropies, that is, of susceptibilities that differ as the external (measuring) magnetic field is rotated with respect to the principal (\parallel, \perp) axis of the molecule.

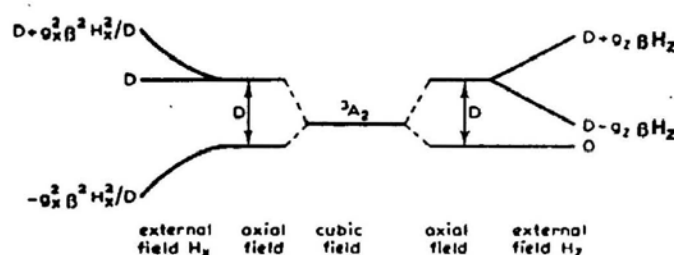


Fig. 5.4 Ni(II) with an internal axial field and an external magnetic field.

If the effect of an external magnetic field \mathbf{H} along the z direction is considered and an interdimer interaction in the molecular field approximation is also allowed for⁹⁰, the Hamiltonian (5-1) becomes

$$\mathbf{H} = -2J\hat{\mathbf{s}}_1 \cdot \hat{\mathbf{s}}_2 - g\beta\mathbf{H}\hat{\mathbf{S}}_z - 2Z'J'\hat{\mathbf{S}}_z \langle \hat{\mathbf{S}}_z \rangle \quad (5-5)$$

where $\hat{\mathbf{S}}_z$ is the operator for the z component of total dimer spin, J' is the

effective interdimer exchange integral, and Z' is the dimer lattice coordination number. Let s be the eigenvalues of \hat{s}_1 or \hat{s}_2 , S the eigenvalues of $\hat{s}_1 + \hat{s}_2$, and M_s the eigenvalues of \hat{S}_z . The eigenvalues of (5-5) may be written as

$$E_c(S, M_s) = E_0(S, M_s) - g\beta H M_s - 2Z'J'M_s \langle \hat{S}_z \rangle \quad (5-6)$$

where $E_0(S, M_s) = -J[S(S+1) - 2s(s+1)]$. For divalent nickel Ni(II), it has two unpaired spins per atom, so that $s = 1$ and $S = 2, 1, 0$. The energy levels $E_0(S, M_s)$ are therefore $E_0(0,0) = +4J$, $E_0(1, M_1) = +2J$ and $E_0(2, M_2) = -2J$, where $M_s = S, S-1, \dots, -S$ and each level is $(2S+1)$ -fold degenerate when H is zero. The magnetic susceptibility, χ , per gram-atom of Ni(II) is given by equation (5-7)

$$\chi = \frac{Ng^2\beta^2 F(J, T)}{[kT - 4Z'J'F(J, T)]} + N\alpha \quad (5-7)$$

where

$$F(J, T) = \frac{1 + 5e^{4J/kT}}{3 + 5e^{4J/kT} + e^{-2J/kT}} \quad (5-8)$$

and $N\alpha$ is the temperature-independent paramagnetism (TIP), and is calculated by using the expression $\frac{8N\beta^2}{10Dq}$. Since Ni(II) can have a large ZFS parameter ($D \approx 5 \sim 10k$), it is necessary to evaluate the effect of single-ion ZFS on the dimer susceptibility. Let the system be quantized along the z direction and assume axial symmetry. In the absence of a magnetic field and neglecting interdimer interaction, the Hamiltonian is

$$H_0 = -2J\hat{s}_1 \cdot \hat{s}_2 - D(\hat{s}_{1z}^2 + \hat{s}_{2z}^2) \quad (5-9)$$

where D is the parameter measuring the ZFS of the ground state. Let an external magnetic field \mathbf{H} be applied along the x, y , or z direction, the Hamiltonian becomes

$$\mathbf{H} = \mathbf{H}_0 + g_i \beta \mathbf{H} \hat{\mathbf{S}}_i \quad (5-10)$$

where $i = x, y$, or z . When the external field is along the z direction, the eigenvalues E_n of (5-10) are given exactly by first-order perturbation theory since the $\Psi_{0,n}$ are eigenfunctions of $\hat{\mathbf{S}}_z$, therefore

$$E_n = E_{0,n} + g_z \beta \mathbf{H} \langle \Psi_{0,n} | \hat{\mathbf{S}}_z | \Psi_{0,n} \rangle. \quad (5-11)$$

When the external field is along the x direction, the first-order perturbation energy is zero because $\hat{\mathbf{S}}_x$ has no diagonal elements with $\Psi_{0,n}$. Therefore the second-order perturbation term must be calculated. With the help of the energy level diagram of Ni(II) in a weak tetragonal field, Fig. 5.4, in which \mathbf{H}_x and \mathbf{H}_y are equal to one another, and the treatment of Van Vleck's approach, the field-independent susceptibilities can be expressed as⁹¹

$$\chi_{||} = \chi_z = \frac{2Ng_z^2 \beta^2}{kT} F_1(J, D, T) \quad (5-12)$$

and

$$\begin{aligned} \chi_{\perp} = \chi_x = \chi_y \\ = 2Ng_z^2 \beta^2 \left[\frac{1}{D} F_2(J, D, T) + \frac{3C_2^2}{3J - \delta} F_3(J, D, T) \right. \\ \left. + \frac{3C_1^2}{3J + \delta} F_4(J, D, T) \right] \end{aligned} \quad (5-13)$$

where

$$F_0(J, D, T) = 2 + e^{D/kT} + 2e^{4J/kT} + e^{J/kT} e^{-\delta/kT} + e^{J/kT} e^{\delta/kT} + 2e^{4J/kT} e^{D/kT} \quad (5-14)$$

$$F_1(J, D, T) = \frac{e^{4J/kT} + 4e^{4J/kT} e^{D/kT} + 1}{F_0(J, D, T)} \quad (5-15)$$

$$F_2(J, D, T) = \frac{e^{D/kT} + 2e^{4J/kT} e^{D/kT} - 2e^{4J/kT} - 1}{F_0(J, D, T)} \quad (5-16)$$

$$F_3(J, D, T) = \frac{e^{4J/kT} - e^{J/kT} e^{\delta/kT}}{F_0(J, D, T)} \quad (5-17)$$

$$F_4(J, D, T) = \frac{e^{4J/kT} - e^{J/kT} e^{-\delta/kT}}{F_0(J, D, T)} \quad (5-18)$$

$$\delta = [(3J + D)^2 - 8JD]^{1/2} \quad (5-19)$$

$$C_1 = 2\sqrt{2}D [(9J - D + 3\delta)^2 + 8D^2]^{-1/2} \quad (5-20)$$

$$C_2 = (9J - D + 3\delta)[(9J - D + 3\delta)^2 + 8D^2]^{-1/2} \quad (5-21)$$

The magnetic susceptibility which can be calculated through (5-12) and (5-13) is the molecular susceptibility while the one which can be experimentally measured is the crystal susceptibility, the two are identical only when the site symmetry of the metal ion is equal to the point symmetry of the crystal space group. In general, however, only measurements on powdered samples are performed, which yield the average magnetic susceptibility, $\bar{\chi}$. In this case there is no way of obtaining the principal molecular values and directions. The quantity $\bar{\chi}$ is defined as

$$\bar{\chi} = \frac{1}{3}(\chi_{||} + 2\chi_{\perp}) \quad (5-22)$$

Taking $g_x = g_y = g_z = g$ (a very good approximation for Ni(II)) and expressing J and D in units of k , the powder susceptibility per gram-atom of Ni(II) is

$$\bar{\chi} = \frac{Ng^2\beta^2}{3} \left[\frac{1}{kT} F_1(J, D, T) + \frac{2}{D} F_2(J, D, T) + \frac{6C_2^2}{3J - \delta} F_3(J, D, T) + \frac{6C_1^2}{3J + \delta} F_4(J, D, T) \right] + N\alpha \quad (5-23)$$

To derive a susceptibility equation including the effect of both ZFS and interdimer interaction the term $-2Z'J'\hat{S}_i \cdot \langle \hat{S}_i \rangle$ is added to the Hamiltonian (5-10). Proceeding as above Eq. (5-24) is obtained

$$\bar{\chi} = \frac{Ng^2\beta^2}{3} \left[\frac{F_1(J, D, T)}{kT - 4Z'J'F_1(J, D, T)} + \frac{2F'(J, D, T)}{1 - 4Z'J'F'(J, D, T)} \right] + N\alpha \quad (5-24)$$

where

$$F'(J, D, T) = \frac{1}{D} F_2(J, D, T) + \frac{3C_2^2}{3J - \delta} F_3(J, D, T) + \frac{3C_1^2}{3J + \delta} F_4(J, D, T) \quad (5-25)$$

An important feature of the magnetic susceptibility is that it is temperature dependent. The effective magnetic moment

$$\mu_{eff} = \left[\frac{3k}{N\beta^2} (\bar{\chi} - N\alpha) T \right]^{1/2} \quad (5-26)$$

is usually much less so, and it is used for a quick characterization of the magnetic properties of the ions.

5. 5. Magnetic Exchange in Binuclear Co(II) Complexes

Cobalt (II) with three unpaired electrons exhibits an important orbital contribution (esp. at high temperatures). In interpreting the magnetic data to obtain estimates of the exchange parameters, there is a much more difficult problem than in the Ni(II) case. For example, if both Co(II) and Ni(II) are in approximately octahedral coordination with a tetragonal distortion, the $^3A_{2g}$ ground term of Ni(II) is split (to first order) only by exchange, whereas the $^4T_{1g}$ ground term of Co(II) is split by both spin-orbit coupling and the low-symmetry field even in the absence of exchange. A further complication which arises in the Co(II) case is that the three " t_{2g} " orbitals contain only one unpaired spin, and since in the symmetry of a binuclear complexes these three orbitals cannot be equivalent, the strength of the exchange will depend on which one is occupied on each ion. This not only contributes substantially to the magnetic anisotropy of the complex, but also means that more than one exchange parameter is required to describe its magnetic properties.

Clearly, the magnetic behaviour of a binuclear Co(II) complexes can be interpreted at several levels of approximation. For example, a relatively simple method to treat the varying-temperature magnetic data for the binuclear Co(II) complexes is to ignore the effects of the orbital degeneracy, which is equivalent to assuming that there is a distortion from octahedral symmetry large enough to

split the ${}^4T_{1g}$ terms by an energy $\gg kT$, with the orbital singlet levels lowest [Co(II) ion in a tetrahedral environment has a spin of 3/2 and is orbitally nondegenerate (4A_2 ground term)]; the spin states are assumed to be coupled by an isotropic Heisenberg exchange interaction. As in the Ni(II) case, the observed decrease in the magnetic moment with decreasing temperature is ascribed mainly to an exchange term $-2J\hat{s}_1\cdot\hat{s}_2$ in the Hamiltonian. The susceptibility of a pair of Co(II) ions is given by⁹²

$$\chi_m = \frac{Ng^2\beta^2}{kT} \left[\frac{14 + 5e^{-6x} + 3e^{-10x}}{7 + 5e^{-6x} + 3e^{-10x} + e^{-12x}} \right] + \chi_{TIP} \quad (5-27)$$

where $x = J/kT$, χ_{TIP} is the so-called Temperature-Independent Paramagnetism caused by the magnetic field (second-order Zeeman effect of ground term)⁹³. In principle, χ_{TIP} can be calculated theoretically⁴⁸, however, it is usually calculated by some empirical expressions, sometimes even guessing a value is used in making the TIP correction.

Certainly, this model, in which the temperature dependence of the magnetic moment is assumed to be due largely to exchange (J), is obviously inappropriate. The effective moment of an octahedral Co(II) complex normally decreases with temperature, as a result of the splitting of the ${}^4T_{1g}$ ground term by spin-orbit coupling and distortion, and both of these effects are larger than the exchange interaction J , which is only of the order of a few wave numbers. Therefore, any further treatment should take these two effects into account. Here only the modification of the spin-orbit coupling will be briefly discussed below. Unfortunately, in doing so it has to introduce two new parameters, both of rather uncertain value, so that the accuracy of the results will not be high.

The lowest orbital states of the free Co(II) are 4F and 4P (See Fig. 3.1). In the presence of the cubic field, the lowest 4F state splits into two orbital triplets (symmetry 4T_2 and 4T_1) and a singlet (4A_2) with the 4T_1 triplet lowest. The 4P term is not split by the cubic field and remains an orbital triplet with symmetry 4T_1 . Since the 4P and ground-orbital triplet (4T_1) have the same symmetry, the cubic field mixes a little 4P character into the ground ${}^4T_1(F)$ state. However, the matrix elements of \hat{L} within the state of 4T_1 are exactly the same as the matrix elements of $-(3/2)\hat{L}$ between the associated P functions⁹⁴. In group theoretical language one refers to the structural isomorphism of 4T_1 and 4P . Since free-ion spin-orbit coupling is expressed as $\lambda \hat{L} \cdot \hat{s}$ [where $\lambda \approx -180\text{cm}^{-1}$ for Co(II)], the effect of this coupling in the field can be represented by the operator $H_{Ls} = -\lambda(\hat{L}_1 \cdot \hat{s}_1 + \hat{L}_2 \cdot \hat{s}_2)$ acting on product functions derived from pseudo- 4P states of the ions 1 and 2 in a binuclear Co(II) complex⁹⁴. This operator must, however, be modified to take account of (1) mixing of metal and ligand wavefunctions as a result of covalency (which causes the true matrix elements of \hat{L} to be smaller than those obtained using pure d wavefunctions) and, (2) mixing of the strong-field determinantal wavefunctions due to interelectronic repulsion. The first can be allowed for by introducing an orbital reduction factor κ as an empirical parameter⁹⁵, and the second by multiplying \hat{L} by another numerical factor A , whose value can, in principle, be estimated independently from spectroscopic data⁹³. The free-ion coupling constant λ is thus replaced by $\kappa A \lambda$, and the complete perturbation is represented by the Hamiltonian (5-28),

$$H = \kappa A \lambda (\hat{L}_1 \cdot \hat{s}_1 + \hat{L}_2 \cdot \hat{s}_2) - 2J \hat{s}_1 \cdot \hat{s}_2 \quad (5-28)$$

and the quantities to be determined by curve fitting to the experimental data are κ , A and J . Since the dependence of χ_m on κ , A and J can not be expressed analytically, the usual method of least squares is not applicable, and a trial-and-error fit is necessary. κ , A and J are therefore varied by small amounts, and contours of the mean squared deviation are plotted until a minimum is located for each binuclear Co(II) complex⁴⁸.

CHAPTER 6

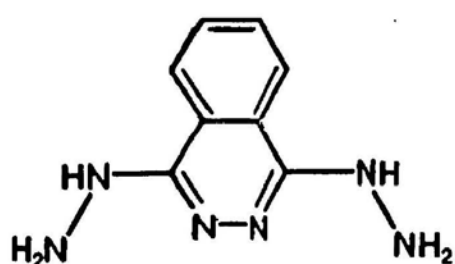
SOME BINUCLEATING, SEXADENTATE PHTHALAZINE HYDRAZONE LIGANDS

Tetradentate pyridylaminophthalazine (PAP) ligands (27) have generated many binuclear complexes with Cu(II), Co(II), Co(III) and Ni(II) salts^{63-65,67-73,75,77-80}. Significantly, the Cu(II) complexes have been shown to be useful models for the active sites of copper metalloproteins containing binuclear copper centers, especially from the standpoint of magnetic, structural, and electrochemical properties.

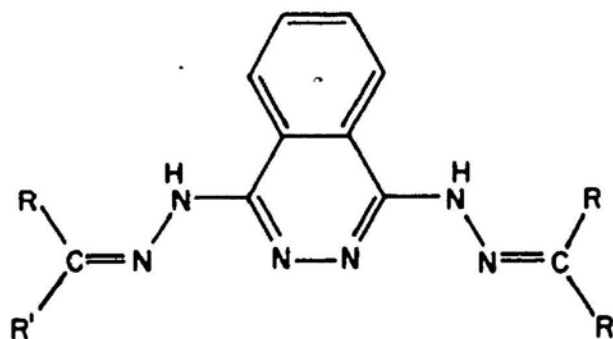
In an attempt to expand this group of compounds to include other polyfunctional ligands which might show similar properties, this project has involved the synthesis and study of the coordination chemistry of three other ligands derived from 1,4-dihydrazinophthalazine (DHPH), which is a reactive intermediate and acts as a tetradentate binucleating ligands in its own right⁶² (See Fig. 6.1). Theoretically, the reaction of DHPH with appropriate aldehydes/ketones should yield Schiff-base adducts (hydrazones) with six donor atoms arranged in a manner which would favour the formation of binuclear complexes, whose exogenous bridging site would be able to be varied. Besides, the well-known deprotonation reactions of hydrazones suggest that both neutral and anionic ligands could be present. Finally, many extensions of the system could be envisioned by using a variety of aldehydes and ketones. Therefore the three DHPH derivatives

PMP, PPA and PMI shown in Fig. 6.1 were prepared with ease.

The ligands PMP, PPA and PMI were chosen for study here because they should form five-membered chelate rings, thus having the potential for the formation of systems with large metal-metal separations, and also because they present alternatives to the other model ligands already studied (N_4 donors) by offering each metal three potential donor sites.



DHPH



Ligands

Ligand	R	R'
PMP(33)	H	
PPA(34)	CH ₃	
PMI(35)	H	

Fig. 6.1 The intermediate DHPH and its derivatives; binucleating phthalazine ligands PMP, PPA, and PMI.

6. 1. The Binucleating Ligand PMP

The synthesis of this ligand was carried out according to the literature procedure⁹⁶. The ligand 1,4-dihydrazinophthalazine-bis(6-methyl-2-pyridinecarboxal-dimine), **33**, henceforth referred to as PMP, was directly prepared by the reaction of the DHPH with 6-methyl-2-pyridinecarboxaldehyde, in which both reactants, in the ratio of 1:2, were mixed in hot methanol and refluxed for three hours. Reddish-orange crystals formed upon cooling which were filtered and recrystallized from ethanol (Mp $\sim 130^{\circ}\text{C}$) (See Experimental Section).

PMP has two N-H protons, at least one of which seems to be replaceable, as will be shown in some cases. The ligand can coordinate two transition metals with its six nitrogen donors to form a binuclear structure by reacting readily with the salt in the ratio of 1:2, both in water and/or organic solvents. In particular, PMP is found to be quite reactive toward the transition metal ions Co(II) and Ni(II). The resulting complexes are adducts with the formula $[\text{M}_2(\text{PMP})\text{X}]\text{X}_3 \cdot n\text{H}_2\text{O}$, in which the two metals are bound to a single PMP ligand in a doubly-bridged structural arrangement [a binuclear 2:1 (metal : ligand) structure], and with the formula $[\text{M}_2(\text{PMP})_2]\text{Y}_4 \cdot n\text{H}_2\text{O}$, in which the two metal centers are sandwiched between the two adjacent PMP ligands (a binuclear 1:1 mode) [where M = Co(II) and Ni(II); X = Cl and Br; Y = ClO_4 and BF_4]. Both species exhibit reduced magnetic moments in many cases, which is believed to be the result of a spin-spin magnetic coupling between the two metal centers due to a superexchange interaction *via* the -N-N- bond in the phthalazine ring and/or the bridging group X⁸⁰.

6. 2. The Binucleating Ligand PPA

This ligand was prepared in terms of the published procedure⁸³. The ligand 1,4-dihydrazinophthalazine-bis(2-pyridineacetaldoxime), **34**, henceforth PPA, was directly synthesized by reaction of the DHPH (1 equiv.) and 2-acetyl-pyridine (2 equiv.) in refluxing methanol and obtained as orange crystals (Mp. 185 - 187 °C) (See Experimental Section).

Structurally, this ligand is an analogue of PMP, but the methyl group is bound to the azomethine carbon atom. It should have analogous physical/chemical properties to the ligand PMP and form similar Co(II)/Ni(II) complexes to those of PMP as well. Indeed, in this study the ligand PPA not only behaves as a hexadentate chelating ligand to form μ -bridged binuclear Co(II)/Ni(II) complexes with the 2:1 mode, as it did in the copper compound **31**, but also acts as a binucleating ligand with six nitrogen donors to two adjacent transition metals in the 1:1 fashion, as its PMP analogue does.

6. 3. The Binucleating Ligand PMI

The ligand 1,4-dihydrazinophthalazine-bis(N-methyl-2-imidazolecarboxaldimine), **35**, henceforward PMI, was produced by a reported procedure⁷⁴, in which PMI was directly synthesized by the condensation of the precursors, DHPH (1 equiv.) and N-methylimidazole carboxaldehyde (2 equiv.), in refluxing methanol for 3 hours, and collected as yellow crystals (Mp. 238 - 241 °C). Further details on its synthesis will be given in the Experimental Section.

The ligand PMI, which involves N-methylimidazole peripheral donor groups, reacts readily with Co(II)/Ni(II) salts to give highly coloured products which include both binuclear 2:1 and 1:1 derivatives. The reactions of Co(II)/Ni(II) perchlorate and tetrafluoroborate with PMI parallel the same reactions involving PMP and PPA, in both cases binuclear 1:1 species are obtained. The binuclear PMI complexes formed are expected to have the similar physical/chemical properties to their PMP and PPA counterparts, since they contain similar donor groups in an equivalent geometric arrangement.

SECTION II RESULTS AND DISCUSSION

CHAPTER 7

BINUCLEAR COBALT(II)/NICKEL(II) COMPLEXES
OF THE LIGANDS PMP, PPA AND PMI

The ligands PMP, PPA and PMI react readily with alcoholic and aqueous solutions of Co(II)/Ni(II) salts to form two series of binuclear complexes with general formulae $[M_2LX]X_3$ (2:1), or $[M_2L_2]Y_4$ (1:1) where $M = \text{Co(II)}$ and Ni(II) ; $L = \text{PMP, PPA, and PMI}$; $X = \text{Cl, Br, and NO}_3$; $Y = \text{NO}_3, \text{ClO}_4, \text{and BF}_4$. The majority of the complexes have been obtained as fine crystalline products. However, only a few of these crystals collected are suitable for X-ray analysis. The rest of the compounds have been isolated in the form of powders. The elemental analyses are quoted in Tables 7.1 and 7.2, in which some metal analyses are not very satisfactory but they still do support the formulae suggested. The microanalytical data for these complexes also indicate that in some cases the solvent molecules in the compounds are still present after being dried under vacuum, suggesting their coordinating behaviour. Generally, these complexes are intensely coloured, and very soluble in water as well as soluble in most common organic solvents.

The binuclear chloride complexes of the ligand PMP were prepared by reacting a methanol solution of PMP and an aqueous solution of the related metal salt in a molar ratio of 1:2 under reflux. The solutions were filtered hot and allowed to stand at room temperature for crystallization. The crystals formed and were

Table 7.1 Analytical data for the binuclear Co(II) complexes of the ligands PMP, PPA and PMI.

No.	Complex	Mol. Wt	Found/(Calcd) (%)			
		Colour ^a	C	H	N	Co
36	[Co ₂ (PMP)Cl(H ₂ O) ₄]Cl ₃ ·4H ₂ O	799.80 Red	32.81 (33.01)	4.64 (4.50)	13.79 (14.00)	15.20 (14.74)
37	[Co ₂ (PMP)Br(H ₂ O) ₄]Br ₃ ·3H ₂ O	959.57 D.brown	27.55 (27.52)	3.67 (3.75)	11.54 (11.67)	11.08 (12.28)
38	[Co ₂ (PMP) ₂](NO ₃) ₄ ·4EtOH	1341.88 Black	48.49 (46.50)	3.77 (4.77)	21.54 (20.87)	8.09 (8.78)
39	[Co ₂ (PMP) ₂](ClO ₄) ₄ ·EtOH	1353.67 R.violet	41.63 (40.78)	3.64 (3.40)	16.72 (16.55)	7.80 (8.71)
40	[Co ₂ (PMP-H) ₂](BF ₄) ₂ ·4H ₂ O	1153.54 Black	46.11 (45.78)	4.04 (3.99)	19.17 (19.42)	6.17 (10.22)
41	[Co ₂ (PPA)Cl(MeOH)Cl ₃]	687.68 R.violet	40.31 (40.13)	3.24 (3.49)	16.36 (16.29)	13.40 (17.14)
42	[Co ₂ (PPA-H)Br(H ₂ O) ₂ Br ₂]0.5EtOH	811.60 R.black	34.17 (34.00)	2.83 (3.33)	13.76 (13.80)	11.80 (14.52)
43	[Co ₂ (PPA) ₂](ClO ₄) ₄ ·EtOH	1353.67 D.violet	41.55 (40.77)	3.39 (3.40)	16.85 (16.55)	8.44 (8.71)
44	[Co ₂ (PPA-H) ₂](BF ₄) ₂ ·EtOH·3H ₂ O	1181.52 D.brown	46.52 (46.72)	3.41 (4.23)	18.60 (18.96)	7.84 (9.96)
45	[Co ₂ (PMI)Cl(H ₂ O) ₄]Cl ₃ ·1.5H ₂ O	732.78 R.brown	29.40 (29.48)	4.00 (3.82)	18.87 (19.10)	16.13 (16.08)
46	[Co ₂ (PMI)Br(H ₂ O) ₄]Br ₃ ·0.5H ₂ O	892.50 Brown	24.10 (24.20)	3.03 (3.03)	15.53 (15.69)	10.92 (13.21)
47	[Co ₂ (PMI)(OH ₂)(NO ₃) ₄]EtOH·0.5H ₂ O	812.91 Brown	29.38 (29.52)	2.97 (3.32)	24.68 (24.11)	13.39 (14.50)
48	[Co ₂ (PMI) ₂](ClO ₄) ₄ ·EtOH	1309.66 R.black	35.01 (34.82)	3.35 (3.21)	21.27 (21.38)	7.60 (9.00)
49	[Co ₂ (PMI) ₂](BF ₄) ₄ ·2EtOH	1305.08 Black	37.19 (36.78)	3.56 (3.68)	21.45 (21.45)	8.36 (9.03)

a: D.brown means Dark brown, R.violet Reddish violet, and R.black Reddish black, etc.

Table 7.2 Analytical data for the binuclear Ni(II) complexes of the ligands PMP, PPA and PMI

No.	Complex	Mol.Wt	Found/(Calcd) (%)			
		Colour ^a	C	H	N	Ni
50	$[\text{Ni}_2(\text{PMP})\text{Cl}(\text{H}_2\text{O})_4]\text{Cl}_3 \cdot 4.5\text{H}_2\text{O}$	808.36 Green	32.62 (32.66)	4.57 (4.58)	13.72 (13.85)	13.09 (14.53)
51	$[\text{Ni}_2(\text{PMP})\text{Br}(\text{H}_2\text{O})_4]\text{Br}_3 \cdot 0.5\text{MeOH} \cdot \text{H}_2\text{O}$	939.10 O.green	28.76 (28.75)	3.48 (3.41)	11.90 (11.93)	11.63 (12.50)
52	$[\text{Ni}_2(\text{PMP})(\text{OH}_2)(\text{H}_2\text{O})_4](\text{NO}_3)_4 \cdot \text{MeOH}$	883.52 Brown	31.13 (31.24)	3.75 (3.85)	19.27 (19.01)	12.59 (13.29)
53	$[\text{Ni}_2(\text{PMP})_2](\text{ClO}_4)_4 \cdot 4\text{H}_2\text{O}$	1379.28 Brown	38.14 (38.27)	3.66 (3.48)	15.92 (16.23)	8.38 (8.51)
54	$[\text{Ni}_2(\text{PMP})(\text{PMP-H})](\text{BF}_4)_3 \cdot 5.5\text{H}_2\text{O}$	1267.92 Orange	41.65 (41.65)	3.90 (3.94)	17.57 (17.67)	5.34 (9.28)
55	$[\text{Ni}_2(\text{PPA})\text{Cl}(\text{H}_2\text{O})_4]\text{Cl}_3 \cdot 2\text{H}_2\text{O}$	763.32 Green	34.21 (34.59)	3.72 (4.19)	14.80 (14.67)	15.32 (15.38)
56	$[\text{Ni}_2(\text{PPA-H})\text{Br}(\text{EtOH})(\text{H}_2\text{O})\text{Br}_2]\text{EtOH} \cdot 0.5\text{H}_2\text{O}$	871.14 Green	35.74 (35.82)	3.13 (3.90)	12.70 (12.86)	11.69 (13.48)
57	$[\text{Ni}_2(\text{PPA})_2](\text{NO}_3)_4 \cdot 4\text{H}_2\text{O}$	1229.50 G.brown	43.19 (42.94)	3.71 (3.90)	22.80 (22.77)	12.95 (9.55)
58	$[\text{Ni}_2(\text{PPA})_2](\text{ClO}_4)_4 \cdot 6\text{H}_2\text{O}$	1415.32 O.green	37.38 (37.31)	3.44 (3.67)	15.73 (15.83)	8.14 (8.30)
59	$[\text{Ni}_2(\text{PPA})_2](\text{BF}_4)_4 \cdot 4\text{H}_2\text{O}$	1328.70 R.brown	39.84 (39.74)	3.53 (3.61)	16.98 (16.86)	8.65 (8.84)
60	$[\text{Ni}_2(\text{PMI})\text{Cl}(\text{H}_2\text{O})_4]\text{Cl}_3 \cdot 2\text{H}_2\text{O}$	741.32 Y.green	28.97 (29.13)	3.93 (4.05)	18.69 (18.89)	14.24 (15.84)
61	$[\text{Ni}_2(\text{PMI})\text{Br}(\text{H}_2\text{O})_4]\text{Br}_3 \cdot 3.5\text{H}_2\text{O}$	946.13 L.green	22.83 (22.83)	2.98 (3.49)	14.58 (14.79)	12.59 (12.41)
62	$[\text{Ni}_2(\text{PMI})(\text{OH}_2)(\text{NO}_3)_4]\text{EtOH} \cdot 1.5\text{H}_2\text{O}$	830.48 Mustard	28.88 (28.90)	3.39 (3.49)	23.82 (23.60)	13.31 (14.14)
63	$[\text{Ni}_2(\text{PMI})_2](\text{ClO}_4)_4 \cdot 4\text{H}_2\text{O}$	1335.28 Y.orange	32.11 (32.35)	3.33 (3.30)	20.56 (20.97)	8.07 (8.79)
64	$[\text{Ni}_2(\text{PMI})_2](\text{BF}_4)_4 \cdot 6\text{H}_2\text{O}$	1320.74 Brown	32.63 (32.71)	3.47 (3.03)	21.02 (21.20)	8.88 (8.89)

a: O.green represents Olive green, G.brown Greenish brown, R.brown Reddish brown, Y.green Yellowish green, and L.green Lime green, etc.

isolated by decanting the mother liquor and washing with a methanol/ether mixture. The crystal structures of the reddish-brown Co(II) complex and the green Ni(II) compound have been determined (See Chapter 8). The bromide, nitrate, perchlorate and tetrafluoroborate complexes were prepared in a similar manner. Introducing a small amount of water into the preparation seems quite helpful for the formation of crystalline solids. However, this is not appropriate for the preparation of binuclear PMI complexes, in which the fine crystalline powders of the PMI compounds formed in cool absolute (or 95%) ethanol solution that was filtered immediately after refluxing.

For the PPA complexes, both solvent systems mentioned above were employed in their preparations so as to obtain the satisfactory products. Broadly, the PPA compounds are more soluble than PMP ones, which makes it more difficult to form crystalline solids. Crystalline products were only obtained in some cases, but they were not found to be suitable for the X-ray structure study. According to the elemental analyses, the binuclear PPA bromide complexes contain just three bromide groups. The charge deficiency associated with these bromides can be rationalized by the presence of a deprotonated PPA ligand, like the ligand in 31. Such a feature has also shown up in the Co(II) tetrafluoroborate compounds of PMP and PPA (40 and 44), in which both ligands in these 1:1 species have lost one proton.

Another interesting phenomenon deserving to be mentioned is that in some cases the complex is able to possess totally different colours when a different solvent is used in its preparation. This significant change in colour may suggest a change in the chromophore around the metal centers and/or possibly an involve-

ment of the solvent in the coordination sphere of the center. The latter situation is supported by the fact that the colour of DMF solutions of the PMI compounds changes gradually. This change can be followed by UV/VIS spectroscopy, in which the charge transfer absorption of the compound shifts and/or splits up into two bands, which probably implies that the DMF molecule has coordinated to the metal center by replacing a small molecule/anion coordinated or even the nitrogen donor of the ligand, since DMF itself is a very strong donor.

Generally, the preparations of the binuclear cobalt complexes are more difficult than those of their nickel counterparts. Sometimes a careful choice of solvents or special treatment is required. No precaution was taken to exclude air during their preparation. However, the magnetic data on some cobalt complexes suggest that the Co(II) compounds may be partially oxidized by air during their syntheses, and so further preparation of these compounds should be carried out in a nitrogen atmosphere.

The perchlorate and tetrafluoroborate complexes were originally expected to have the binuclear 2:1 molecular formulae, like their halide counterparts. However, the elemental analyses indicate that their empirical formulae are just $[ML]Y_2 \cdot mS \cdot nH_2O$ ($M = Co$ and Ni ; $L = PMP, PPA$ and PMI ; $Y = ClO_4$ and BF_4 ; and $S =$ solvent). According to the studies of the ligand $DHPII$ and its complex **15** as well as other related ligands and their corresponding complexes, the molecular formulae of the ClO_4 and BF_4 complexes should be twice their empirical formulae and be written as $[M_2L_2]Y_4 \cdot 2mS \cdot 2nH_2O$, i.e., they have the binuclear 1:1 structure, as will be supported by their spectral and magnetic data. Their magnetic properties are definitely consistent with a structure containing

pairs of $M(II)$ ions with a weak antiferromagnetic exchange interaction (See Chapter 10). The nitrate complexes appear less well defined. Both 1:1(38) and 2:1(47) nitrate species are possible in terms of their elemental analyses and spectral data. This coordination behaviour that normally coordinating anions (such as Cl^- and Br^-) associate with the binuclear 2:1 species while poorly coordinating donor groups (e.g., ClO_4^- and BF_4^-) result in the 1:1 derivatives signifies that the metal centers in these systems need a relatively strong ligand-field environment and, the three ligands PMP, PPA and PMI in the 1:1 complexes can provide the centers with stronger coordinating donors than the perchlorate and tetrafluoroborate groups.

CHAPTER 8

CRYSTAL AND MOLECULAR STRUCTURES OF THE
BINUCLEAR HALIDE COMPLEXES OF THE LIGAND PMP

The binuclear chloride complexes of the ligand PMP, $(\mu\text{-PMP})(\mu\text{-chloro})\text{-tetraaquo-dicobalt(II)-trichloride-4.0H}_2\text{O}$ (**36**) and $(\mu\text{-PMP})(\mu\text{-chloro})\text{-tetraaquo-dinickel(II)-trichloride-4.5H}_2\text{O}$ (**50**), have been characterized by an X-ray crystal structural study. The crystallographic data collection and refinement of the structures are given as follows.

8. 1. Crystal structure of $[\text{Co}_2(\text{PMP})\text{Cl}(\text{H}_2\text{O})_4]\text{Cl}_3 \cdot 4.0\text{H}_2\text{O}$ (**36**)

A. Collection of X-ray Intensity Data

A reddish-brown single crystal (approximately $0.20 \times 0.20 \times 0.20$ mm) of the title compound **36** was used for the structural determination. Diffraction data were measured at room temperature (22°C) by employing a Picker four-circle diffractometer with graphite-monochromatized $\text{MoK}\alpha$ radiation [$\lambda(\text{MoK}\alpha_1) = 0.70930 \text{ \AA}$]. The $\theta - 2\theta$ scan technique was used, and individual reflection profiles were analysed⁹⁷ to $2\theta_{\text{max}} = 49.9^\circ$. The measured reflections numbered 5337 in all, of which 3097 were independent and 2204 reflections with $I(\text{intensity})_{\text{net}} > 2.5\sigma(I_{\text{net}})$ were considered significant, and used in the analysis. The measured intensities were corrected for Lorentz and polarization effects, but

absorption corrections were not made (because of the relatively small value of μ_r). No extinction correction was needed. The cell parameters were obtained by the least-squares refinement of the diffractometer setting angles of 62 well centred reflections with 2θ between 45 - 50 °. The pertinent crystal data are outlined in Table 8.1.

B. Solution and Refinement of the structure

The structure of **36** was solved by direct methods with the program MULTAN⁹⁸. The atomic positions were refined with full-matrix least-squares techniques by minimizing the function $\sum w(\Delta F)^2$ (the weighting scheme was $w^{-1} = \sigma_F^2$). All non-hydrogen atoms were refined anisotropically, whereas all hydrogen atoms were refined with isotropic temperature factors (the calculated H-atoms were fixed at their calculated thermal parameter values because one was refined to a negative value). The hydrogen atoms of the water molecules and the methyl groups were found by Fourier difference maps. The final values of the discrepancy indices were $R = 0.040$ and $R_w = 0.043$ for the significant reflections while $R = 0.075$ and $R_w = 0.086$ for all data with unit weights based on counting statistics (σ_F^2). Final atomic positions of the atoms and equivalent isotropic temperature factors are given in Table 8.2. All calculations were carried out with the NRCVAX system of programmes⁹⁹. The source of atomic scattering factors is specified in ref. 100. Anisotropic thermal parameters for the non-hydrogen atoms, further bond distances and angles, and related structural data are available in the Appendix and/or the Supplementary Material.

Table 8.1 Summary of Crystal Data and Diffraction Data Collection.

formula	$\text{Co}_2\text{C}_{22}\text{H}_{28}\text{Cl}_4\text{N}_8\text{O}_4 \cdot 4.0\text{H}_2\text{O}(\mathbf{36})$	$\text{Ni}_2\text{C}_{22}\text{H}_{28}\text{Cl}_4\text{N}_8\text{O}_4 \cdot 4.5\text{H}_2\text{O}(\mathbf{50})$
mol. wt	799.80	808.38
cryst. size, mm ³	0.20x0.20x0.20	0.15x0.15x0.20
cryst syst	trigonal	trigonal
space group	$P3_121$	$P3_221$
a, Å	17.1624(14)	17.1237(4)
c, Å	10.2358(7)	10.21360(20)
V, Å ³	2611.01	2593.01
Z	3	3
$\rho(\text{calcd})$, g cm ⁻³	1.53	1.56
μ , mm ⁻¹	1.31	4.73
radiation; λ , Å	MoK α_1 ; 0.70930	CuK α ; 1.54056
$2\theta_{\text{max}}$, deg.	49.9	110.0
no. of indep. reflexns	3097	2124
no. of signif. reflexns	2204	1992
final R(R _w)†	0.040(0.043)	0.040(0.054)
temp for data collcn, °C	22	22

† $R = \sum (|F_o| - |F_c|) / \sum |F_o|$, $R_w = [\sum w(|F_o| - |F_c|)^2 / \sum w |F_o|^2]^{1/2}$.

Table 8.2 Atomic parameters X, Y, Z and BISO for 36. E.S.Ds. refer to the last digit printed.

ATOM	X	Y	Z	BISO†
CO	0.02300(6)	0.74759(5)	0.98773(8)	2.41(4)
CL 1	0.77515(12)	0.77515	1	2.99(9)
CL 2	0.56512(11)	0.22334(11)	0.99536(18)	3.86(9)
CL 0	0.8031 (3)	0.7867 (3)	0.6370 (4)	6.88(24)
O 1	0.6363 (3)	0.7568 (4)	0.7377 (4)	4.4 (3)
O 2	0.6225 (3)	0.7486 (3)	1.1919 (4)	3.65(25)
O 3	0.4934 (4)	0.2370 (4)	0.7132 (6)	5.3 (3)
N 1	0.5574 (3)	0.6034 (3)	0.9937 (5)	2.34(24)
N 2	0.4295 (3)	0.6115 (3)	0.9733 (5)	2.7 (3)
N 3	0.4856 (3)	0.7016 (3)	0.9787 (5)	2.5 (3)
N 4	0.6131 (3)	0.8719 (3)	0.9926 (5)	2.9 (3)
C 1	0.2775 (4)	0.3232 (4)	0.9953 (7)	3.2 (3)
C 2	0.3217 (4)	0.4140 (4)	0.9895 (6)	2.7 (3)
C 3	0.4157 (4)	0.4624 (4)	0.9938 (6)	2.2 (3)
C 4	0.4697 (4)	0.5593 (4)	0.9894 (5)	2.1 (3)
C 5	0.4577 (5)	0.7571 (5)	0.9797 (7)	3.2 (4)
C 6	0.5270 (5)	0.8521 (4)	0.9863 (6)	2.8 (3)
C 7	0.5023 (5)	0.9178 (5)	0.9886 (7)	3.7 (4)
C 8	0.5707 (6)	1.0084 (5)	0.9996 (7)	4.6 (5)
C 9	0.6573 (5)	1.0261 (5)	1.0065 (7)	3.67(14)
C10	0.6769 (5)	0.9583 (4)	1.0028 (7)	3.5 (4)
C11	0.7721 (6)	0.9778 (5)	1.0115 (9)	5.3 (5)
O 4	0.0341 (17)	0.03412	0	0.1 (6)
O 5	0.9475 (18)	0.9388 (19)	0.765 (3)	4.7 (6)
H 1	0.227 (4)	0.301 (4)	0.998 (6)	3.6
H 2	0.295 (4)	0.441 (4)	0.982 (6)	3.7
H 5	0.387 (5)	0.729 (5)	0.970 (6)	4.2
H 7	0.460 (5)	0.906 (5)	0.991 (6)	5.0
H 8	0.561 (5)	1.039 (5)	0.996 (7)	5.8
H 9	0.712 (4)	1.096 (4)	1.024 (7)	4.6
H N2	0.388 (4)	0.590 (4)	0.989 (6)	3.5
H11A	0.819 (5)	1.046 (5)	1.005 (7)	6.2 (3)
H11B	0.783 (4)	0.960 (4)	0.949 (6)	4.2 (4)
H11C	0.788 (6)	0.964 (6)	1.082 (8)	7.8 (3)
H101	0.605 (4)	0.760 (4)	0.737 (5)	2.9 (5)
H201	0.684 (7)	0.753 (6)	0.740 (9)	9.97(22)
H102	0.666 (5)	0.754 (5)	1.254 (7)	5.6 (3)
H202	0.583 (3)	0.729 (4)	1.242 (5)	2.0 (5)
H103	0.528 (4)	0.296 (5)	0.687 (7)	4.2 (4)
H203	0.505 (5)	0.230 (5)	0.783 (7)	6.0 (3)

* E.S.Ds are the equivalent isotropic Debye-Waller temperature factors.

† BISO is the mean of the principal axes of the thermal ellipsoid.

C. Description of the Structure of **36**

The crystal structure **36** consists of a binuclear $[\text{Co}_2(\text{PMP})\text{Cl}(\text{H}_2\text{O})_4]^{3+}$ cation, three chloride anions and four lattice water molecules. A structural representation of this binuclear species is presented in Fig. 8.1, together with the atomic numbering system used. Relevant interatomic distances and angles are listed in Table 8.3 and 8.4. There is essentially a two-fold axis in the molecule, which passes through the chlorine bridge and the central-point of the phthalazine group. The $[\text{Co}_2(\text{PMP})\text{Cl}(\text{H}_2\text{O})_4]^{3+}$ system is nearly planar, with the two cobalt atoms and the bridging Cl atom co-planar with the ligand. The two cobalt(II) ions are linked by a chlorine bridge and a phthalazine via its diazine nitrogen pair [N(1)-N(1A)]. The equatorial coordination of each octahedral metal center is completed by the hydrazone and pyridine nitrogen donors, and the two axial coordination sites of the center are occupied by two water molecules, which are tightly bound to the cobalt atom [Co-O(1) 2.057 Å and Co-O(2) 2.090 Å]. The two cobalt octahedra are quite distorted and separated by a distance of 3.712 Å with a chlorine bridge angle of 100.56°. Major in-plane deformations occur due to the juxtaposition of the two five-membered chelate rings.

8. 2. Crystal Structure of $[\text{Ni}_2(\text{PMP})\text{Cl}(\text{H}_2\text{O})_4]\text{Cl}_3 \cdot 4.5\text{H}_2\text{O}$ (**50**)

A. Collection of X-ray Intensity Data

A green single crystal (approximately 0.15 x 0.15 x 0.20 mm) of the title compound **50** was collected which appeared to be suitable for a detailed structure determination. The diffraction data were measured at room temperature (22 °C)

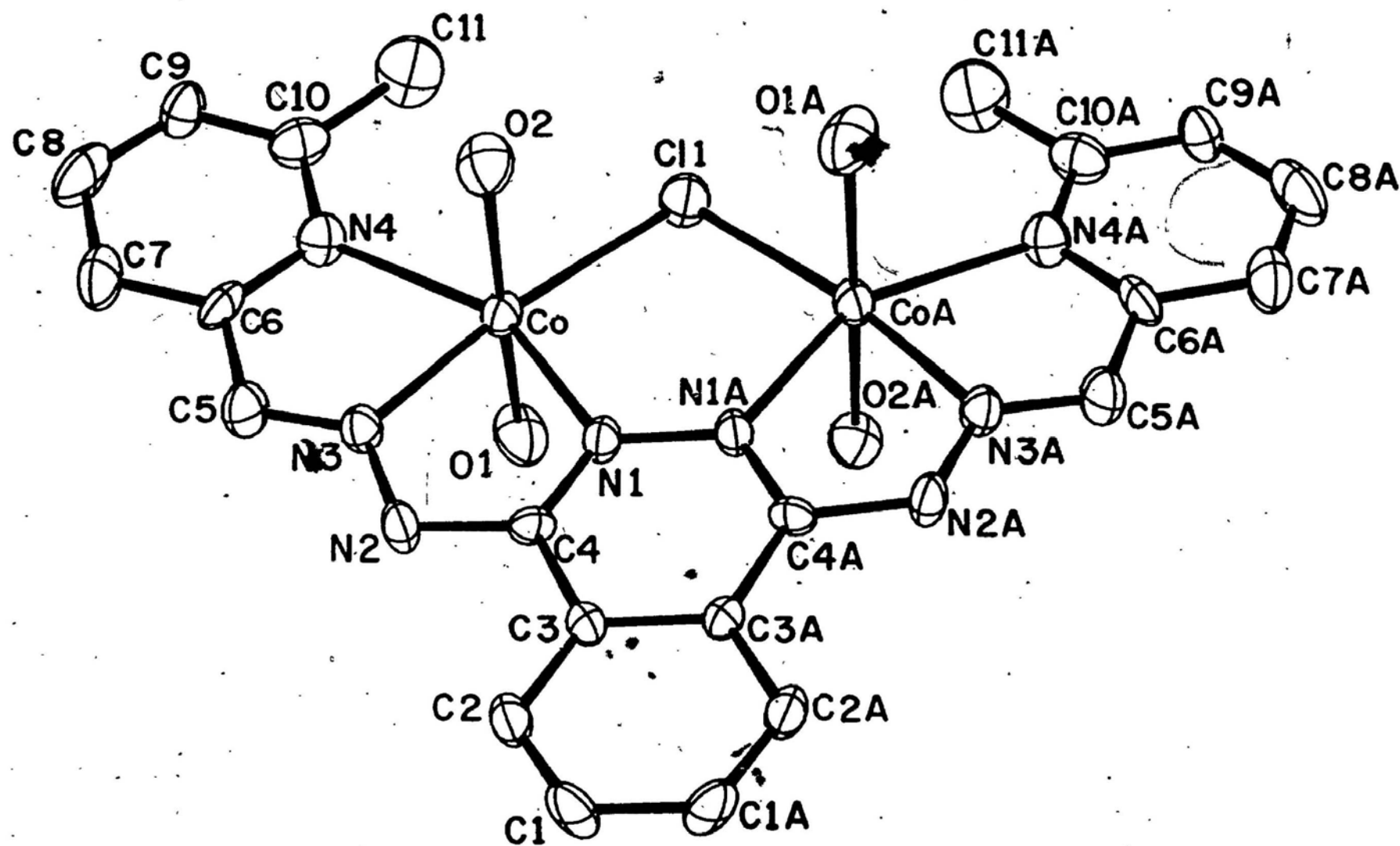


Fig. 8.1

Structural representation of $[\text{Co}_2(\text{PMP})\text{Cl}(\text{H}_2\text{O})_4]^{3+}$, **36**, with hydrogen atoms omitted (40% probability thermal ellipsoids).

Table 8.3 Interatomic Distances (\AA) and Angles (deg.) Relevant to the Cobalt Coordination Spheres in $[\text{Co}_2(\text{PMP})\text{Cl}(\text{H}_2\text{O})_4]\text{Cl}_3 \cdot 4.0\text{H}_2\text{O}(\mathbf{36})$.

Co-CoA	3.7121(16)	O(1)-Co-O(2)	174.37(20)
Co-Cl(1)	2.4131(16)	O(1)-Co-N(1)	95.20(20)
Co-O(1)	2.057(4)	O(1)-Co-N(3)	92.66(20)
Co-O(2)	2.090(4)	O(1)-Co-N(4)	90.44(20)
Co-N(1)	2.147(4)	O(2)-Co-N(1)	88.83(19)
Co-N(3)	2.082(5)	O(2)-Co-N(3)	92.24(19)
Co-N(4)	2.223(5)	O(2)-Co-N(4)	88.10(19)
Cl(1)-Co-O(1)	88.21(14)	N(1)-Co-N(3)	73.91(18)
Cl(1)-Co-O(2)	87.41(13)	N(1)-Co-N(4)	149.05(18)
Cl(1)-Co-N(1)	96.71(13)	N(3)-Co-N(4)	75.45(19)
Cl(1)-Co-N(3)	170.62(14)	Co-Cl(1)-CoA	100.56(8)
Cl(1)-Co-N(4)	113.90(14)		

Table 8.4 Interatomic Distances (\AA) and Angles (degree) relevant to the ligand in $[\text{Co}_2(\text{PMP})\text{Cl}(\text{H}_2\text{O})_4]\text{Cl}_3 \cdot 4.0\text{H}_2\text{O}(\mathbf{36})$.

N(1)-N(1)A	1.374(9)	C(2)-C(3)	1.398(8)
N(1)-C(4)	1.305(7)	C(3)-C(3)A	1.394(11)
N(2)-N(3)	1.354(7)	C(3)-C(4)	1.445(8)
N(2)-C(4)	1.386(8)	C(5)-C(6)	1.461(9)
N(3)-C(5)	1.261(8)	C(6)-C(7)	1.389(8)
N(4)-C(6)	1.343(9)	C(7)-C(8)	1.409(11)
N(4)-C(10)	1.336(8)	C(8)-C(9)	1.362(12)
C(1)-C(1)A	1.361(13)	C(9)-C(10)	1.363(10)
C(1)-C(2)	1.352(9)	C(10)-C(11)	1.498(11)
N(1)A-N(1)-C(4)	119.9(5)	N(1)-C(4)-C(3)	123.8(5)
N(3)-N(2)-C(4)	115.7(5)	N(2)-C(4)-C(3)	120.5(5)
Co-N(3)-N(2)	117.3(3)	N(3)-C(5)-C(6)	116.0(6)
Co-N(3)-C(5)	119.9(5)	N(4)-C(6)-C(5)	117.6(5)
N(2)-N(3)-C(5)	122.8(5)	N(4)-C(6)-C(7)	122.5(6)
C(6)-N(4)-C(10)	118.2(5)	C(5)-C(6)-C(7)	119.9(6)
C(1)A-C(1)-C(2)	121.0(5)	C(6)-C(7)-C(8)	118.3(7)
C(1)-C(2)-C(3)	119.9(5)	C(7)-C(8)-C(9)	117.6(6)
C(2)-C(3)-C(3)A	119.1(5)	C(8)-C(9)-C(10)	121.1(7)
C(2)-C(3)-C(4)	124.6(5)	N(4)-C(10)-C(9)	122.3(7)
C(3)A-C(3)-C(4)	116.3(5)	N(4)-C(10)-C(11)	116.7(6)
N(1)-C(4)-N(2)	115.6(5)	C(9)-C(10)-C(11)	121.0(6)

by employing a Nonius CAD4 automatic four-circle diffractometer with graphite monochromated $\text{CuK}\alpha$ radiation [$\lambda(\text{CuK}\alpha) = 1.54056 \text{ \AA}$]. The $\theta - 2\theta$ scan technique was used and individual reflection profiles were analysed⁹⁷ to $2\theta_{\text{max}} = 110.0^\circ$. The measured reflections totalled 2288, of which 2124 were independent and, 1992 reflections with $I_{\text{net}} > 2.5\sigma(I_{\text{net}})$ were considered reliable and used in the analysis. The measured intensities were corrected for Lorentz and polarization effects, but the absorption corrections were not made. No extinction correction was needed. The cell parameters were obtained by the least-squares fitting of the setting angles of 45 well centred reflections with 2θ in the range $90.0 - 96.0^\circ$. The pertinent crystal data are outlined in Table 8.1.

B. Solution and Refinement of the structure

The structure of **50** was determined by direct methods using the program MULTAN⁹⁸. The atomic positions were refined with full-matrix least-squares techniques by minimizing the function $\sum w(\Delta F)^2$. All the non-hydrogen atoms were refined with anisotropic temperature factors, whereas all the hydrogen atoms were refined isotropically. The H-atoms of the methyl groups were located from the usual Fourier difference syntheses, but attempts to determine the H-atoms of the water molecules were not successful. The final values of the discrepancy indices were $R_1 = 0.049$ and $R_w = 0.054$ for the significant reflections while $R = 0.054$ and $R_w = 0.070$ for all data with unit weights based on counting statistics. The final atomic positional parameters and equivalent isotropic temperature factors are given in Table 8.5. All the calculations were performed with the NRCVAX system of programs⁹⁹. The atomic scattering factors were taken from the usual source¹⁰⁰. The anisotropic thermal parameters for the

Table 8.5 Atomic parameters X, Y, Z, and BISO for 50. E.S.Ds. refer to the last digit printed*.

ATOM	X	Y	Z	BISO†
NI	0.37939(9)	0.25555(10)	0.00972(12)	2.52(7)
CL 1	0.22983(17)	0.22983	0	2.96(12)
CL 2	0.43231(15)	0.77582(15)	0.00470(22)	3.83(12)
CL 0	0.1987 (3)	0.2148 (3)	0.3606 (5)	6.8 (3)
O 1	0.3690 (4)	0.2500 (5)	0.2121 (5)	4.3 (4)
O 2	0.3812 (4)	0.2536 (4)	-0.1947 (5)	3.3 (3)
O 3	0.5044 (5)	0.7652 (5)	0.2885 (7)	5.7 (4)
N 1	0.4418 (4)	0.3962 (4)	0.0042 (6)	2.4 (4)
N 2	0.5696 (5)	0.3870 (5)	0.0225 (8)	2.9 (5)
N 3	0.5133 (5)	0.2971 (5)	0.0209 (6)	2.4 (4)
N 4	0.3814 (5)	0.1284 (5)	0.0086 (7)	3.1 (5)
C 1	0.7228 (6)	0.6761 (7)	0.0026 (10)	3.4 (5)
C 2	0.6780 (5)	0.5839 (6)	0.0096 (8)	2.6 (5)
C 3	0.5835 (6)	0.5371 (6)	0.0055 (7)	2.3 (4)
C 4	0.5293 (6)	0.4399 (6)	0.0110 (7)	2.3 (4)
C 5	0.5388 (7)	0.2406 (6)	0.0185 (9)	3.1 (5)
C 6	0.4670 (6)	0.1449 (5)	0.0146 (7)	2.8 (5)
C 7	0.4883 (8)	0.0770 (7)	0.0086 (10)	3.8 (6)
C 8	0.4195 (9)	-0.0111 (7)	0.0019 (10)	4.3 (7)
C 9	0.3325 (9)	-0.0282 (7)	-0.0060 (10)	4.4 (7)
C10	0.3158 (7)	0.0427 (6)	-0.0004 (9)	3.7 (6)
C11	0.2213 (9)	0.0255 (10)	-0.0106 (16)	5.4 (8)
O 4	0.9665 (24)	0.96648	1	14.3 (12)
O 5	0.940 (3)	0.991 (3)	0.900 (4)	19.4 (13)
H 1	0.766 (7)	0.693 (7)	0.025 (10)	4.1
H 2	0.717 (6)	0.556 (6)	0.019 (7)	3.3
H 5	0.611 (7)	0.258 (7)	0.023 (8)	4.0
H 7	0.554 (7)	0.095 (7)	0.010 (9)	4.9
H 8	0.426 (8)	-0.055 (8)	-0.019 (11)	5.6
H 9	0.273 (7)	-0.089 (7)	-0.019 (9)	4.9
H N2	0.613 (7)	0.406 (7)	0.022 (10)	3.8
H11A	0.196 (9)	-0.038 (10)	0.011 (12)	8.0 (37)
H11B	0.207 (8)	0.050 (7)	0.065 (10)	6.1 (28)
H11C	0.214 (8)	0.037 (8)	-0.088 (12)	7.7 (38)

* E.S.Ds are the equivalent isotropic Debye-Waller temperature factors.

† BISO is the mean of the principal axes of the thermal ellipsoid.

non-hydrogen atoms and the related structural data are given in the Appendix and/or the Supplementary Material.

C. Description of the Structure of **50**

The crystal structure **50** is composed of a binuclear $[\text{Ni}_2(\text{PMP})\text{Cl}(\text{H}_2\text{O})_4]^{3+}$ cation, three chloride anions and 4.5 lattice water molecules. A structural representation of this binuclear cation, together with the atomic labelling system used, is shown in Fig. 8.2. Selected bond lengths and bond angles are listed in Table 8.6 and 8.7. The structure **50** is essentially the same as its cobalt counterpart **36**, and there appear no significant differences between their bond parameters (length and angle). The binuclear cation is almost planar, and lies on a two-fold axis which passes through the central-point of the phthalazine group and the chlorine bridge. The equatorial coordination of the two Ni(II) centers is made up of a chlorine group and six nitrogen donors of a PMP ligand, in which the Ni(II) ions are doubly bridged by this chlorine and the diazine group, with two water molecules completing a distorted octahedral arrangement about each metal center. The Ni-Ni distance is 3.678 Å and the Ni-Cl-Ni bridge angle 101.6°. Again the major in-plane deformations occur as a result of the juxtaposition of the two five-membered chelate rings. By contrast with the complexes **31** and **32**, much larger metal-metal separations are found in **36** and **50**, and they are attributed to the presence of the 6-methyl substituent on the pyridine rings of the ligand PMP, in which the bulky methyl groups are in a position to force the two metal centers apart by virtue of their proximity to the binuclear center themselves.

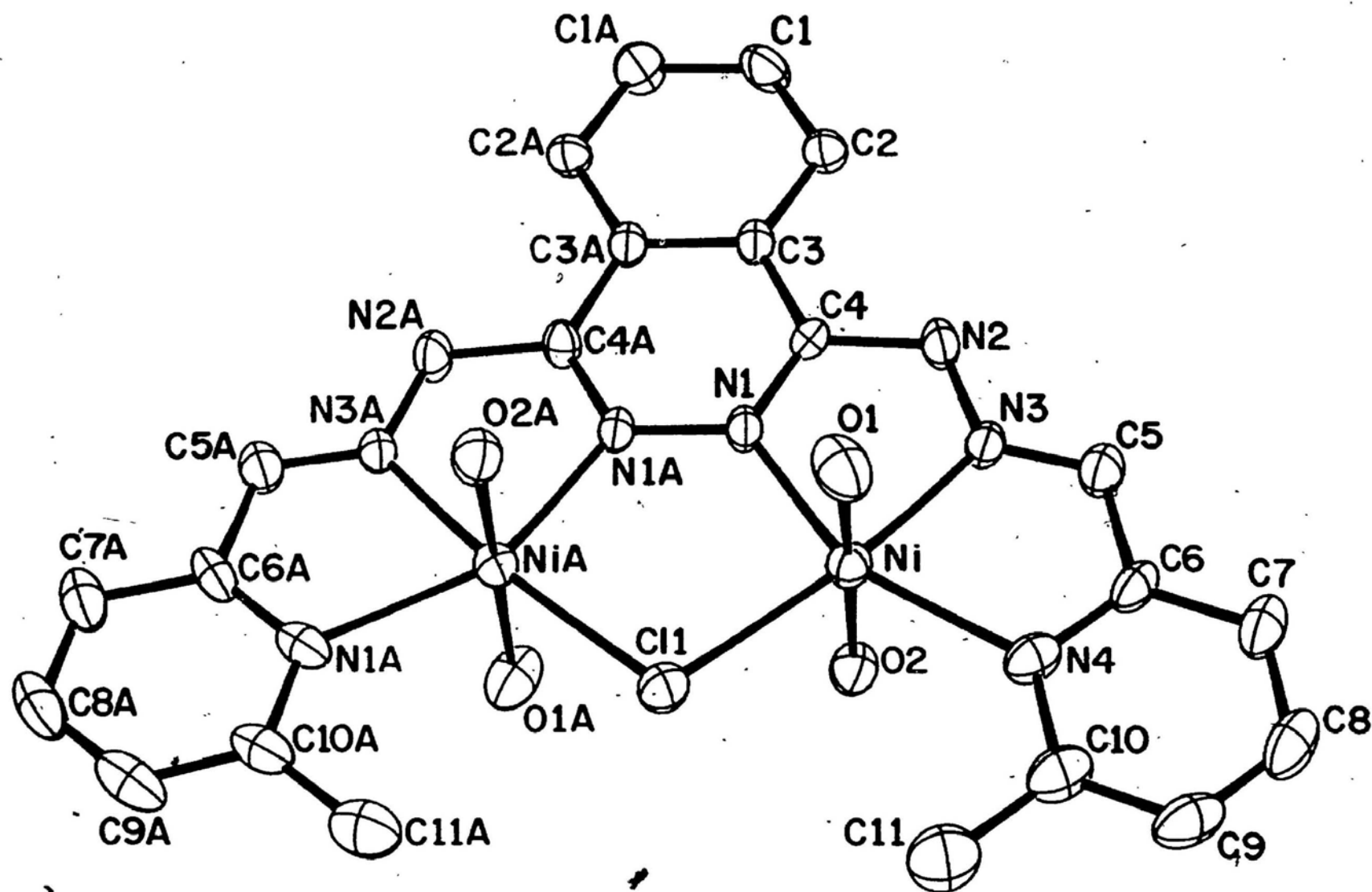


Fig. 8.2

Structural representation of $[\text{Ni}_2(\text{PMP})\text{Cl}(\text{H}_2\text{O})_4]^{3+}$, **50**, with hydrogen atoms omitted (40% probability thermal ellipsoids).

Table 8.6 Interatomic Distances (\AA) and Angles (deg.) Relevant to the Nickel Coordination Spheres in $[\text{Ni}_2(\text{PMP})\text{Cl}(\text{H}_2\text{O})_4]\text{Cl}_3 \cdot 4.5\text{H}_2\text{O}(\mathbf{50})$.

Ni-NiA	3.6784(27)	O(1)-Ni-O(2)	176.15(24)
Ni-Cl(1)	2.3738(23)	O(1)-Ni-N(1)	93.0(3)
Ni-O(1)	2.072(5)	O(1)-Ni-N(3)	90.94(25)
Ni-O(2)	2.088(5)	O(1)-Ni-N(4)	90.2(3)
Ni-N(1)	2.091(7)	O(2)-Ni-N(1)	89.35(23)
Ni-N(3)	2.036(7)	O(2)-Ni-N(3)	92.21(24)
Ni-N(4)	2.194(8)	O(2)-Ni-N(4)	88.36(23)
Cl(1)-Ni-O(1)	88.45(16)	N(1)-Ni-N(3)	76.2(3)
Cl(1)-Ni-O(2)	88.76(15)	N(1)-Ni-N(4)	152.9(3)
Cl(1)-Ni-N(1)	95.45(19)	N(3)-Ni-N(4)	76.9(3)
Cl(1)-Ni-N(3)	171.57(21)	Ni-Cl(1)-Ni	101.57(12)
Cl(1)-Ni-N(4)	111.48(22)		

Table 8.7 Interatomic Distances (Å) and Angles (deg.) relevant to the Ligand in $[\text{Ni}_2(\text{PMP})\text{Cl}(\text{H}_2\text{O})_4]\text{Cl}_3 \cdot 4.5\text{H}_2\text{O}(\mathbf{50})$.

N(1)-N(1)A	1.354(13)	C(2)-C(3)	1.402(12)
N(1)-C(4)	1.300(11)	C(3)-C(3)A	1.382(16)
N(2)-N(3)	1.347(10)	C(3)-C(4)	1.445(12)
N(2)-C(4)	1.391(11)	C(5)-C(6)	1.478(12)
N(3)-C(5)	1.245(11)	C(6)-C(7)	1.383(12)
N(4)-C(6)	1.349(12)	C(7)-C(8)	1.375(10)
N(4)-C(10)	1.333(12)	C(8)-C(9)	1.369(18)
C(1)-C(1)A	1.386(20)	C(9)-C(10)	1.381(15)
C(1)-C(2)	1.370(13)	C(10)-C(11)	1.495(17)
Ni-N(1)-N(1)A	123.8(5)	N(1)-C(4)-N(2)	115.7(7)
Ni-N(1)-C(4)	116.1(5)	N(1)-C(4)-C(3)	123.6(8)
N(1)A-N(1)-C(4)	120.2(7)	N(2)-C(4)-C(3)	120.7(7)
N(3)-N(2)-C(4)	116.0(7)	N(3)-C(5)-C(6)	116.2(9)
Ni-N(3)-N(2)	115.9(5)	N(4)-C(6)-C(5)	116.6(7)
Ni-N(3)-C(5)	119.9(6)	N(4)-C(6)-C(7)	122.6(8)
N(2)-N(3)-C(5)	124.0(8)	C(5)-C(6)-C(7)	120.7(9)
C(6)-N(4)-C(10)	117.6(8)	C(6)-C(7)-C(8)	118.8(10)
C(1)A-C(1)-C(2)	121.0(8)	C(7)-C(8)-C(9)	118.8(9)
C(1)-C(2)-C(3)	118.5(8)	C(8)-C(9)-C(10)	119.4(10)
C(2)-C(3)-C(3)A	120.4(8)	N(4)-C(10)-C(9)	122.7(10)
C(2)-C(3)-C(4)	123.4(8)	N(4)-C(10)-C(11)	117.1(10)
C(3)A-C(3)-C(4)	116.2(8)	C(9)-C(10)-C(11)	120.2(10)

CHAPTER 9

SPECTROSCOPY AND STRUCTURES OF THE BINUCLEAR
PMP, PPA AND PMI COMPLEXES

9. 1. The Infrared Spectra Of The Binuclear Complexes

A. The Characteristic Absorption of the Pyridine Ring

The infrared spectra of the ligands PMP and PPA exhibit bands at 993 and 990 cm^{-1} respectively, which can be associated with pyridine ring breathing modes of vibration. According to a previous report⁶³, it is evident that the pyridine ring has coordinated to the metal center if this characteristic absorption shifts to higher energy (above 1000 cm^{-1}). The absorptions in the range 1002 - 1020 cm^{-1} (Tables 9.1 and 9.2) for the complexes **36** - **44** and **50** - **58**, typically shifted to higher energy by 10 - 30 cm^{-1} , indicate the involvement of the pyridine ring in coordination and suggest that PMP and PPA behave as hexadentate ligands in all these compounds. The strong absorption at 1050 cm^{-1} for **59**, associated with ionic BF_4 groups, masks this characteristic band of the pyridine residue. The coordination of the pyridine ring has been verified by an X-ray analysis of the compounds **36** and **50**, in which both pyridine nitrogen donors of the ligand PMP coordinate to two metals of the complexes to complete the equatorial coordination of the binuclear center (See Fig. 8.1 and 8.2). It is reasonable to assume that this situation prevails for all the 2:1 species. For the 1:1 derivatives

Table 9.1 Infrared spectral data for the binuclear Co(II) complexes.

No.	Complex	Assignment (cm ⁻¹) ^a		
		H ₂ O/ROH	Pyridine	Ligand/Anion
36	[Co ₂ (PMP)Cl(H ₂ O) ₄]Cl ₃ ·4H ₂ O	3600,3340(vs,br) (H ₂ O)	1010 (sh)	300(Co-O)(sh) 242(Co-Cl) _t
37	[Co ₂ (PMP)Br(H ₂ O) ₄]Br ₃ ·3H ₂ O	3560,3300(vs,br) (H ₂ O)	1010 (sh)	304(Co-O)(sh) 223(Co-Br) _t
38	[Co ₂ (PMP) ₂](NO ₃) ₄ ·4EtOH	3510(w,br) (EtOH)	1006 (sh)	1755(rw) (NO ₃)
39	[Co ₂ (PMP) ₂](ClO ₄) ₄ ·EtOH	3550(w) (EtOH)	1004 -	1090,930,625(s,sh) (ClO ₄)
40	[Co ₂ (PMP-H) ₂](BF ₄) ₂ ·4H ₂ O	3540(ms) (H ₂ O)	1010 -	1070(s,br) (BF ₄)
41	[Co ₂ (PPA)Cl(MeOH)Cl ₃]	3410(slw) (MeOH)	1020 (sh)	205(Co-Cl) _t 248(Co-Cl) _b
42	[Co ₂ (PPA-H)Br(H ₂ O) ₂ Br ₂]0.5EtOH	3540,3400(ms) (H ₂ O,EtOH)	1015 (sh)	275,230(Co-Br) _t 214(Co-Br) _b
43	[Co ₂ (PPA) ₂](ClO ₄) ₄ ·EtOH	3500(w) (EtOH)	1010 -	1080,932,622(s,sh) (ClO ₄)
44	[Co ₂ (PPA-H) ₂](BF ₄) ₂ ·EtOH·3H ₂ O	3540(ms) (H ₂ O,EtOH)	1010 -	1060(s,br) (BF ₄)
45	[Co ₂ (PMI)Cl(H ₂ O) ₄]Cl ₃ ·1.5H ₂ O	3600,3410(vs,br) (H ₂ O)	- -	322(Co-O)(sh) 230(Co-Cl) _b
46	[Co ₂ (PMI)Br(H ₂ O) ₄]Br ₃ ·0.5H ₂ O	3590,3420(vs,br) (H ₂ O)	- -	320(Co-O)(sh) 204(Co-Br) _b
47	[Co ₂ (PMI)(OH ₂)(NO ₃) ₄]EtOH·0.5H ₂ O	3400(ms) (OH ₂ ,EtOH)	- -	1755,1736(ν ₁ + ν ₄) (Co-ONO ₂)
48	[Co ₂ (PMI) ₂](ClO ₄) ₄ ·EtOH	3500(w) (EtOH)	- -	1095,930,620(s,sh) (ClO ₄)
49	[Co ₂ (PMI) ₂](BF ₄) ₄ ·2EtOH	3520(w) (EtOH)	- -	1050(s,br) (BF ₄)

^a: s means strong, vs very strong, ms medium strong, w weak, slw slightly weak, rw relatively weak, br broad, sh sharp, t terminal, and b bridging, etc.

Table 9.2 Infrared spectral data for the binuclear Ni(II) complexes.

No.	Complex	Assignment (cm ⁻¹) ^a		
		H ₂ O/ROH	Pyridine	Ligand/Anion
50	[Ni ₂ (PMP)Cl(H ₂ O) ₄]Cl ₃ ·4.5H ₂ O	3600,3330(vs,br) (H ₂ O)	1010 (sh)	314(Ni-O)(sh) 255(Ni-Cl) _b
51	[Ni ₂ (PMP)Br(H ₂ O) ₄]Br ₃ ·0.5MeOH·H ₂ O	3550,3340(vs,br) (H ₂ O)	1007 (sh)	315(Ni-O)(sh) 212(Ni-Br) _b
52	[Ni ₂ (PMP)(OH ₂)(H ₂ O) ₄](NO ₃) ₄ ·MeOH	3560,3320(vs,br) (H ₂ O, MeOH)	1002 (sh)	1750(rw) (NO ₃)
53	[Ni ₂ (PMP) ₂](ClO ₄) ₄ ·4H ₂ O	3500(ms) (H ₂ O)	1010 -	1100,930,620(s,sh) (ClO ₄)
54	[Ni ₂ (PMP)(PMP-H)](BF ₄) ₃ ·5.5H ₂ O	3540(ms) (H ₂ O)	1004 -	1060(s,br) (BF ₄)
55	[Ni ₂ (PPA)Cl(H ₂ O) ₄]Cl ₃ ·2H ₂ O	3460(vs,br) (H ₂ O)	1008 (sh)	300(Ni-O)(sh) 242(Ni-Cl) _b
56	[Ni ₂ (PPA-H)Br(EtOH)(H ₂ O)Br ₂]EtOH·0.5H ₂ O	3410(ms) (H ₂ O, EtOH)	1020 (sh)	258(Ni-Br) _t 210(Ni-Br) _b
57	[Ni ₂ (PPA) ₂](NO ₃) ₄ ·4H ₂ O	3540,3380(ms) (H ₂ O)	1018 (sh)	1740(rw) (NO ₃)
58	[Ni ₂ (PPA) ₂](ClO ₄) ₄ ·6H ₂ O	3600,3420(ms) (H ₂ O)	1010 -	1090,935,622(s,sh) (ClO ₄)
59	[Ni ₂ (PPA) ₂](BF ₄) ₄ ·4H ₂ O	3590,3460(ms) (H ₂ O)	- -	1050(s,br) (BF ₄)
60	[Ni ₂ (PMI)Cl(H ₂ O) ₄]Cl ₃ ·2H ₂ O	3540,3400(vs,br) (H ₂ O)	- -	344(Ni-O)(sh) 235(Ni-Cl) _b
61	[Ni ₂ (PMI)Br(H ₂ O) ₄]Br ₃ ·3.5H ₂ O	3580,3420(vs,br) (H ₂ O)	- -	346(Ni-O)(sh) 207(Ni-Br) _b
62	[Ni ₂ (PMI)(OH ₂)(NO ₃) ₄]EtOH·1.5H ₂ O	3420(slw) (H ₂ O, EtOH)	- -	1750,1730(ν ₁ + ν ₄) (Ni-ONO ₂)
63	[Ni ₂ (PMI) ₂](ClO ₄) ₄ ·4H ₂ O	3500(ms) (H ₂ O)	- -	1100,928,620(s,sh) (ClO ₄)
64	[Ni ₂ (PMI) ₂](BF ₄) ₄ ·6H ₂ O	3600,3500(s) (H ₂ O)	- -	1060(s,br) (BF ₄)

a: s means strong, vs very strong, ms medium strong, sh sharp, br broad, slw slightly weak, t terminal, and b bridging, etc.

the pyridine-nitrogen coordination still appears to exist but in a rather different structural arrangement, as will be discussed later.

B. The Absorptions of Water/Solvent molecules

All complexes prepared exhibit a broad multiple absorption in the high energy region (in the range $3300 - 3600 \text{ cm}^{-1}$) of their infrared spectra. By comparison with the spectra of the ligands, this broad absorption is assigned to the coordinated and/or lattice water/alcoholic solvent molecules, although it is difficult to make specific assignments in this area. The very strong broad absorptions in this range displayed by most of the binuclear halide complexes and a nickel nitrate compound of PMP (52) indicate the presence of the coordinated water and/or alcoholic molecules, as can be supported by a sharp strong absorption in the low energy region ($300 - 346 \text{ cm}^{-1}$) of their infrared spectra, which is associated with a Co-O or Ni-O stretch (See Tables 9.1 and 9.2). The slightly weak bands around $3400 - 3420 \text{ cm}^{-1}$ in the spectra of the PMI nitrate complexes, 47 and 62, are assigned to the O-H stretch of a bridging water.

C. The IR Spectra of the Binuclear Halide Complexes

A very rich infrared absorption is observed for all the binuclear halide complexes in the low energy region ($200 - 350 \text{ cm}^{-1}$). The characteristic bands between $230 - 255 \text{ cm}^{-1}$ of the spectra for all the chloride complexes are associated with the M-Cl vibration of a bridging chlorine. The spectrum of 41 differs somewhat from the other chloride complexes, showing no bands associated with water and the appearance of a strong absorption at 295 cm^{-1} , assigned to a Co-Cl stretch of a terminal chlorine, which is absent in the other compounds. The

characteristic absorption in the range $204 - 223 \text{ cm}^{-1}$ is observed in all the spectra of the bromide compounds, which is assigned to the M-Br stretch of a bridging bromine, whereas the strong band between $230 - 275 \text{ cm}^{-1}$ shown by **42** and **56** is associated with a M-Br stretch of a terminal bromine, which is also absent in the other compounds (Tables 9.1 and 9.2). The infrared spectra of PMP complexes **36**, **37**, **50** and **51**, PPA complexes **42** and **56**, and PMI complexes **45**, **46**, **60** and **61** are almost identical respectively, with respect to band positions and relative intensities, indicating very similar structures between them respectively. All the complexes of these three groups, together with PPA chloride compounds **41** and **55**, are suggested having the same basic structural unit as the PMP chloride compounds **36** and **50** (whose structures have been determined by the X-ray crystallography), i.e., the two pseudo-octahedral metal centers are doubly-bridged, fixed in the molecular plane by a single hexadentate ligand as well as a halogen donor, and axially coordinated by halogen atoms and/or water/solvent molecules, as will be also supported by the electronic spectra and magnetic data.

D. The IR Spectra of the binuclear perchlorate complexes

All the cobalt perchlorate complexes exhibit a relatively weak absorption around 3500 cm^{-1} in the high energy region of their IR spectra (Table 9.1), which is assigned to the lattice ethanol molecule of these compounds. This weak absorption is also consistent with their elemental analyses: a single ethanol molecule per complex molecule. Their nickel counterparts, on the other hand, reveal a relatively strong and broad high energy absorption between $3420 - 3600 \text{ cm}^{-1}$ in their IR spectra (Table 9.2), indicating the presence of water molecules. However, by contrast with the very strong and broad high energy bands in the

spectra of 50 - 52, these water molecules of the ClO_4 complexes are only considered as the water of crystallization; in other words, they do not exist in the coordination sphere of the metal center. All the perchlorate compounds show a rather broad absorption in the range $1080 - 1100 \text{ cm}^{-1}$ (ν_3), a weak band around 930 cm^{-1} (ν_1) and a sharp absorption between $620 - 625 \text{ cm}^{-1}$ (ν_4)¹⁰¹, definitely indicating the presence of tetrahedral ionic perchlorate. Since both the perchlorate groups and water/ethanol molecules do not behave as the coordinating ligands in these binuclear 1:1 species, all the coordination sites of the two metal centers must be completely occupied by the nitrogen atom donors from the two ligands. This is of significance concerning the proposed binuclear structure of the 1:1 derivatives, as will be discussed later.

E. The IR spectra of the Tetrafluoroborate Complexes

The tetrafluoroborate anion, with the same point group symmetry as the perchlorate ion, has the same fundamental vibrations as the perchlorate. Therefore the IR spectra of the tetrafluoroborate complexes are supposed to be very similar to those of the perchlorate counterparts. Indeed, the IR spectra of the BF_4 compounds exhibit a broad and intense band between $1050 - 1070 \text{ cm}^{-1}$, which is assigned to the ν_3 vibration of a ionic tetrafluoroborate¹⁰², signifying that tetrafluoroborate group remains ionic in these compounds. Relatively weak absorptions in the range $3460 - 3600 \text{ cm}^{-1}$ are observed for all these BF_4 compounds, and again they are assigned to the lattice water and/or alcoholic solvent molecules (Tables 9.1 and 9.2). The spectral similarity between the BF_4 and ClO_4 complexes suggests their molecular similarity and that the same 1:1 structural unit is present in these derivatives.

F. The IR Spectra of the Nitrate Complexes

The nitrate complexes seem to be somewhat varied. Five complexes may fall into two groups: on the one hand, they are divisible into the binuclear 2:1 species (**47**, **52** and **62**) and the 1:1 derivatives (**38** and **57**) according to their elemental analyses, on the other hand, they are classifiable under two headings, complexes with ionic nitrate group (**38**, **52** and **57**) or those with coordinated nitrate (**47** and **62**) in the light of their infrared spectra. Usually, the $\nu_1 + \nu_4$ combination band between 1700 - 1800 cm^{-1} in the IR spectra of the nitrate complexes reveals some structural information¹⁰³. The presence of only one nitrate combination band in the range 1740 - 1755 cm^{-1} for **38**, **52** and **57** is assigned to the vibration of an ionic nitrate group, whereas two absorptions at/around 1730 and 1750 cm^{-1} in the spectra of **47** and **62** can be associated with monodentate nitrate (Tables 9.1 and 9.2). The absence of a high energy nitrate combination band in the 2:1 nitrate compounds, indicative of the presence of a nitrate bridge, suggests that some group, rather than the nitrate, serves as the second bridge besides the diazine group of the ligand. This group is proposed to be a water molecule due to the fact that a moderate and clear absorption between 3320 - 3420 cm^{-1} shows up in the IR spectra of these complexes, which is assigned to O-H stretch of bridging water. The three binuclear 2:1 nitrate compounds are proposed to possess the similar structural unit to those of the halide compounds (See Chapter 11). As for the binuclear 1:1 nitrate complexes, they are assumed to have the same basic structure as the perchlorate compounds. The feature that the nitrate compounds possess both the binuclear 2:1 and 1:1 structural modes is also in agreement with the fact that the nitrate group is a ligand lying between the strong coordinating donor (e.g., Cl and Br) and the poor donor (e.g., ClO_4 and

BF₄).

9. 2. The Electronic Spectra Of The Binuclear Complexes

The solution electronic spectra of all the complexes prepared are recorded and displayed in Tables 9.3 and 9.4. All the electronic spectra are characterized by the appearance of absorptions below 16700 cm⁻¹, which can be assigned to d-d transition of the Co(II) and Ni(II) ions, and very intense ($\epsilon = 9800 - 46000$ l mol⁻¹ cm⁻¹) visible absorptions in the range 19000 - 23000 cm⁻¹, which are obviously charge transfer in origin. According to these electronic spectra, together with the results from the IR spectra, two important conclusions on the stereochemistry of the metal center and the coordination geometry of the 1:1 species can be drawn.

A. The Stereochemistry of the Metal Center

The Co(II) complexes exhibit near infrared bands between 6290 - 7400 cm⁻¹ ($\epsilon = 1 - 66$ l mol⁻¹ cm⁻¹), which are assigned to the $\nu_1({}^4T_{2g} \leftarrow {}^4T_{1g})$ transition of the octahedral Co(II) metal centers (See Chapter 3). No bands can be associated with the ν_2 transition since the transition to ${}^4A_{2g}$ is, as usual, too weak to be observed. However, a fairly intense ($\epsilon = 2000 - 8000$ l mol⁻¹ cm⁻¹) shoulder in the range 15400 - 16100 cm⁻¹ for these Co(II) compounds could perhaps be assigned to the ν_3 transition in the pseudo-octahedral Co(II) center, although its high intensity is not typical of such bands. This may have arisen through "intensity stealing", in which the crystal field states generally increase in intensity as they move into the blue, where they can couple with higher energy wavefunc-

Table 9.3 Electronic spectral data for the binuclear Co(II) complexes†.

No.	Complex	Assignment O_h (cm^{-1})/(ϵ l mol ⁻¹ cm ⁻¹)		
		ν_1	ν_3	MLCT
36	$[\text{Co}_2(\text{PMP})\text{Cl}(\text{H}_2\text{O})_4]\text{Cl}_3 \cdot 4\text{H}_2\text{O}$	6900 (49.4)	15400 (5400)	19000 (13700)
37	$[\text{Co}_2(\text{PMP})\text{Br}(\text{H}_2\text{O})_4]\text{Br}_3 \cdot 3\text{H}_2\text{O}$	6290 (43.7)	15400 (2500)	19000 (13800)
38	$[\text{Co}_2(\text{PMP})_2](\text{NO}_3)_4 \cdot 4\text{EtOH}$	7100 (4.9)	16000 (6800)	20400 (32800)
39	$[\text{Co}_2(\text{PMP})_2](\text{ClO}_4)_4 \cdot \text{EtOH}$		15400 (4100)	20000 (24800)
40	$[\text{Co}_2(\text{PMP-H})_2](\text{BF}_4)_2 \cdot 4\text{H}_2\text{O}$	7100 (1.3)		19000 (19000)
41	$[\text{Co}_2(\text{PPA})\text{Cl}(\text{MeOH})\text{Cl}_3]$	6780 (38.9)	15600 (3800)	20000 (9800)
42	$[\text{Co}_2(\text{PPA-H})\text{Br}(\text{H}_2\text{O})_2\text{Br}_2] \cdot 0.5\text{EtOH}$	6350 (35.3)	16100 (5400)	19600 (10500)
43	$[\text{Co}_2(\text{PPA})_2](\text{ClO}_4)_4 \cdot \text{EtOH}$	7400 (4.2)	15400 (3200)	20400 (26400)
44	$[\text{Co}_2(\text{PPA-H})_2](\text{BF}_4)_2 \cdot \text{EtOH} \cdot 3\text{H}_2\text{O}$	7400 (3.1)	15400 (3000)	20200 (29800)
45	$[\text{Co}_2(\text{PMI})\text{Cl}(\text{H}_2\text{O})_4]\text{Cl}_3 \cdot 1.5\text{H}_2\text{O}$	6900 (66.0)	15400 (8100)	21300 (9550)
46	$[\text{Co}_2(\text{PMI})\text{Br}(\text{H}_2\text{O})_4]\text{Br}_3 \cdot 0.5\text{H}_2\text{O}$	6580 (56.4)	15700 (7500)	20800 (9200)
47	$[\text{Co}_2(\text{PMI})(\text{OH}_2)(\text{NO}_3)_4]\text{EtOH} \cdot 0.5\text{H}_2\text{O}$	7400 (7.76)	15700 (6500)	21500 (9900)
48	$[\text{Co}_2(\text{PMI})_2](\text{ClO}_4)_4 \cdot \text{EtOH}$	7400 (22.4)	15400 (7900)	20800 (20360)
49	$[\text{Co}_2(\text{PMI})_2](\text{BF}_4)_4 \cdot 2\text{EtOH}$	7400 (29.7)	15750 (7200)	21700 (17790)

† The spectra recorded here are solution spectra in DMF.

Table 9.4 Electronic spectral data for the binuclear Ni(II) complexes[†].

No.	Complex	Assignment ν_1 ν_2 MLCT O_h (cm^{-1})/(ϵ ; $\text{lnol}^{-1}\text{cm}^{-1}$)		
		ν_1	ν_2	MLCT
50	$[\text{Ni}_2(\text{PMP})\text{Cl}(\text{H}_2\text{O})_4]\text{Cl}_3 \cdot 4.5\text{H}_2\text{O}$	9900 (36.0)	15400 (30.0)	19600 (13600)
51	$[\text{Ni}_2(\text{PMP})\text{Br}(\text{H}_2\text{O})_4]\text{Br}_3 \cdot 0.5\text{MeOH} \cdot 11\text{H}_2\text{O}$	9600 (41.0)	15400 (33.0)	19600 (22600)
52	$[\text{Ni}_2(\text{PMP})(\text{OH}_2)(\text{H}_2\text{O})_4](\text{NO}_3)_4 \cdot \text{MeOH}$	12500 (22.5)	15750 (3450)	20000 (21500)
53	$[\text{Ni}_2(\text{PMP})_2](\text{ClO}_4)_4 \cdot 4\text{H}_2\text{O}$	12800 (51.8)	15600 (384)	19600 (45600)
54	$[\text{Ni}_2(\text{PMP})(\text{PMP-H})](\text{BF}_4)_3 \cdot 5.5\text{H}_2\text{O}$	12700 (44.7)	-	20000 (35000)
55	$[\text{Ni}_2(\text{PPA})\text{Cl}(\text{H}_2\text{O})_4]\text{Cl}_3 \cdot 2\text{H}_2\text{O}$	11800 (34.4)	-	22700 (4860)
56	$[\text{Ni}_2(\text{PPA-H})\text{Br}(\text{EtOH})(\text{H}_2\text{O})\text{Br}_2]\text{EtOH} \cdot 0.5\text{H}_2\text{O}$	11400 [†] (41.6)	15400 (256)	20800 (10500)
57	$[\text{Ni}_2(\text{PPA})_2](\text{NO}_3)_4 \cdot 4\text{H}_2\text{O}$	12500 (51.5)	15400 (820)	20200 (33100)
58	$[\text{Ni}_2(\text{PPA})_2](\text{ClO}_4)_4 \cdot 6\text{H}_2\text{O}$	12500 (66.3)	15600 (9480)	20000 (40200)
59	$[\text{Ni}_2(\text{PPA})_2](\text{BF}_4)_4 \cdot 4\text{H}_2\text{O}$	12500 (63.0)	-	20000 (45500)
60	$[\text{Ni}_2(\text{PMI})\text{Cl}(\text{H}_2\text{O})_4]\text{Cl}_3 \cdot 2\text{H}_2\text{O}$	10900 [†] (26.2)	16700 (22.2)	21700 (14000)
61	$[\text{Ni}_2(\text{PMI})\text{Br}(\text{H}_2\text{O})_4]\text{Br}_3 \cdot 3.5\text{H}_2\text{O}$	10700 [†] (33.3)	16400 (41.6)	21500 (15100)
62	$[\text{Ni}_2(\text{PMI})(\text{OH}_2)(\text{NO}_3)_4]\text{EtOH} \cdot 1.5\text{H}_2\text{O}$	11800 (24.5)	15400 (3600)	20100 [†] (17000)
63	$[\text{Ni}_2(\text{PMI})_2](\text{ClO}_4)_4 \cdot 4\text{H}_2\text{O}$	11900 (45.0)	16700 (7000)	20800 (40100)
64	$[\text{Ni}_2(\text{PMI})_2](\text{BF}_4)_4 \cdot 6\text{H}_2\text{O}$	11900 (43.1)	16700 (8600)	20800 (33100)

[†] The spectra recorded in the Table are solution spectra in DMF.

* Solution spectra in methanol.

tions, usually charge transfer states. On the other hand, the ν_1 absorptions of the binuclear 1:1 derivatives show much lower intensities (See Table 9.3) than those of the binuclear halide complexes, especially in the two tetrafluoroborate compounds **40** and **44**. This may suggest that only a small amount of the octahedral Co(II) species exists in these 1:1 derivatives, whereas the rest of the cobalt ions are probably present in the Co(III) oxidation state with octahedral stereochemistry. Octahedral Co(III) species can generate two bands in their electronic spectra (See § 3.3), but, unfortunately these two bands cannot be observed in the spectra of the 1:1 derivatives as they both fall within the region of the charge transfer absorption and are masked by the very intense CT bands. However, the results from the magnetic data (See § 10.1) seem to support the presence of the Co(III) species in the 1:1 derivatives.

The Ni(II) compounds display two visible bands around 11000 cm^{-1} ($\epsilon = 22 - 66\text{ l mol}^{-1}\text{ cm}^{-1}$) and 16000 cm^{-1} ($\epsilon = 30 - 9500\text{ l mol}^{-1}\text{ cm}^{-1}$), which can be associated with the $\nu_1({}^3T_{2g} \leftarrow {}^3A_{2g})$ and $\nu_2({}^3T_{1g} \leftarrow {}^3A_{2g})$ transitions in a pseudo-octahedral Ni(II) center. Again the unusually high intensities of the ν_2 transition, which are shown by all the nickel nitrate complexes and the 1:1 derivatives, are still ascribed to the intensity stealing. No major splittings of these bands occur, which reflect low symmetry of the six-coordinate Ni(II) centers in these Ni(II) complexes, and so all these assignments are made on the basis of octahedral symmetry.

The binuclear 2:1 halide compounds exhibit the obvious difference in energy of their ν_1 transitions, reflecting the varying chromophores involved, in which the major structural difference between them would be the halogen bridge. Otherwise

they are assumed to be isostructural. The 1:1 compounds of each ligand exhibit the ν_1 transitions at essentially the same energy, implying that the same basic structural unit of the binuclear 1:1 species exists in these derivatives.

B. The Coordination Geometry of the 1:1 Species

According to Tables 9.3 and 9.4, the perchlorate and tetrafluoroborate complexes (the binuclear 1:1 mode) clearly differ from the halogen bridged compounds. Their ν_1 transitions occur in the same energy region but at much higher energy than those equivalent transitions for the halide compounds. This reflects a stronger ligand-field environment around each metal center of the 1:1 species, and is also consistent with the fact that more nitrogen donor groups are surrounding each center of this species by contrast with the 2:1 halide complexes. The very intense charge transfer (CT) absorptions exhibited by these two kinds of species also support this result: the intensities of the CT bands in the 1:1 derivatives are almost twice as intense as those of the 2:1 complexes, suggesting the involvement of more ligands per metal in the 1:1 compounds.

The intense CT absorption in the range $19000 - 23000 \text{ cm}^{-1}$ observed for all the complexes seems to be a characteristic feature associated with the ligands of this sort. As the ligands are unsaturated derivatives with empty and/or relatively low energy π anti-bonding orbitals, the electronic origin of these intense bands in this relatively low-energy region would reasonably be assumed to be "Metal to Ligand Charge Transfer (MLCT)" in nature. Whereas the internal $\pi^* \leftarrow \pi$ transitions of the ligands themselves are supposed to lie at higher energies than those of the MLCT.

It is also of interest to note the striking difference in the MLCT intensities between the 2:1 and 1:1 nitrate derivatives. The nitrate compounds **47**, **52** and **62**, three 2:1 species, are similar in the MLCT intensity to their halide counterparts, suggesting that they are the same sort of species. While those 1:1 nitrate complexes **38** and **57**, like the perchlorate analogues, have much more intense (more than twice) absorptions than those 2:1 complexes, indicating that they do belong to a different group. Besides, the low-energy ν_1 transitions of the 2:1 nitrate complexes occur at higher energy than those of the corresponding halide compounds, even close to those of the 1:1 species. This may be attributed to an oxygen bridge, a stronger ligand than halogen.

C. The Conclusion

All the studies of these IR and electronic spectra come to the major conclusions that (i) the binuclear 1:1 derivatives also contain two OCTAHEDRAL metal centers, (ii) both ligands in the 1:1 complexes can coordinate to the binuclear center in a HEXADENTATE fashion and, consequently, (iii) a proposed structure for this species is illustrated in Fig. 9.1, in which each ligand coordinates the two octahedral centers with the diazine and hydrazone nitrogen-atom donors forming the equatorial coordination and with the two pyridine-ring nitrogen donors occupying the axial coordinate sites which are arranged trans to one another. Molecular models reveal that this speculative structure is very stable apart from a slight strain. However, it must await structural confirmation from X-ray crystallography. Thus far all the collected crystals of these species have been unsuitable for X-ray analysis.

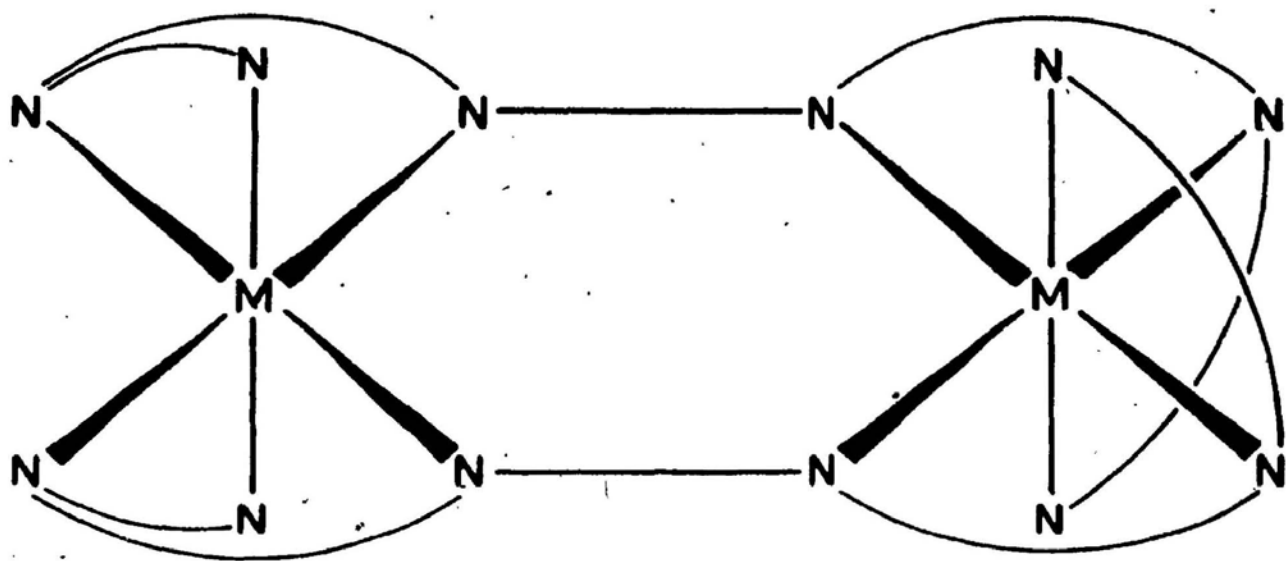


Fig. 9.1

Proposed structure for the binuclear cation $[M_2L_2]^{4+}$ in the binuclear 1:1 derivatives.

CHAPTER 10

MAGNETIC PROPERTIES OF THE BINUCLEAR PMP, PPA AND PMI COMPLEXES

For the binuclear structures the exchange coupling between the metal centers is usually investigated by magnetic susceptibility measurements. The comparison of the magnetic exchange of different compounds may give information about the magnitude of the exchange, the possible exchange mechanism and, the correlation between exchange and geometric parameters. The magnetic susceptibility data for the binuclear Co(II) and Ni(II) complexes prepared are listed in Tables 10.1 and 10.2, respectively. They will be discussed in some detail below.

10. 1. The Room-Temperature Magnetic Moment

The room-temperature magnetic moments (μ_{eff}) for all the binuclear complexes, which are given in Tables 10.1 and 10.2, are calculated from Eqn. (5-26), in which χ_m is the molar susceptibility per metal center corrected for diamagnetic components, and $N\alpha$ the TIP (See p.50). TIP can normally be estimated from the d-d absorptions ($10Dq$), but could not be calculated for the Co(II) compounds here, because only one (ν_1) transition was observed for these Co(II) complexes. Therefore, the estimated correction of 190×10^{-6} c.g.s.u. has been applied in calculating their magnetic moments (See § 5.5).

Table 19.1 Magnetic data for the binuclear Co(II) complexes.

No.	Complex	μ_{eff}^{rt} (BM) [†]	g	J (cm ⁻¹)	θ (K)	$10^2 R$
36	[Co ₂ (PMP)Cl(H ₂ O) ₄]Cl ₃ ·4H ₂ O	4.81 [*] (301K)	2.45(2)	-3.18(10)	-25.7	8.61
37	[Co ₂ (PMP)Br(H ₂ O) ₄]Br ₃ ·3H ₂ O	4.52 [*] (294K)	2.31(2)	-3.16(10)	-26.7	9.02
38	[Co ₂ (PMP) ₂](NO ₃) ₄ ·4EtOH	2.58	-	-	-	-
39	[Co ₂ (PMP) ₂](ClO ₄) ₄ ·EtOH	2.64	-	-	-	-
40	[Co ₂ (PMP-H) ₂](BF ₄) ₂ ·4H ₂ O	1.14	-	-	-	-
41	[Co ₂ (PPA)Cl(MeOH)Cl ₃]	3.90 [*] (296K)	-	-	-	-
42	[Co ₂ (PPA-H)Br(H ₂ O) ₂ Br ₂]0.5EtOH	3.38	-	-	-	-
43	[Co ₂ (PPA) ₂](ClO ₄) ₄ ·EtOH	2.04	-	-	-	-
44	[Co ₂ (PPA-H) ₂](BF ₄) ₂ ·EtOH·3H ₂ O	1.30	-	-	-	-
45	[Co ₂ (PMI)Cl(H ₂ O) ₄]Cl ₃ ·1.5H ₂ O	4.78	-	-	-	-
46	[Co ₂ (PMI)Br(H ₂ O) ₄]Br ₃ ·0.5H ₂ O	4.64	-	-	-	-
47	[Co ₂ (PMI)(OH ₂)(NO ₃) ₄]EtOH·0.5H ₂ O	4.45	-	-	-	-
48	[Co ₂ (PMI) ₂](ClO ₄) ₄ ·EtOH	2.66 [*] (296K)	-	-	-	-
49	[Co ₂ (PMI) ₂](BF ₄) ₄ ·2EtOH	2.71	-	-	-	-

† ; The TIP correction of 190×10^{-6} c.g.s.u. are applied for the calculations of the μ_{eff}^{rt} .

* ; These data come from the variable-temperature magnetic susceptibility measurements, in which the TIP correction was set at 200×10^{-6} c.g.s.u.

All of the binuclear octahedral cobalt complexes exhibit room-temperature magnetic moments generally lower than the value expected for an isolated octahedral Co(II) species (See Tables 10.1 and 3.1), for five binuclear 2:1 complexes **36**, **37**, **45**, **46** and **47** these reduced values lie in the range 4.45 - 4.81 BM, suggesting the possibility of weak antiferromagnetic exchange between the two Co(II) centers in the complex. However, the binuclear 1:1 Co(II) derivatives, together with two Co(II) halide compounds of PPA (**41** and **42**), are characterized by having very low room-temperature magnetic moments. This unusual magnetic behaviour may be attributed to (i) a very strong spin-coupled interaction, (ii) the existence of low spin Co(II) centers, or (iii) the presence of the partially oxidized Co(II)-Co(III) species.

First of all, it seems unlikely that these compounds possess a very strong antiferromagnetic coupling between the Co(II) centers, since the diazine bridge is not a strong superexchange medium, especially upon the consideration of the slightly reduced room-temperature magnetic moment for the Co(II) chloride complex of PMP (**36**), which suggests only a weak spin-coupled interaction between the two Co(II) ions. Secondly, concerning the low-spin Co(II) center, its existence is still within the bounds of possibility since a low-spin Co(II) derivative does occur when the donor atoms are constrained in a planar arrangement like corrins and porphyrins. However, the ligands PMP, PPA and PMI are not likely to force the Co(II) electrons to be paired and also there is no evidence from the spectral data to reveal the presence of square-planar Co(II) centers in these compounds and, finally, it is more likely that these low moments are caused by the partial oxidation of the complexes during syntheses. If so, then the presence of molecular oxygen ($4e^- + O_2 + 2H_2O = 4OH^-$) could be responsible for the oxidation as

well as the deprotonation of **40** and **44**, and the low moment could be due to the presence of a significant proportion of Co(III) in the mixture.

Two cobalt tetrafluoroborate complexes **40** and **44** have unusually low magnetic moments. This is again probably attributable to the occurrence of partial oxidation of the complex to a binuclear Co(III) derivative. If so, the small apparent magnetic moments would reflect the spin-coupled Co(II)-Co(II) content in the 1:1 derivatives, for diamagnetic Co(III) species will not make any contribution towards the spin-exchange interaction. Theoretically, the relative content of the Co(II)-Co(II) species that a complex contains can be worked out by comparing the magnetic susceptibility $\bar{\chi}$ of this complex [which can be calculated by the equation (5-26)] with that of some "standard" binuclear complex with 100-percent Co(II) ions. According to rough estimates taking the structurally-known Co(II) chloride compound **36** as such a standard, only 6.0% and 7.8% spin-coupled Co(II)-Co(II) species exist in the compounds **40** and **44** respectively. In other words, more than 90% Co(II) ions of the complex have been oxidized to diamagnetic Co(III), which appears to coincide with the results from their electronic spectra (See § 9.2).

The PPA halide complexes, **41** and **42**, exhibit relatively much higher μ_{eff} values than those of the 1:1 derivatives, which may reflect that the coordinated halogen could be helpful to the stabilization of the Co(II) ions. This is based on the fact that the electronegative halogen can polarize the metal-halogen bond and make the metal partially positive, which will cause the Co(II) oxidation to Co(III) to be less thermodynamically favoured, in other words, stabilize the Co(II) state. The absence of a halogen in the 1:1 compounds may allow the Co(II) oxidation to

occur more easily.

The room-temperature magnetic moments of all the binuclear nickel complexes, except **54**, lie between 2.8 - 3.2 BM, which seem to be within the accepted range for mononuclear six-coordinate Ni(II) species (See Table 3.1). However, in some cases (See Table 10.2) the binuclear nickel centers of the compounds have been shown to be spin-coupled by variable-temperature magnetic susceptibility measurements, although their room-temperature moments also fall in the non-reduced range for octahedral/pseudo-octahedral Ni(II). This indicates that the determination of the spin exchange for these nickel compounds must rest upon the variable-temperature magnetic susceptibility measurements rather than the room-temperature magnetic moments.

A very low magnetic moment is also obtained for the nickel tetrafluoroborate complex of PMP, **54**, upon the assumption that both nickel ions are paramagnetic (i.e., two octahedral centers). This value is much lower than could be expected by considering the magnetic properties of the other binuclear nickel compounds, and cannot reasonably be explained on the basis of antiferromagnetic exchange (See § 10.2). However if one Ni(II) center is assumed to be diamagnetic, i.e., one center is square planar (See § 4.3), the calculation will give a normal value 3.18 BM for the other nickel center, implying that such an assumption seems reasonable. This suggests that the deprotonated ligand in the 1:1 complex behaves as a strong coordinating ligand and helps to generate the low-spin square-planar metal center.

Table 10.2 Magnetic data for the binuclear Ni(II) complexes†.

No.	Complex	μ_{eff} (BM)	g (ρ)	J (cm^{-1})	D (cm^{-1})	$Z'J'$ (cm^{-1})	$10^2 R$
50	$[\text{Ni}_2(\text{PMP})\text{Cl}(\text{H}_2\text{O})_4]\text{Cl}_3 \cdot 4.5\text{H}_2\text{O}$	3.06 [*] (301K)	2.227 (0.040)	-12.99	7.60	0.040	0.9
51	$[\text{Ni}_2(\text{PMP})\text{Br}(\text{H}_2\text{O})_4]\text{Br}_3 \cdot 0.5\text{MeOH} \cdot \text{H}_2\text{O}$	3.12 [*] (296K)	2.248 (0.042)	-10.6	10.3	0.0010	2.3
52	$[\text{Ni}_2(\text{PMP})(\text{OH}_2)(\text{H}_2\text{O})_4](\text{NO}_3)_4 \cdot \text{MeOH}$	2.86	-	-	-	-	-
53	$[\text{Ni}_2(\text{PMP})_2](\text{ClO}_4)_4 \cdot 4\text{H}_2\text{O}$	2.81	-	-	-	-	-
54	$[\text{Ni}_2(\text{PMP})(\text{PMP-H})](\text{BF}_4)_3 \cdot 5.5\text{H}_2\text{O}$	2.22 [*] (296K)	-	-	-	-	-
55	$[\text{Ni}_2(\text{PPA})\text{Cl}(\text{H}_2\text{O})_4]\text{Cl}_3 \cdot 2\text{H}_2\text{O}$	3.19	-	-	-	-	-
56	$[\text{Ni}_2(\text{PPA-H})\text{Br}(\text{EtOH})(\text{H}_2\text{O})\text{Br}_2]\text{EtOH} \cdot 0.5\text{H}_2\text{O}$	2.99	-	-	-	-	-
57	$[\text{Ni}_2(\text{PPA})_2](\text{NO}_3)_4 \cdot 4\text{H}_2\text{O}$	3.04 [*] (295K)	2.148 (0.0)	-0.35	20.22	0.41	0.84
58	$[\text{Ni}_2(\text{PPA})_2](\text{ClO}_4)_4 \cdot 6\text{H}_2\text{O}$	3.16	-	-	-	-	-
59	$[\text{Ni}_2(\text{PPA})_2](\text{BF}_4)_4 \cdot 4\text{H}_2\text{O}$	3.07 [*] (296K)	2.127 (0.0)	-0.34	20.50	0.30	0.67
60	$[\text{Ni}_2(\text{PMI})\text{Cl}(\text{H}_2\text{O})_4]\text{Cl}_3 \cdot 2\text{H}_2\text{O}$	3.19	-	-	-	-	-
61	$[\text{Ni}_2(\text{PMI})\text{Br}(\text{H}_2\text{O})_4]\text{Br}_3 \cdot 3.5\text{H}_2\text{O}$	3.24	-	-	-	-	-
62	$[\text{Ni}_2(\text{PMI})(\text{OH}_2)(\text{NO}_3)_4]\text{EtOH} \cdot 1.5\text{H}_2\text{O}$	3.18	-	-	-	-	-
63	$[\text{Ni}_2(\text{PMI})_2](\text{ClO}_4)_4 \cdot 4\text{H}_2\text{O}$	3.17	-	-	-	-	-
64	$[\text{Ni}_2(\text{PMI})_2](\text{BF}_4)_4 \cdot 6\text{H}_2\text{O}$	3.18	-	-	-	-	-

† ; E.S.Ds of g , J , D and $Z'J'$ for compounds 50, 51, 57 and 59 are given in Fig. 10.1 - 10.4, respectively.

* ; These data come from the variable-temperature magnetic susceptibility measurements.

10.2 The Variable-Temperature Magnetic Susceptibility

The variable-temperature magnetic susceptibilities (χ) have been measured on dried, powdered samples in the temperature range 5 - 300 K. The results are given in Tables 10.1 and 10.2, illustrated in Fig. 10.1 to 10.8 and detailed as follows for the compounds under discussion.

A. The Binuclear Nickel Complexes

For the binuclear Ni(II) species, an important feature is the zero-field splitting of the $s = 1$ ground state (D), which is often within the same order of magnitude as the electron-spin-exchange integral (J). Therefore the magnetic model used must take this effect into account, besides which, an interdimer exchange ($Z'J'$) should be also included. Thus, the spin Hamiltonian (5-10) becomes as

$$H = -2J\hat{s}_1 \cdot \hat{s}_2 - D(\hat{s}_{1z}^2 + \hat{s}_{2z}^2) - 2Z'J'\hat{S}_i \cdot \langle \hat{S}_i \rangle - g_i\beta H\hat{S}_i \quad (10-1)$$

and then the resulting magnetic susceptibility equation (5-24), $\bar{\chi}(J, D, T, Z'J')$, which is applied to fit the magnetic data measured for the Ni(II) compounds, has been further modified as

$$\chi_m = \bar{\chi}(J, D, T, Z'J')(1 - \rho) + \frac{2Ng^2\beta^2\rho}{3kT} + N\alpha \quad (10-2)$$

in order to account for the monomeric impurity ρ , which represents the fraction of a possible magnetically dilute mononuclear Ni(II) impurity. The floating parameters ($J, D, T, \rho, Z'J'$) giving the best fit are obtained by minimizing the function

$$R = \left[\frac{\sum_i (\chi_i^{obsd} - \chi_i^{calcd})^2}{\sum_i (\chi_i^{obsd})^2} \right]^{1/2} \quad (10-3)$$

with use of a non-linear least-squares regression analysis. The best fit of the theoretical expression (10-2) to the experimental data is illustrated in Fig. 10.1 - 10.4 for the Ni(II) complexes **50**, **51**, **57** and **59** respectively, and the best values of the fitting parameters (g , J and D etc.) for these compounds are gathered in Table 10.2 as well. The values of the function R are also listed, as a measure of the discrepancy between the experimental and calculated curves.

All the results of the variable-temperature susceptibility measurements on these four nickel samples reveal that an antiferromagnetic exchange between the Ni(II) centers is present in these compounds. The complexes **50** and **51** that have substantial antiferromagnetic-exchange centers show very similar g and J values, when an isotropic model without the ZFS (D) or interdimer exchange ($Z'J'$) for an $s = 1$ Ni(II) dimer fit is employed. Considering the large Ni(II)-Ni(II) separation in the dimer, a superexchange pathway must be responsible for the significant antiferromagnetic interaction. Also, the results obviously divide the complexes discussed into two groups: the compounds **57** and **59** (the 1:1 derivatives) having very weak spin couplings with $J > -1 \text{ cm}^{-1}$, and the compounds **50** and **51** (the 2:1 complexes) with much larger exchange integrals. A major difference between these two groups of complexes is the second bridge, i.e., the halogen group for **50** and **51**, indicating that the halogen bridge is a more active magnetic exchange medium than the diazine bridging group, and plays a more important role in the superexchange process.

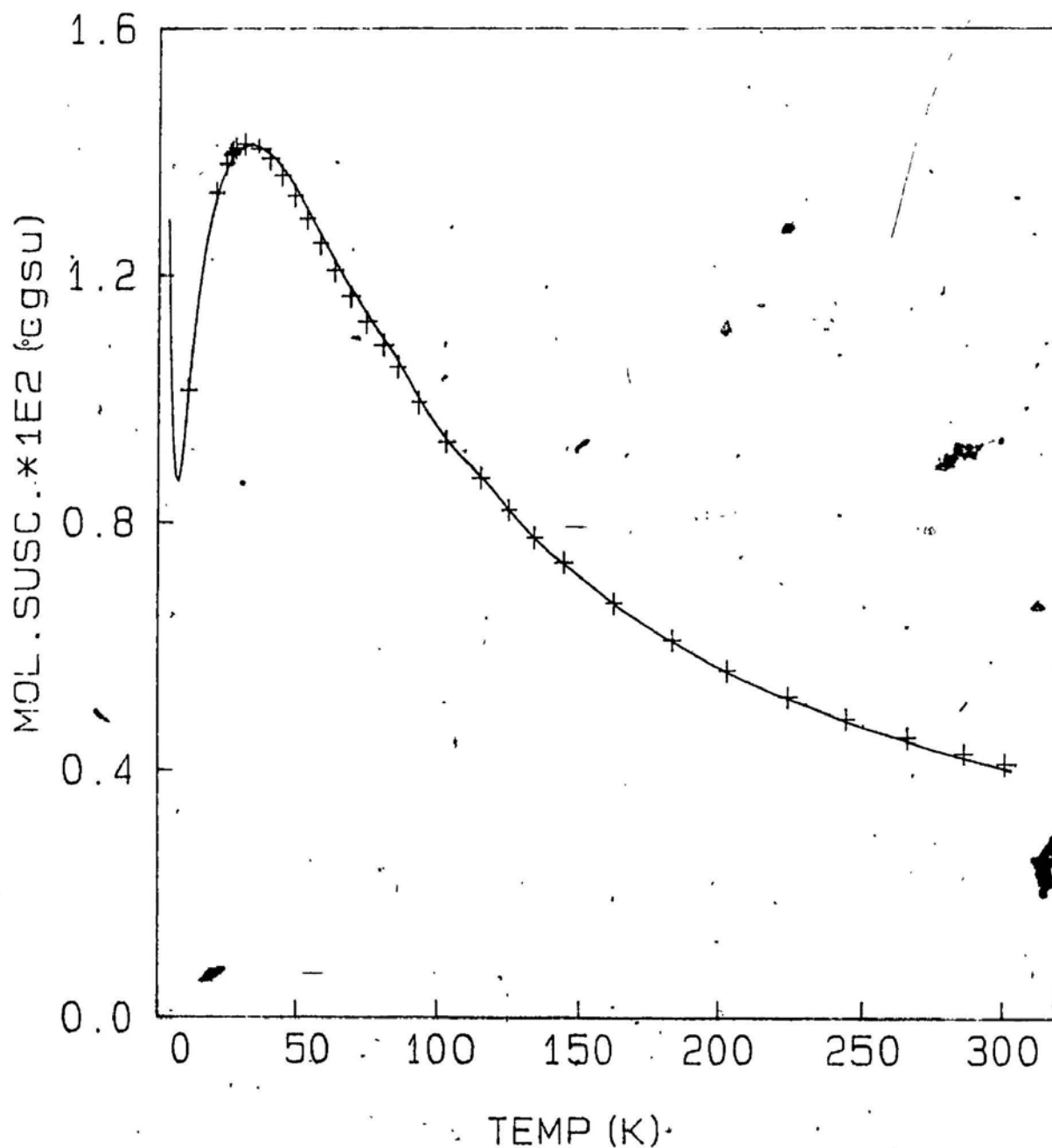


Fig. 10.1

Magnetic susceptibility data for the PMP Ni(II) chloride complex 50. The solid line was calculated from equation (10-2) with $g = 2.227(3)$, $J = -12.99(6) \text{ cm}^{-1}$, $D = 7.60(2) \text{ cm}^{-1}$, $Z'J' = 0.040(2) \text{ cm}^{-1}$ (corrected for 4% paramagnetic impurity).

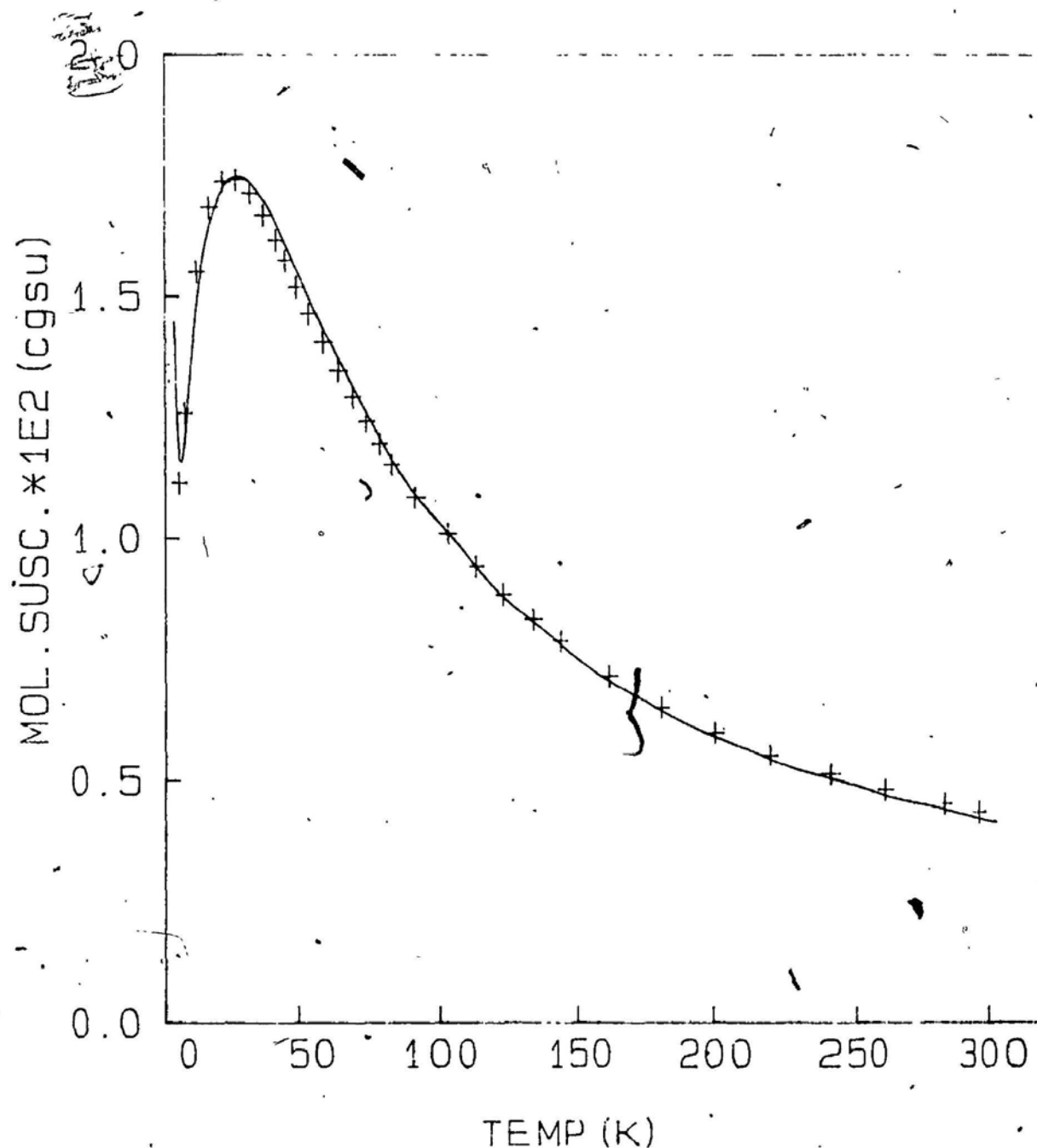


Fig. 10.2

Magnetic susceptibility data for the PMP Ni(II) bromide complex **51**. The solid line was calculated from equation (10-2) with $g = 2.248(8)$, $J = -10.60(1) \text{ cm}^{-1}$, $D = 10.3(1) \text{ cm}^{-1}$, $Z'J' = 0.0010(2) \text{ cm}^{-1}$ (corrected for 4.2% paramagnetic impurity).

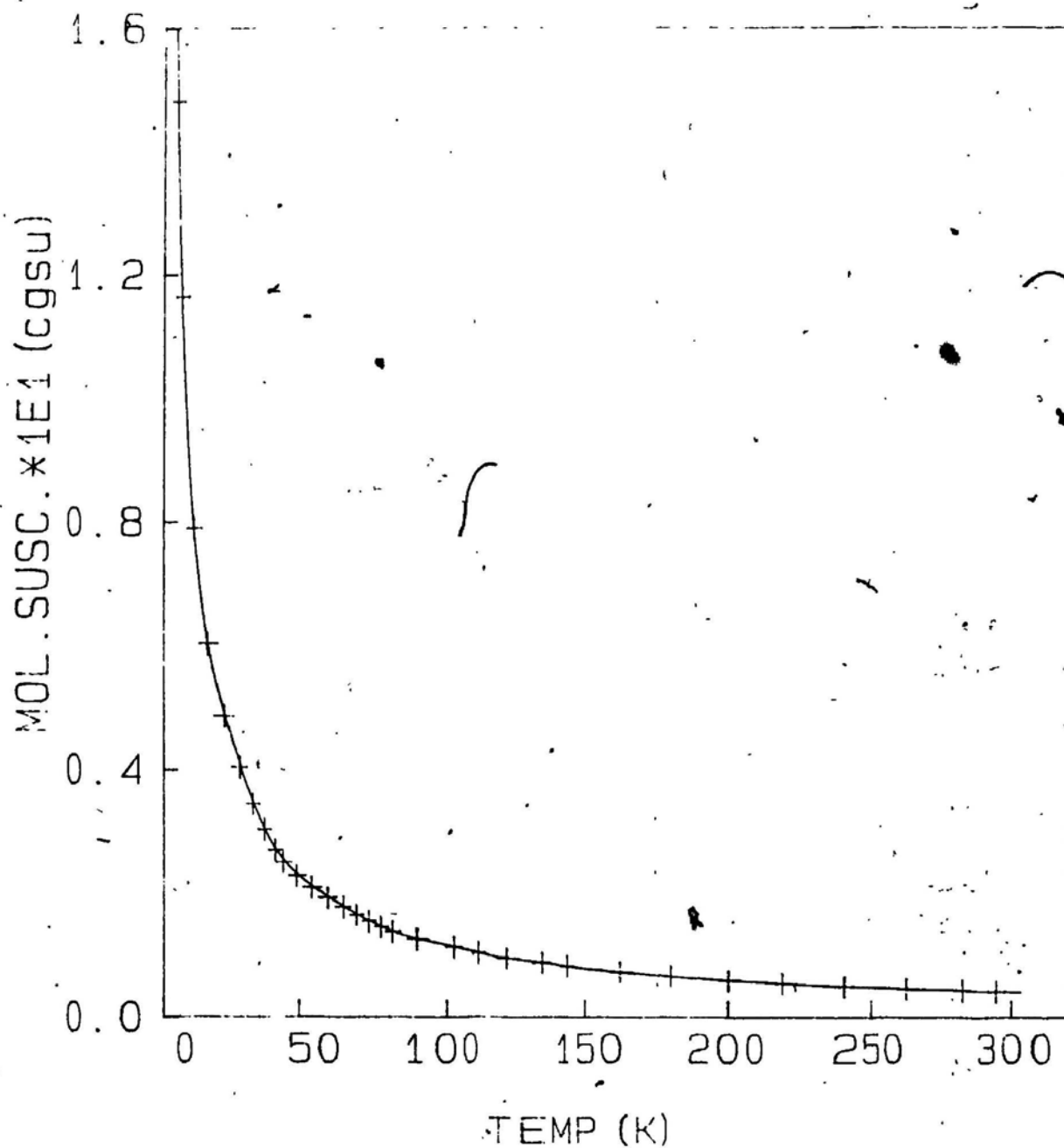


Fig. 10.3

Magnetic susceptibility data for the PPA Ni(II) nitrate complex **57**. The solid line was calculated from equation (10-2) with $g = 2.148(2)$, $J = -0.35(1) \text{ cm}^{-1}$, $D = 20.22(2) \text{ cm}^{-1}$, $Z'J' = 0.41(1) \text{ cm}^{-1}$.

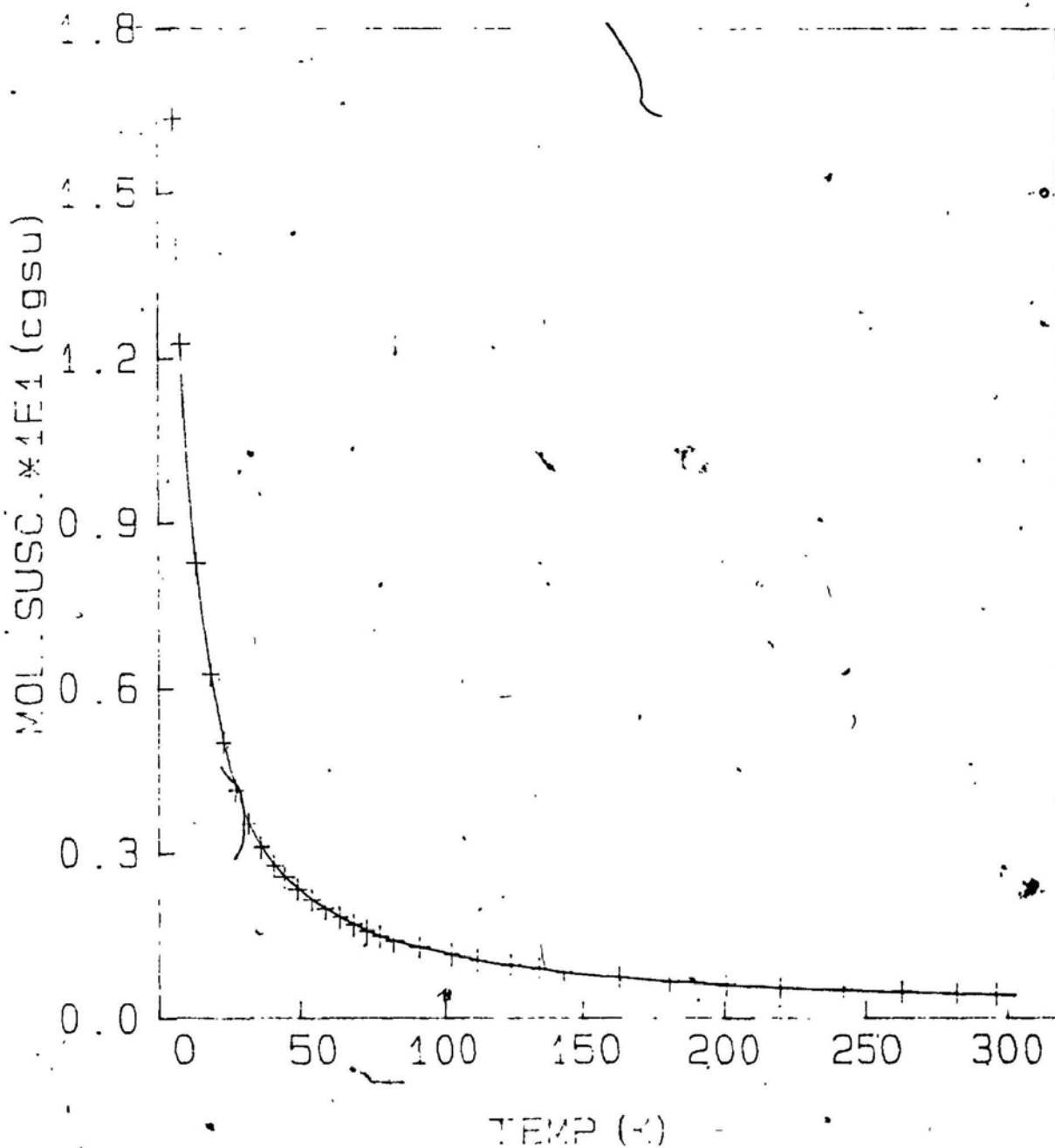


Fig. 10.4

Magnetic susceptibility data for the PPA Ni(II) tetrafluoroborate complex **59**. The solid line was calculated from equation (10-2) with $g = 2.127(2)$, $J = -0.34(1) \text{ cm}^{-1}$, $D = 20.50(1) \text{ cm}^{-1}$, $Z'J' = 0.30(1) \text{ cm}^{-1}$.


The proposed 1:1 structure for the compounds **57** and **59**, involving two phthalazine diazine bridges, would have perhaps been thought to cause stronger antiferromagnetic exchange between its two metal centers considering the magnetic data for the compound **15** ($J = -22.3 \text{ cm}^{-1}$)⁶². However, these species exhibit quite weak antiferromagnetic exchange interactions. This unexpectedly weak exchange may result partially from the twist of the molecular plane surrounding the binuclear center, which will cause a decrease in the overlap of the π molecular orbitals of the bridge system as well as the effective interaction between the magnetic orbitals, thus leading to a decrease of the spin exchange interaction. Recent studies also reveal that the phthalazine bridge is, by contrast with the other related diazine ligand, just a modest and/or relatively weak superexchange medium⁸⁰. It is generally believed that the major part of the superexchange takes place *via* π -electron delocalization of the ligand, but recent observations have shown that magnetic exchange through σ electrons is also very important^{104,105}. Other factors including metal-ligand bond lengths and metal-ligand-metal bond angles should also be taken into account in quantitative discussions about magnetic exchange and structure correlations. The variable-temperature magnetic data measured for compounds **57** and **59** have also been examined by the mononuclear model to find out which treatment of the data produces a better fit. The calculating results indicate that the monomer model gives much higher 10^2R values (3.96 and 3.44 respectively), which means that the model does not fit in with the data very well, thus further confirming the presence of the binuclear dimer in the 1:1 species.

B. The Binuclear Cobalt Complexes

The interpretation of the magnetic data for binuclear Co(II) complexes is much more difficult than that associated with comparable Ni(II) compounds (See § 5.5). In the present study it has been assumed that the orbital angular momentum for Co(II) has been completely quenched and the decrease in magnetic susceptibility of the Co(II) derivatives, as a function of temperature, results solely from an exchange interaction defined by an isotropic Hamiltonian (5-1). The susceptibility of a pair of Co(II) ions has been given by equation (5-27), in which the temperature independent paramagnetism term (χ_{TIP}) can usually be estimated from the d-d bands of the Co(II) ion, but could not be obtained here for these Co(II) complexes, because only one transition (ν_1) was clearly visible in their electronic spectra. The χ_{TIP} term has been set at 200×10^{-6} c.g.s.u., which means a small ($< 2\%$) correction of the data, in the non-linear least-squares regression of the theoretical expression (5-27) to the experimental data.

The best data-fit line has been obtained (See Fig. 10.5 and 10.6), and the best values of the fitting parameters J and g are gathered in Table 10.1. The high average g values are, as usual, typical of binuclear Co(II) derivatives^{64,94}, but the values of the exchange integral around -3.2 cm^{-1} that denotes a weak antiferromagnetic exchange interaction are much smaller than those displayed by the nickel compounds **50** and **51**, as is also typical and normal upon the comparison of the other related analogous Co(II) and Ni(II) derivatives. The plots of μ_{eff} versus temperature (T) and χ_m^{-1} vs. T for **36** and **37** are illustrated in Fig. 10.7 and 10.8 respectively. Both complexes obey the Curie-Weiss law above about 50 K, and give the Weiss constant $\theta = -25.7 \text{ K}$ (**36**) and $\theta = -26.7 \text{ K}$ (**37**)

in the range 50 - 300 K by using a linear regression method to the experimental data points. These negative θ values and the upward curvature of the the reciprocal susceptibility plots at low temperature, together with the negative values of their exchange integral as a whole, undoubtedly indicate the presence of a weak antiferromagnetic spin exchange between the two Co(II) centers of these cobalt complexes under discussion.



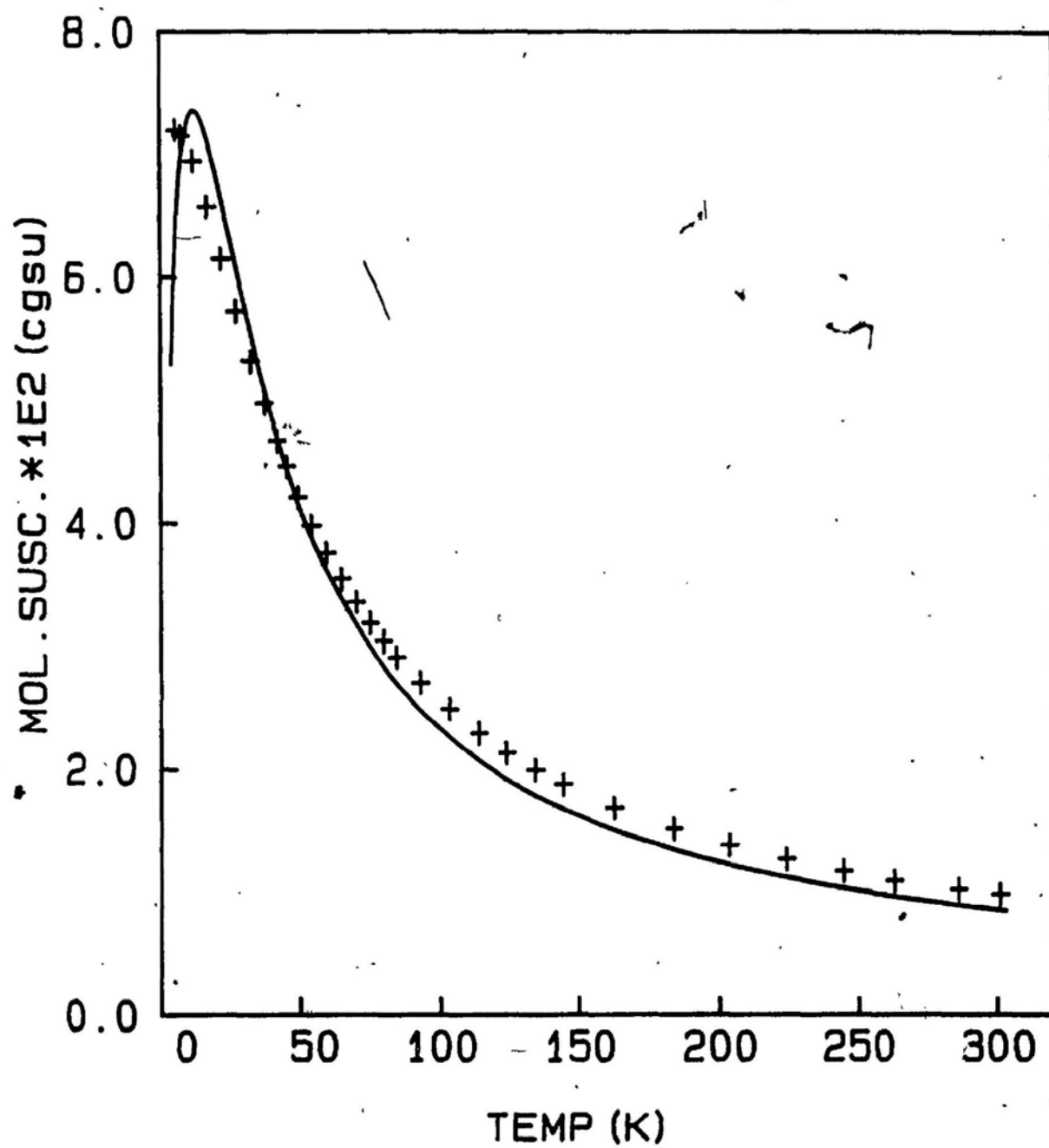


Fig. 10.5

Magnetic susceptibility data for the PMP Co(II) chloride complex **36**. The solid line was calculated from equation (5-27) with $g = 2.45$, $J = -3.18 \text{ cm}^{-1}$.

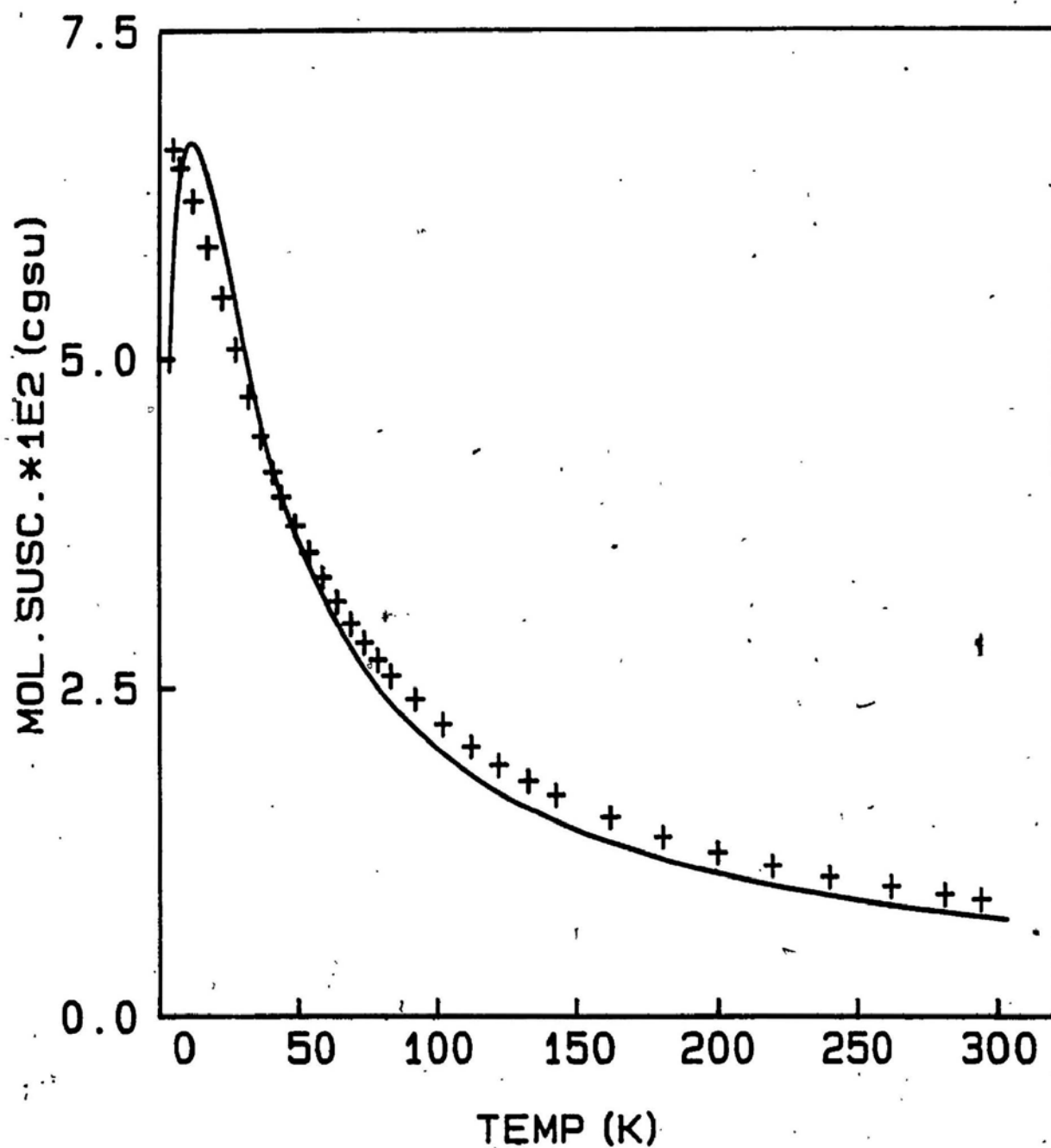


Fig. 10.6

Magnetic susceptibility data for the PMP Co(II) bromide complex **37**. The solid line was calculated from equation (5-27) with $g = 2.31$, $J = -3.16 \text{ cm}^{-1}$.

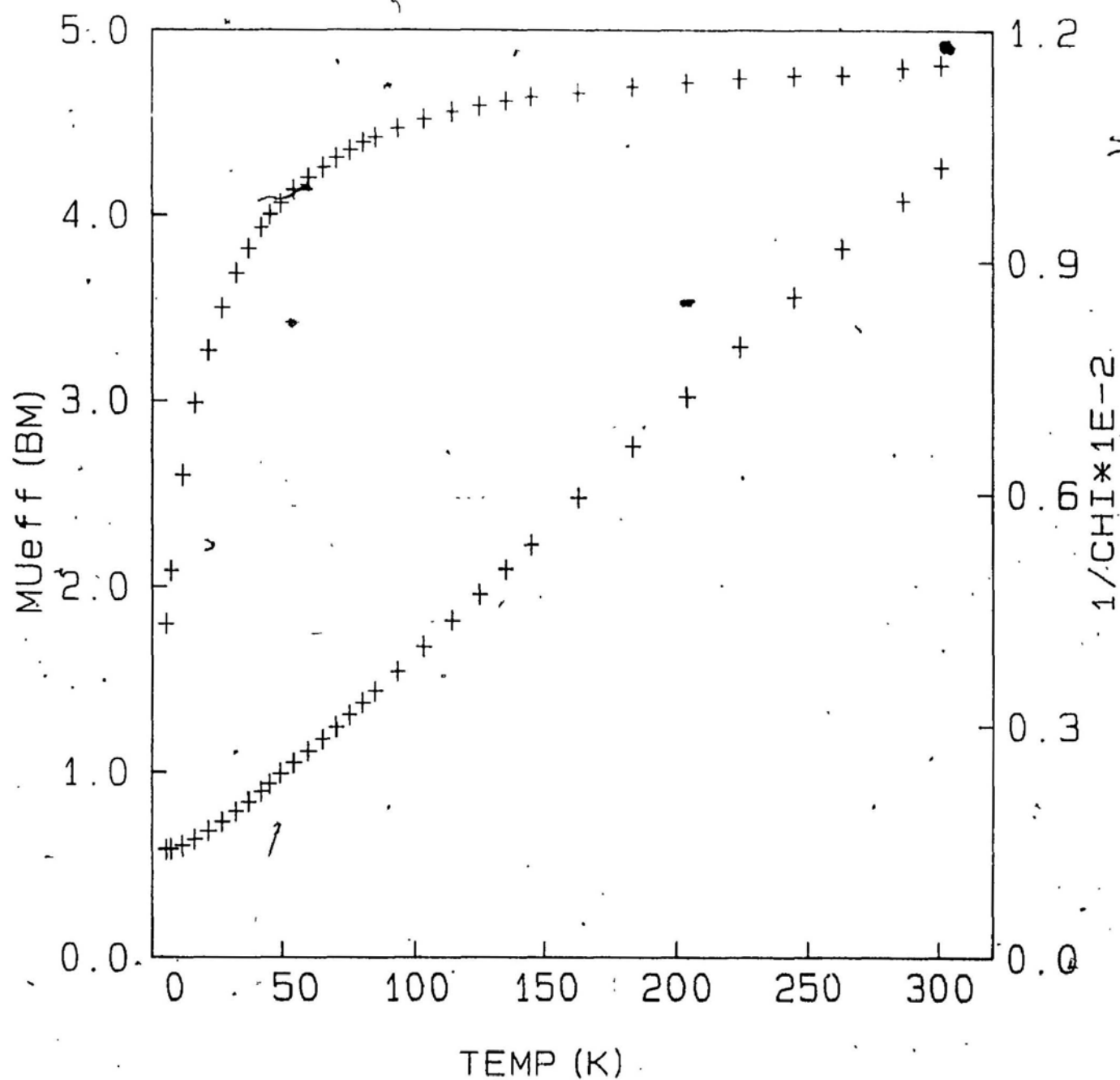


Fig. 10.7

Magnetic data for $[\text{Co}_2(\text{PMP})\text{Cl}(\text{H}_2\text{O})_4]\text{Cl}_3 \cdot 4\text{H}_2\text{O}$, **36**.

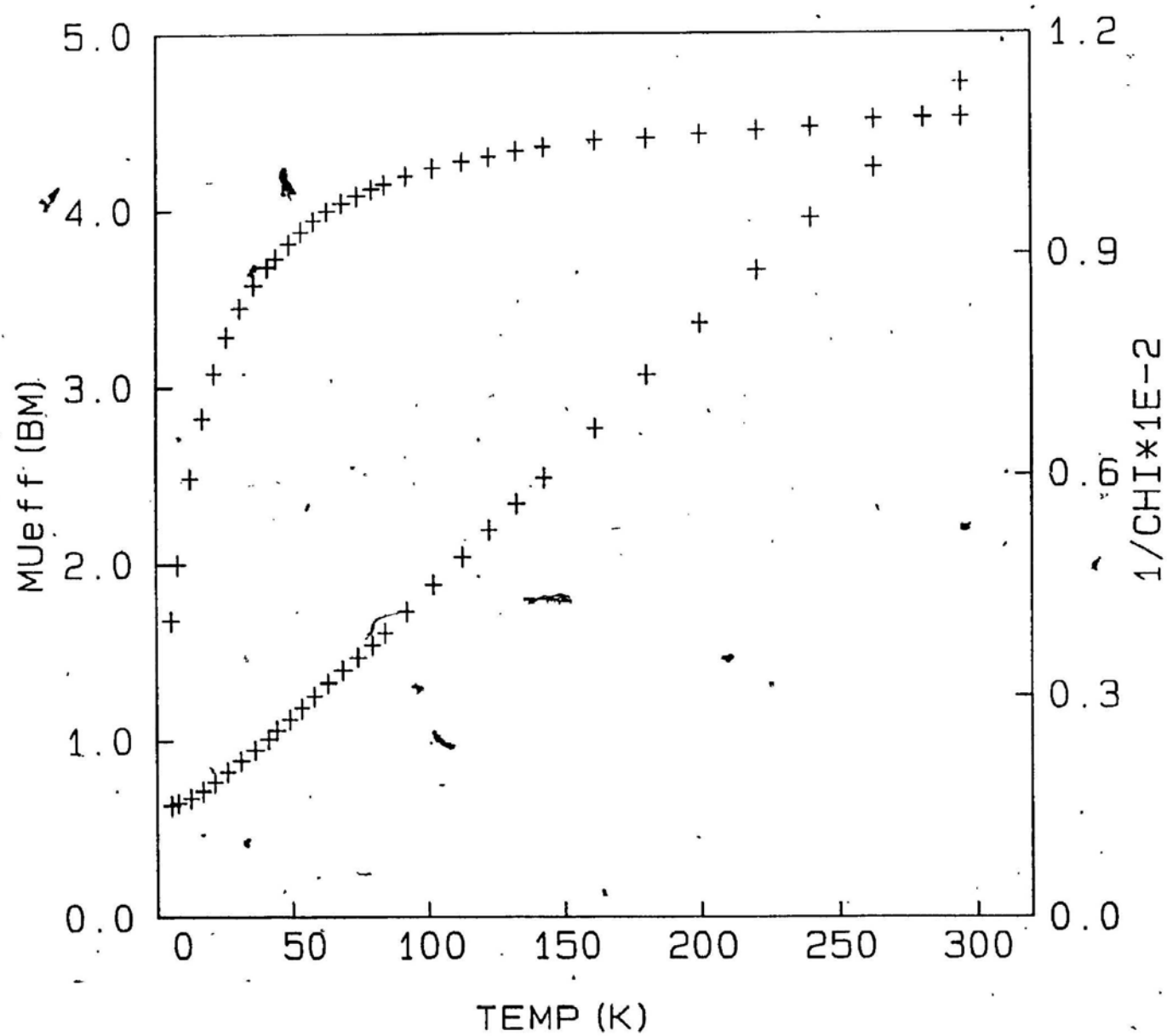


Fig. 10.8

Magnetic data for $[\text{Co}_2(\text{PMP})\text{Br}(\text{H}_2\text{O})_4]\text{Br}_3 \cdot 3\text{H}_2\text{O}$, **37**.

CHAPTER 11

CONCLUDING REMARKS AND SUMMARY

The results described in this study have shown that the three phthalazine hydrazine derivatives prepared are binucleating, hexadentate chelating ligands, and are able to form binuclear complexes with spin-coupled pairs of transition-metal ions. The binuclear transition-metal compounds formed have been characterized by microanalytical, spectroscopic and magnetic studies, and they are divided into two groups: those in which the two metal ions are bound in close proximity to each other by a single hexadentate ligand (binuclear 2:1 species); and those in which the two metals are linked close together by two hexadentate ligands (binuclear 1:1 derivatives). Both groups of compounds exhibit very intense MLCT transitions, and generally reduced room-temperature magnetic moments associated with the magnetic interaction between the two metal ions. The metal centers in both types of compounds are assumed to have distorted octahedral stereochemistries, and are doubly bridged by the ligand diazine group(s) and/or an anion group.

The binuclear 2:1 species include all the halide compounds and three nitrates. The infrared and electronic spectra of these complexes are very similar within each subgroup reflecting close similarities between the respective structures. The basic structural unit for these compounds is embodied in the representatives of this group, the PMP halide complexes **36** and **50**, whose structures

have been determined by X-ray crystallography. In the three nitrate complexes, the PMP one, **52**, is proposed to have essentially the same cation structure as the PMP chloride compound **50**, except that the bridging chlorine is replaced by a water bridge, while the other two PMI nitrates **47** and **62**, with the water bridge and four monodentate nitrate groups coordinating axially, are suggested to possess the structure given in Fig. 11.1, in which two metal atoms are symmetrically coordinated by the ligand and other donor groups.

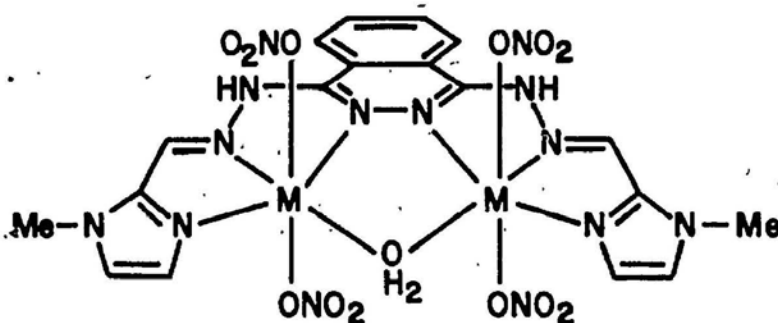


Fig. 11.1 The proposed binuclear structure for **47** and **62**.

Three PPA halide complexes seem to have some differences in their coordination spheres involving both coordinated halogen and solvent. In the cobalt chloride complex **41**, the two Co(II) ions are both six-coordinated but in different coordinating environments: one Co(II) center has a chloride group at its sixth coordination site, while the other has a methanol molecule (See Fig. 11.2). This situation also possibly happens in the case of the nickel bromide complex **56**, in which an ethanol and a water molecule occupy axial sites of the two centers. Here different isomers would be possible, depending on whether the bromine atoms were bound to the same nickel center or one on each nickel ion. The same situa-

tion also exists for the cobalt bromide complex **42**. It is hard to determine which configuration actually exists for these two bromide compounds based on the available information.

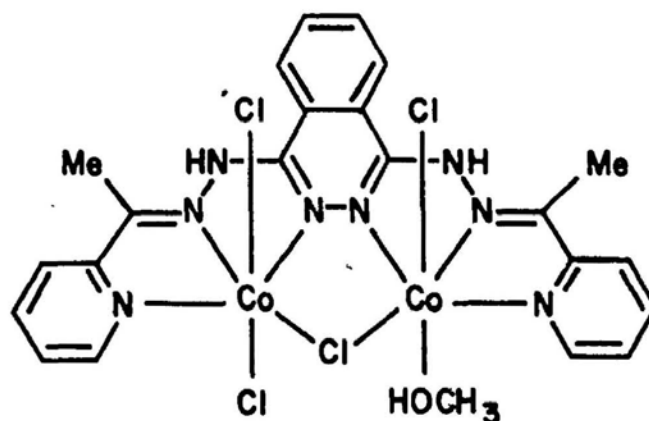


Fig. 11.2 The proposed binuclear structure for **41**.

The binuclear 1:1 derivatives include the perchlorate and tetrafluoroborate complexes as well as two nitrates, **38** and **57**. The stoichiometries of these derivatives indicate that only one metal atom and one ligand are involved in the empirical formulae ($[ML]Y_2 \cdot mS \cdot nH_2O$). However, by comparing with the binuclear 2:1 species as well as other related ligand systems and their complexes, the electronic spectra of the 1:1 derivatives are most simply interpreted by a binuclear structure with two ligands, i.e., the molecular formula is twice the empirical one, and their magnetic behaviour at room temperature and between 5 - 300 K also indicate the presence of pairs of metal ions with a weak antiferromagnetic exchange interaction. The similarities between the infrared spectra of these 1:1 derivatives reveal that these compounds are closely related and probably have the same cation structural unit. The IR spectra further indicate that the ClO_4 , BF_4 and NO_3 groups of these compounds remain in an ionic state and the water/solvent

molecule are also present but only in the crystal lattice. Therefore the binuclear cation involves just two hexadentate ligands bound to the two octahedral metal centers. A structural representation for the 1:1 binuclear complexes is illustrated in Fig. 9.1, in which the two pseudo-octahedral metal ions are symmetrically situated between the two adjacent hexadentate ligands, with the diazine and azomethine nitrogen donors coordinating equatorially and the peripheral-ring nitrogen atoms occupying axial sites.

SECTION III EXPERIMENTAL AND MISCELLANEOUS

CHAPTER 12

EXPERIMENTAL

12. 1. Elemental Analysis And Physical Measurements

A. Elemental Analysis

The C, H and N analyses were carried out by the Canadian Microanalytical Service Ltd., New Westminster, British Columbia, Canada. Cobalt and nickel analyses were determined by atomic absorption spectroscopy using a Varian Techtron AA5 instrument on solutions obtained by the digestion of the samples in concentrated HNO_3 .

B. Infrared Spectra

All the infrared spectra were run as solid mulls, between sodium chloride ($4000 - 600 \text{ cm}^{-1}$) and cesium iodide ($600 - 200 \text{ cm}^{-1}$) plates, using 'Nujol' as mulling agent in the region $4000 - 200 \text{ cm}^{-1}$, with a Perkin-Elmer Model 283 Spectrometer.

C. Electronic Spectra

Electronic spectra of both solutions and solid mulls were recorded by a Cary 17 Spectrophotometer. The samples of the solid spectra were prepared as relatively strong mulls in 'Nujol' and pasted onto filter paper held between two glass microscope slides, then the ends of the slides were sealed with adhesive tape. The

sample and the blank of 'Nujol', which is on filter paper placed between the similar glass slides, were mounted with adhesive tapes on the solution cell mounts in the instrument. The spectra were run in the range 300 - 1200 nm. The solution spectra were run in DMF or methanol solutions from 300 - 1600 nm.

D. Magnetic Measurements

The room-temperature magnetic moments were measured using a Cahn model 7600 Faraday magnetic susceptibility system. Variable-temperature (in the range 5 - 300 K) magnetic susceptibility data were obtained by using an Oxford Instruments Superconducting Faraday Magnetic Susceptibility System with a Sartorius 4432 microbalance. The measurements were performed using a main solenoid field of 1.5 Tesla and a gradient field of 10 Tm^{-1} . The susceptibility data have been corrected for diamagnetism (Pascal corrections), temperature independent paramagnetism, and the presence of monomer impurity (nickel complexes only). $\text{HgCo}(\text{NCS})_4$ was used as a calibration standard.

E. X-ray Crystallography

X-ray diffraction data were collected by Dr. E. J. Gabe and his co-workers in the Division of Chemistry, the National Research Council of Canada, Ottawa, Canada. The X-ray data, together with pertinent details on the data collection and instrumentation have been included in Chapter 8.

12. 2. The Syntheses Of The Ligands

Commercial available solvents and starting chemicals were directly used in

the syntheses without further purification.

A. The Precursor DHPH

The aqueous solution of hydrazine, which was prepared by mixing 8 ml 50% aqueous acetic acid (dilute glacial 1:1) and 20 ml 85% hydrazine monohydrate , was added to a solution of phthalonitrile (12.8 g) dissolved in 25 ml *p*-dioxane. The resulting mixture was incubated in oil bath at 95 °C with stirring for 3 hr. Upon cooling, yellow crystals formed which were filtered off and recrystallized from 500 ml water to give pale yellow needle crystals (Mp. 190 - 192 °C , Yield: 82.2%).

B. The Ligand PMP

DHPH (3.80 g, 20 mmol) and 6-methyl-2-pyridine-carboxaldehyde (4.85 g, 40 mmol) were reacted together in hot methanol (100 ml) under reflux overnight with the formation of a deep reddish-orange solution, whose volume was reduced to 30 ml after refluxing. On cooling in the refrigerator for several days, the resulting reddish-orange ligand was obtained by filtration and recrystallized from ethanol (500 ml) [Mp. 129 - 132 °C , Yield: 2.40 g (63.2%)].

C. The Ligand PPA

DHPH (3.80 g, 20mmol) and 2-acetylpyridine (4.85g, 40mmol) were reacted in hot methanol (80 ml) under reflux for 4 hr. On cooling in the refrigerator overnight, orange crystals formed, which were filtered off, washed with ethanol and dried in air [Mp. 185 - 187 °C , Yield: 4.40 g (51.0%)].

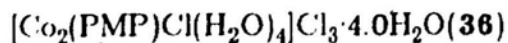
D. The Ligand PMI

i] *n*-BuLi (88 ml of 2.5 M solution in hexane-) was added to dry (distilled over sodium benzophenone ketyl) THF (200 ml) in an atmosphere of dry nitrogen and the mixture cooled to -75°C in a dry ice/methanol bath. *N*-methylimidazole (16 ml, 0.20-mol) dissolved in dry THF (50 ml) was added dropwise to the solution of *n*-BuLi in THF over a period of 1/2 hr and the mixture was stirred for a further 1/2 hr at -75°C . 25 ml DMF mixed in dry THF (20 ml) was added dropwise over a period of 1/2 hr and the mixture allowed to warm up to room temperature overnight. A saturated aqueous solution of NH_4Cl (200 ml) was added to the mixture and the solvent volume reduced by using a rotary evaporator. The solution was extracted 5 times with chloroform and the combined chloroform extracts reduced in volume. The product, *N*-methylimidazole-2-carboxaldehyde, was obtained as colourless crystals after fractionating the combined extracts under vacuum ($62 - 75^{\circ}\text{C}$, 1.15 mm Hg). Yield: 4.46 g (20.7%).

ii]. DHPH (3.80 g, 20 mmol) and *N*-methylimidazole-2-carboxaldehyde (4.40 g, 40 mmol) were refluxed together in methanol (80 ml) for 3 hr. Yellow crystals formed on cooling, which were filtered off, washed with pet. ether, and dried under vacuum [Mp. $238 - 240^{\circ}\text{C}$, Yield: 2.82 g (41.9%)].

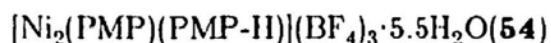
12. 3. The Syntheses Of The Complexes

Metal salts were used as commercially available hydrates without further purification.



$\text{CoCl}_2 \cdot 6\text{H}_2\text{O}$ (0.50 g, 2.1 mmol) was dissolved in hot water (5 ml) and added to a solution of PMP (0.40 g, 1.0 mmol) dissolved in refluxing methanol (30 ml). The mixture was refluxed for 2 hr with the formation of a dark-brown solution, then filtered hot, and allowed to stand at room temperature and the volume reduced to 10 - 15 ml by evaporation in air. Reddish-brown crystals formed, which were collected by decanting the mother liquor, washed with a 1:1 methanol/ether mixture and dried with nitrogen gas.

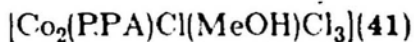
The other PMP compounds **37**, **40** and **50 - 53** were prepared in the same way. They precipitated as nice crystals/crystallites or powders, which were isolated by filtration, washing and drying under vacuum at room temperature. The two PMP cobalt complexes **38** and **39** were also synthesized in the same manner except that ethanol (95%) was used as the solvent in their preparations to obtain the satisfactory products.



$\text{Ni}(\text{BF}_4)_2 \cdot 6\text{H}_2\text{O}$ (0.70g, 2.0 mmol) was dissolved in 5 ml of hot water, and added to a solution of PMP (0.40 g, 1.0 mmol) dissolved in refluxing methanol (30 ml). The mixture was filtered immediately after boiling on a steam-bath for 5 min, and the filtrate was refluxed for another 30 min with the formation of a dark greenish-brown solution. The solution was left to stand at ambient temperature. Orange crystals formed and were isolated by filtration, washing with the methanol/ether mixture and drying under vacuum at room temperature.

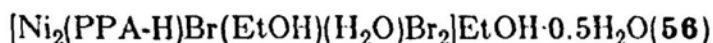
The two PPA nickel compounds **57** and **59** were prepared in the same

manner. They were isolated as reddish-brown crystalline solids. The PPA cobalt complex **44** was synthesized in the same fashion employing ethanol (95%) as the solvent in its preparation and obtained as a dark-brown product.



$\text{CoCl}_2 \cdot 6\text{H}_2\text{O}$ (0.50g, 2.1 mmol) was completely dissolved in hot methanol (30 ml), and added to a solution of PPA (0.40 g, 1.0 mmol) dissolved in refluxing methanol (80 ml). The mixture was refluxed for 2 hr with the formation of an intense reddish-brown solution. The solution was filtered on cooling, reduced to 20 ml in volume, and allowed to stand in a stoppered flask placed in the refrigerator for days. A reddish-violet crystalline powder formed and was separated by filtration, washing with dry methanol and ether, and drying under vacuum at room temperature.

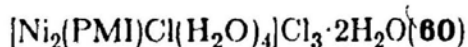
The two PPA nickel complexes **55** and **58** were prepared in the same way. They were collected as green crystals and olive-green crystallites respectively. The PPA cobalt compound **43** was produced in the same manner employing absolute ethanol as the solvent in its preparation. A dark-violet product was obtained.



$\text{NiBr}_2 \cdot 3\text{H}_2\text{O}$ (0.48g, 2.0 mmol) was fully dissolved in hot ethanol (95%, 15 ml), and then added to a solution of PPA (0.40 g, 1.0 mmol) dissolved in refluxing ethanol (95%, 30 ml) containing a few drops of 48% hydrobromic acid. The mixture was refluxed for 2 hr with the formation of a green solution, then filtered hot, and allowed to stand in a stoppered flask overnight. Green crystalline solid formed on the walls of the flask, which was filtered off, washed with the

ethanol/ether mixture and dried under vacuum at room temperature.

The cobalt bromide complex of PPA (42) was prepared in a same manner without the addition of the hydrobromic acid in the preparation. The product was obtained as reddish-black crystalline powder.



$\text{NiCl}_2 \cdot 6\text{H}_2\text{O}$ (0.60g, 2.5 mmol) was completely dissolved in warm absolute ethanol (20 ml) by stirring, and then added to a solution of PMI (0.40 g, 1.1 mmol) dissolved in refluxing absolute ethanol (70 ml). The mixture was refluxed for 1 hr with the formation of an intense greenish-brown solution, then filtered hot, and left to stand for several days. Upon slow evaporation of the solution to 20 ml in air, yellowish-green crystals were deposited. The product was filtered off, washed with absolute-ethanol/ether mixture, and dried under vacuum at room temperature.

The PMI nickel complexes 61 - 64 and the PMI cobalt complexes 47 - 49 were prepared in the same fashion . They precipitated as crystalline solids or powders, and were isolated by filtration, washing with the mixture of absolute ethanol and ether, and dried under vacuum at room temperature. The PMI cobalt compounds 45 and 46 were also produced by the same method but using 95% ethanol as the solvent system in their preparation. They were collected as brown crystallites.

REFERENCES

1. a) P. K. Coughlin, S. J. Lippard, *J. Am. Chem. Soc.*, **103**, 3228, 1981.
 b) A. E. Martin, J. E. Bulkowski, *J. Org. Chem.*, **47**, 415, 1982.
- 2 A. E. Martin, J. E. Bulkowski, *J. Am. Chem. Soc.*, **104**, 1484, 1982.
- 3 Y. Agnus, R. Louis, R. Weiss, *J. Am. Chem. Soc.*, **101**, 3381, 1979.
- 4 S. M. Nelson, *Pure & Appl. Chem.*, **52**, 2461, 1980.
- 5 J. J. Grzybowski, P. H. Merrell, F. L. Urbach, *Inorg. Chem.*, **17**, 3078, 1978.
- 6 J. M. Lehn, *Pure & Appl. Chem.*, **52**, 2441, 1980.
- 7 P. L. Burk, J. A. Osborn, M. T. Youjnou, Y. Agnus, R. Louis, R. Weiss, *J. Am. Chem. Soc.*, **103**, 1273, 1981.
- 8 K. D. Karlin, P. L. Dahlstrom, L. T. Dipierro, R. A. Simon, J. Zubietta, *J. Coord. Chem.*, **11**, 61, 1981.
- 9 J. P. Collman, M. Marrocco, P. Denisevich, C. Koval, F. C. Anson, *J. Electroanal. Chem.*, **101**, 117, 1979.
- 10 D. A. Buckingham, M. J. Gunter, L. N. Mander, *J. Am. Chem. Soc.*, **100**, 2899, 1978.
- 11 C. K. Chang, *J. Am. Chem. Soc.*, **99**, 2819, 1977.
- 12 P. J. Sadler, *Inorg. Perspect. Biol. Med.*, **1**, 233, 1978.
- 13 W. A. Hendrickson, In *Invertebrate O₂-binding Proteins*, J. N. Lamy, J. Lamy, Eds; Marcel Dekker, Basel, 1981, p. 503.
- 14 a) E. I. Solomon, In *Copper Proteins*, T. G. Spiro, Ed.; Wiley-Interscience, New York, 1981, Chap. 2.
 b) M. S. Co, K. O. Hodgson, T. K. Eccles, R. Lontie, *J. Am. Chem. Soc.*, **103**, 984, 1981.
 c) W. P. J. Gaykema, W. G. J. Hol, J. M. Vereijken, N. M. Soeter, H. J. Bak, J. J. Beintema, *Nature (London)*, **309**, 23, 1984.
 d) M. E. Winkler, L. Lerch, E. I. Solomon, *J. Am. Chem. Soc.*, **103**, 7001, 1981.
- 15 M. Erecinska, D. F. Wilson, *Arch. Biochem. Biophys.*, **188**, 1, 1978.
- 16 C. A. Reed, J. T. Landrum, *FEBS Lett.*, **106**, 265, 1979.
- 17 L. Powers, B. Chance, Y. Ching, P. Angiolollo, *Biophys. J.*, **34**, 465, 1981.
- 18 J. A. Fee, In *Metals in Biology, No. 13, Copper Proteins*, H. Sigel Ed.; Marcel Dekker, Basel, 1981, Chap. 8.
- 19 K. G. Strothkamp, S. J. Lippard, *Biochemistry*, **20**, 7488, 1981.

- 20 J. P. Gisselbrecht, M. Gross, A. H. Alberts, J. M. Lehn, *Inorg. Chem.*, **19**, 1986, 1980.
- 21 J. P. Collman, P. Denisovich, Y. Konai, M. Marrocco, C. Koval, F. C. Anson, *J. Am. Chem. Soc.*, **102**, 6027, 1980.
- 22 E. Yeager, *Electrochim. Acta*, **29**, 1725, 1984.
- 23 A. van der Putten, A. Elzing, W. Visscher, E. Barendrecht, *J. Chem. Soc. Chem. Commun.*, 477, 1986.
- 24 R. Robson, *Inorg. Nucl. Chem. Lett.*, **6**, 125, 1970.
- 25 R. Robson, *Aust. J. Chem.*, **23**, 2217, 1970.
- 26 W. Newton, J. R. Postgate, C. Rodriguez-Barrucco, Eds; In *Recent Developments in Nitrogen Fixation*, Academic Press, London, 1977.
- 27 N. H. Pilkington, R. Robson, *Aust. J. Chem.*, **23**, 2225, 1970.
- 28 U. Casellato, P. A. Vigato, D. E. Fenton, M. Vidali, *Chem. Soc. Rev.*, **8**, 199, 1979.
- 29 R. W. Stotz, R. C. Stoufer, *J. Chem. Soc. Chem. Commun.*, 1682, 1970.
- 30 B. F. Hoskins, R. Robson, G. A. Williams, *Inorg. Chim. Acta*, **16**, 121, 1976.
- 31 R. R. Gagné, C. A. Koval, T. J. Smith, M. C. Cimolino, *J. Am. Chem. Soc.*, **101**, 4571, 1979.
- 32 R. R. Gagné, C. L. Spiro, T. J. Smith, C. A. Hannam, W. R. Thies, A. K. Shienke, *J. Am. Chem. Soc.*, **103**, 4073, 1981.
- 33 S. L. Lambert, C. L. Spiro, R. R. Gagne, D. N. Hendrickson, *Inorg. Chem.*, **21**, 68, 1982.
- 34 C. L. Spiro, S. L. Lambert, T. J. Smith, E. N. Duesler, R. R. Gagne, D. N. Hendrickson, *Inorg. Chem.*, **20**, 1229, 1981.
- 35 R. R. Gagné, R. P. Kreh, J. A. Dodge, *J. Am. Chem. Soc.*, **101**, 6917, 1979.
- 36 B. F. Hoskins, R. Robson, H. A. Schaap, *Inorg. Nucl. Chem. Lett.*, **8**, 21, 1975.
- 37 I. Dickson, R. Robson, *Inorg. Chem.*, **13**, 1301, 1974.
- 38 W. Rosen, *Inorg. Chem.*, **10**, 1832, 1971.
- 39 M. G. B. Drew, J. Nelson, S. M. Nelson, *J. Chem. Soc. Dalton Trans.*, 1678, 1981.
- 40 W. J. Stratton, D. H. Busch, *J. Am. Chem. Soc.*, **82**, 4834, 1960.
- 41 W. J. Stratton, *Inorg. Chem.*, **9**, 517, 1970.
- 42 W. J. Stratton, P. J. Ogren, *Inorg. Chem.*, **9**, 2588, 1970.
- 43 C. J. O'Connor, R. J. Romanach, D. M. Robertson, E. E. Eduok, F. R. Fronczek, *Inorg. Chem.*, **22**, 449, 1983.
- 44 T. C. Woon, L. K. Thompson, P. Robichaud, *Inorg. Chim. Acta*, **90**, 201, 1984.

- 45 F. S. Keij, R. A. G. de Graaff, J. G. Haasnoot, J. Reedijk, *J. Chem. Soc. Dalton Trans.*, 2004, 1984.
- 46 R. Prius, P. J. M. W. L. Birker, J. G. Haasnoot, G. C. Verschoor, J. Reedijk, *Inorg. Chem.*, **24**, 4128, 1985.
- 47 P. W. Ball, A. B. Blake, *J. Chem. Soc. A*, 1415, 1969.
- 48 P. W. Ball, A. B. Blake, *J. Chem. Soc. Dalton Trans.*, 852, 1974.
- 49 A. M. M. Lanfredi, A. Tiripicchio, M. Ghedini, G. De Munno, *Acta Crystallogr. Sect. B*, **38**, 1165, 1982.
- 50 M. Ghedini, G. De Munno, G. Denti, A. M. M. Lanfredi, A. Tiripicchio, *Inorg. Chim. Acta*, **57**, 87, 1982.
- 51 G. De Munno, G. Denti, P. Dapporto, *Inorg. Chim. Acta*, **74**, 199, 1983.
- 52 G. De Munno, G. Denti, *Acta Crystallogr. Sect. C*, **40**, 616, 1984.
- 53 P. Dapporto, G. De Munno, A. Segà, C. Meali, *Inorg. Chim. Acta*, **83**, 171, 1984.
- 54 L. K. Thompson, T. C. Woon, D. B. Murphy, E. J. Gabe, F. L. Lee, Y. Le Page, *Inorg. Chem.*, **24**, 4719, 1985.
- 55 L. Rosenb erg, L. K. Thompson, E. J. Gabe, F. L. Lee, *J. Chem. Soc. Dalton Trans.*, 625, 1986.
- 56 T. C. Woon, R. McDonald, S. K. Mandal, L. K. Thompson, A. W. Addison, *J. Chem. Soc. Dalton Trans.*, 2381, 1986.
- 57 L. K. Thompson, S. K. Mandal, E. J. Gabe, F. L. Lee, A. W. Addison, *Inorg. Chem.*, **26**, 657, 1987.
- 58 D. M. Dooley, R. A. Scott, J. Ellinghaus, E. I. Solomon, H. B. Gray, *Proc. Natl. Acad. Sci. U. S. A.*, **75**, 309, 1978.
- 59 S. K. Mandal, L. K. Thompson, M. J. Newlands, F. L. Lee, Y. Lepage, J. P. Charland, E. J. Gabe, *Inorg. Chim. Acta*, **122**, 199, 1986.
- 60 S. K. Mandal, L. K. Thompson, E. J. Gabe, F. L. Lee, J. P. Charland, *Inorg. Chem.*, **26**, 2384, 1987.
- 61 L. K. Thompson, S. K. Mandal, L. Rosenberg, F. L. Lee, E. J. Gabe, *Inorg. Chim. Acta*, **133**, 81, 1987.
- 62 J. E. Andrew, A. B. Blake, *J. Chem. Soc. A*, 1408, 1969.
- 63 L. K. Thompson, V. T. Chacko, J. A. Elvidge, A. B. P. Lever, R. V. Parish, *Can. J. Chem.*, **47**, 4141, 1969.
- 64 A. B. P. Lever, L. K. Thompson, W. M. Reiff, *Inorg. Chem.*, **11**, 104, 1972.
- 65 A. B. P. Lever, L. K. Thompson, W. M. Reiff, *Inorg. Chem.*, **11**, 2292, 1972.
- 66 D. A. Sullivan, G. J. Palenik, *Inorg. Chem.*, **16**, 1127, 1977.
- 67 J. A. Doull, L. K. Thompson, *Can. J. Chem.*, **58**, 221, 1980.

- 68 J. C. Dewan, L. K. Thompson, *Can. J. Chem.*, **60**, 121, 1982.
- 69 D. V. Bautista, J. C. Dewan, L. K. Thompson, *Can. J. Chem.*, **60**, 2583, 1982.
- 70 G. Marongiu, E. C. Lingafelter, *Acta Crystallogr. Sect. B*, **38**, 620, 1982.
- 71 G. Bullock, F. W. Hartstock, L. K. Thompson, *Can. J. Chem.*, **61**, 57, 1983.
- 72 L. K. Thompson, *Can. J. Chem.*, **61**, 579, 1983.
- 73 F. W. Hartstock, L. K. Thompson, *Inorg. Chim. Acta*, **72**, 227, 1983.
- 74 P. Robichand, L. K. Thompson, *Inorg. Chim. Acta*, **85**, 137, 1984.
- 75 L. K. Thompson, A. W. Hanson, B. S. Ramaswamy, *Inorg. Chem.*, **23**, 2459, 1984.
- 76 L. K. Thompson, F. W. Hartstock, P. Robichand, A. W. Hanson, *Can. J. Chem.*, **62**, 2755, 1984.
- 77 L. K. Thompson, F. W. Hartstock, L. Rosenberg, T. C. Woon, *Inorg. Chim. Acta*, **97**, 1, 1985.
- 78 S. K. Mandal, L. K. Thompson, A. W. Hanson, *J. Chem. Soc. Chem. Commun.*, 1709, 1985.
- 79 S. K. Mandal, T. C. Woon, L. K. Thompson, M. J. Newlands, E. J. Gabe, *Aust. J. Chem.*, **39**, 1007, 1985.
- 80 L. K. Thompson, F. L. Lee, E. J. Gabe, *Inorg. Chem.*, **27**, 39, 1988.
- 81 L. K. Thompson, *Ph. D. Thesis*, Univ. of Manchester, Inst. of Sci. & Tech., 1968.
- 82 A. B. P. Lever, B. S. Ramaswamy, S. P. Pickens, *Inorg. Chim. Acta*, **46**, L59, 1980.
- 83 L. K. Thompson, S. K. Mandal, E. J. Gabe, J. P. Charland, *J. Chem. Soc. Chem. Commun.*, 1537, 1986.
- 84 A. Abragam, B. Bleaney, *Electron Paramagnetic Resonance of Transition Ions*, Clarendon Press, Oxford, 1970.
- 85 I. Bertini, C. Luchinat, A. Scozzafava, *Structure and Bonding*, **48**, 45, 1982.
- 86 I. Bertini, C. Luchinat, In *Metal Ions in Biological Systems*, H. Sigel Ed., **15**, 101, 1983.
- 87 R. L. Carlin, *Transition Metal Chemistry*, **1**, 1, 1965.
- 88 D. Nicholls, In *Comprehensive Inorganic Chemistry*, Vol. 3, p. 1109, Pergamon Press, Oxford, 1973.
- 89 J. H. van Vleck, *Electric and Magnetic Susceptibilities*, Oxford Univ. Press, 1965.
- 90 A. P. Ginsberg, M. E. Lines, *Inorg. Chem.*, **11**, 2289, 1972.
- 91 A. P. Ginsberg, R. L. Martin, R. W. Bookes, R. C. Sherwood, *Inorg. Chem.*, **11**, 2884, 1972.

- 92 A. Earnshaw, J. Lewis, *J. Chem. Soc.*, **369**, 1961.
- 93 B. N. Figgis, *Introduction to Ligand Fields*, Interscience, New York, N. Y., 1966.
- 94 J. S. Griffith, *The Theory of Transition Metal Ions*, Cambridge U. P., New York, 1961.
- 95 M. Gerloch, J. R. Miller, *Progr. Inorg. Chem.*, **10**, 1, 1968.
- 96 T. Wen, L. K. Thompson, F. L. Lee, E. J. Gabe, *Inorg. Chem.*, in press.
- 97 D. F. Grant, E. J. Gabe, *J. Appl. Crystallogr.*, **11**, 114, 1978.
- 98 G. Germain, P. Main, M. M. Woolfson, *Acta Crystallogr. Sect. A: Cryst. Phys. Diffr. Theor. Gen. Crystallogr.*, **A27**, 368, 1971.
- 99 E. J. Gabe, F. L. Lee, Y. Le Page, *Crystallographic Computing III*; G. Sheldrick, C. Kruger, R. Goddard, Eds; Charendon Press, Oxford, 1985, p. 187.
- 100 International Tables for X-ray Crystallography; Kynoch Press, Birmingham, England, 1974, Vol. IV, Table 2.2B, p. 99.
- 101 B. J. Hathaway, A. E. Underhill, *J. Chem. Soc.*, **3091**, 1961.
- 102 N. N. Greenwood, *J. Chem. Soc.*, **3811**, 1959.
- 103 A. B. P. Lever, E. Mantovani, B. S. Ramaswamy, *Can. J. Chem.*, **49**, 1957, 1971.
- 104 O. Kahn, *Inorg. Chim. Acta*, **62**, 3, 1983.
- 105 M. S. Haddad, S. R. Wilson, D. J. Hodgson, D. N. Hendrickson, *J. Am. Chem. Soc.*, **103**, 384, 1981.

APPENDIX A

SOME X-RAY DATA FOR COMPLEXES 36 and 50

Table A.1 U(I,J) or U values (x100) for the complex 50. E.S.D's refer to the last digit printed.

Atom	U11(U)	U22	U33	U12	U13	U23
NI	3.23(8)	2.91(8)	3.58(7)	1.63(7)	0.07(6)	0.11(7)
CL 1	3.63(12)	2.94	4.46(18)	1.47(14)	-0.01(7)	0.01
CL 2	4.66(13)	4.07(13)	6.41(13)	2.63(11)	0.67(10)	0.29(11)
CL 0	9.2 (4)	8.1 (3)	9.7 (3)	5.4 (3)	-0.3 (3)	0.8 (3)
O 1	5.0 (4)	8.0 (5)	4.4 (3)	4.1 (4)	0.0 (3)	-0.2 (3)
O 2	4.4 (3)	4.3 (3)	4.5 (3)	2.6 (3)	0.2 (3)	-0.3 (3)
O 3	5.3 (5)	6.4 (5)	8.1 (5)	1.6 (4)	-1.3 (4)	-0.7 (4)
N 1	2.7 (4)	2.9 (4)	4.1 (4)	1.9 (4)	0.2 (3)	0.0 (3)
N 2	2.6 (4)	3.1 (5)	5.9 (5)	1.8 (4)	-0.3 (4)	0.0 (3)
N 3	3.0 (4)	2.6 (4)	4.1 (4)	1.7 (4)	0.3 (3)	0.0 (3)
N 4	4.7 (5)	2.6 (5)	4.1 (4)	1.4 (4)	0.2 (4)	0.5 (3)
C 1	2.5 (5)	3.8 (6)	6.2 (6)	1.1 (5)	-0.9 (5)	0.1 (5)
C 2	2.7 (5)	2.7 (5)	4.3 (5)	1.1 (4)	0.0 (4)	0.2 (4)
C 3	3.1 (5)	3.1 (5)	3.0 (4)	2.0 (4)	0.0 (4)	0.0 (4)
C 4	3.2 (5)	2.4 (5)	3.3 (4)	1.6 (5)	-0.3 (4)	-0.6 (4)
C 5	3.8 (6)	3.2 (5)	5.2 (6)	2.0 (5)	0.0 (4)	0.1 (4)
C 6	5.5 (6)	2.5 (5)	3.2 (4)	2.5 (5)	-0.5 (4)	0.0 (4)
C 7	6.7 (7)	4.4 (6)	4.8 (6)	4.0 (6)	0.0 (5)	0.2 (4)
C 8	8.8 (9)	4.1 (6)	4.7 (6)	4.3 (7)	0.1 (6)	0.7 (5)
C 9	7.5 (9)	2.8 (5)	5.0 (6)	1.6 (6)	-0.7 (5)	0.3 (5)
C10	5.6 (7)	2.9 (6)	4.5 (5)	1.3 (5)	0.4 (5)	0.7 (4)
C11	5.7 (8)	4.4 (8)	9.1 (11)	1.5 (6)	0.6 (7)	0.9 (7)
O 4	18.1 (15)					
O 5	24.5 (17)					
H 1	5.1					
H 2	4.2					
H 5	5.1					
H 7	6.2					
H 8	7.1					
H 9	6.2					
H N2	4.8					
H11A	10.1 (46)					
H11B	7.8 (36)					
H11C	9.8 (48)					

ANISOTROPIC TEMPERATURE FACTORS ARE OF THE FORM -
 $TEMP = -2 \cdot \pi^2 \cdot (H \cdot H \cdot U_{11} \cdot \sin^2 \theta + 2 \cdot H \cdot K \cdot U_{12} \cdot \sin \theta \cos \theta + \dots)$

Table A.2 U(I,J) or U values (x100) for the complex 36. E.S.D's refer to the last digit printed.

Atom	U11(U)	U22	U33	U12	U13	U23
CO	3.09(4)	2.60(4)	3.72(3)	1.61(4)	-0.05(4)	-0.14(4)
CL 1	2.98(8)	2.99	4.93(14)	1.14(9)	0.15(5)	-0.15
CL 2	4.58(9)	3.71(9)	6.89(11)	2.45(8)	0.42(8)	0.29(9)
CL 0	8.9 (3)	9.0 (3)	9.8 (3)	5.68(23)	0.06(22)	1.15(22)
O 1	6.6 (3)	8.5 (4)	3.52(23)	5.2 (3)	-0.14(24)	0.5 (3)
O 2	4.8 (3)	5.3 (3)	4.11(23)	2.8 (3)	0.68(24)	0.14(24)
O 3	5.4 (3)	6.6 (4)	7.4 (4)	2.3 (3)	-1.4 (3)	0.0 (3)
N 1	2.6 (3)	2.4 (3)	4.2 (3)	1.53(23)	-0.04(22)	-0.10(21)
N 2	2.0 (3)	2.3 (3)	5.9 (4)	1.15(22)	-0.24(24)	0.10(24)
N 3	3.4 (3)	3.1 (3)	3.6 (3)	2.02(24)	-0.12(23)	0.22(21)
N 4	3.7 (3)	2.9 (3)	4.2 (3)	1.57(24)	0.5 (3)	0.5 (3)
C 1	1.7 (3)	3.4 (3)	6.3 (4)	0.7 (3)	-0.5 (3)	0.7 (3)
C 2	3.1 (3)	3.8 (4)	4.0 (3)	2.2 (3)	-0.4 (3)	0.1 (3)
C 3	2.2 (3)	2.8 (3)	3.4 (3)	1.4 (3)	-0.21(24)	-0.2 (3)
C 4	2.4 (3)	1.8 (3)	3.0 (3)	0.50(23)	-0.29(24)	-0.2 (3)
C 5	5.2 (4)	3.8 (4)	4.3 (4)	3.1 (3)	-0.4 (3)	0.2 (3)
C 6	5.6 (4)	2.4 (3)	3.3 (3)	2.5 (3)	-0.1 (3)	-0.6 (3)
C 7	6.2 (5)	5.2 (4)	4.5 (4)	4.3 (4)	0.2 (3)	0.4 (3)
C 8	10.3 (7)	3.7 (4)	5.1 (5)	4.8 (5)	-0.8 (5)	-0.6 (3)
C 9	4.65(17)					
C10	4.7 (4)	2.8 (3)	4.9 (4)	1.1 (3)	-0.2 (3)	-0.2 (3)
C11	5.2 (5)	5.0 (5)	8.6 (7)	1.5 (4)	0.7 (5)	0.2 (5)
O 4	12.8 (7)					
O 5	18.6 (7)					
H 1	4.6					
H 2	4.7					
H 5	5.4					
H 7	6.3					
H 8	7.4					
H 9	5.8					
H N2	4.4					
H11A	7.9 (4)					
H11B	5.3 (5)					
H11C	9.9 (4)					
H101	3.7 (6)					
H201	12.6 (3)					
H102	7.1 (4)					
H202	2.5 (6)					
H103	5.3 (5)					
H203	7.6 (4)					

ANISOTROPIC TEMPERATURE FACTORS ARE OF THE FORM —

$$\text{TEMP} = -2 \cdot \pi^2 \cdot (h^2 \cdot U_{11} \cdot \text{ASTAR} \cdot \text{ASTAR} + \dots + 2 \cdot h \cdot k \cdot U_{12} \cdot \text{ASTAR} \cdot \text{BSTAR} + \dots)$$

APPENDIX B

V-T MAGNETIC SUSCEPTIBILITY DATA
OF SOME COMPLEXES

Table B.1 Magnetic data for the complex 50 and 51.

No.	50		51	
	T (K)	χ (cgsu)	T (K)	χ (cgsu)
1	1.1413E+001	1.0137E-002	1.1134E-002	5.7248E+000
2	2.1030E+001	1.3324E-002	1.2580E-002	8.1140E+000
3	2.4607E+001	1.3796E-002	1.5493E-002	1.2740E+001
4	2.6342E+001	1.3941E-002	1.6833E-002	1.7319E+001
5	2.7058E+001	1.3988E-002	1.7354E-002	2.2051E+001
6	2.8143E+001	1.4046E-002	1.7395E-002	2.6945E+001
7	3.1609E+001	1.4111E-002	1.7110E-002	3.2062E+001
8	3.6386E+001	1.4038E-002	1.6659E-002	3.6733E+001
9	4.0061E+001	1.3883E-002	1.6133E-002	4.1488E+001
10	4.4177E+001	1.3610E-002	1.5720E-002	4.5043E+001
11	4.9031E+001	1.3273E-002	1.5169E-002	4.9185E+001
12	5.3790E+001	1.2904E-002	1.4616E-002	5.3868E+001
13	5.8760E+001	1.2497E-002	1.4040E-002	5.8760E+001
14	6.4023E+001	1.2061E-002	1.3452E-002	6.3936E+001
15	6.9219E+001	1.1640E-002	1.2908E-002	6.9014E+001
16	7.4320E+001	1.1238E-002	1.2403E-002	7.4080E+001
17	7.9540E+001	1.0862E-002	1.1937E-002	7.9150E+001
18	8.4204E+001	1.0506E-002	1.1505E-002	8.3838E+001
19	9.2642E+001	9.9361E-003	1.0826E-002	9.2179E+001
20	1.0306E+002	9.2994E-003	1.0081E-002	1.0241E+002
21	1.1375E+002	8.7068E-003	9.4018E-003	1.1287E+002
22	1.2424E+002	8.1938E-003	8.8205E-003	1.2321E+002
23	1.3428E+002	7.7456E-003	8.3181E-003	1.3321E+002
24	1.4452E+002	7.3444E-003	7.8783E-003	1.4314E+002
25	1.6257E+002	6.6893E-003	7.1478E-003	1.6218E+002
26	1.8314E+002	6.0927E-003	6.4935E-003	1.8076E+002
27	2.0326E+002	5.6064E-003	5.9694E-003	2.0069E+002
28	2.2347E+002	5.1851E-003	5.5111E-003	2.2080E+002
29	2.4431E+002	4.8277E-003	5.1246E-003	2.4123E+002
30	2.6509E+002	4.5236E-003	4.7981E-003	2.6204E+002
31	2.8575E+002	4.2617E-003	4.5173E-003	2.8176E+002
32	3.0074E+002	4.0940E-003	4.3377E-003	2.9595E+002

Table B.2 Magnetic data for the complex 57 and 59.

57			59	
No.	T (K)	χ (cgsu)	T (K)	χ (cgsu)
1	5.7150E+000	1.4800E-001	5.8026E+000	1.6332E-001
2	7.8050E+000	1.1627E-001	8.1336E+000	1.2240E-001
3	1.2595E+001	7.8820E-002	1.2679E+001	8.2529E-002
4	1.7221E+001	6.0272E-002	1.7286E+001	6.2438E-002
5	2.1899E+001	4.8597E-002	2.2029E+001	5.0082E-002
6	2.6850E+001	4.0350E-002	2.6941E+001	4.1435E-002
7	3.1805E+001	3.4393E-002	3.2076E+001	3.5268E-002
8	3.6633E+001	3.0232E-002	3.6761E+001	3.0968E-002
9	4.1264E+001	2.6968E-002	4.1453E+001	2.7592E-002
10	4.4318E+001	2.4963E-002	4.5012E+001	2.5558E-002
11	4.9062E+001	2.2760E-002	4.9108E+001	2.3344E-002
12	5.3751E+001	2.0885E-002	5.3926E+001	2.1385E-002
13	5.8640E+001	1.9234E-002	5.8592E+001	1.9770E-002
14	6.3821E+001	1.7725E-002	6.3908E+001	1.8230E-002
15	6.8911E+001	1.6465E-002	6.9151E+001	1.6847E-002
16	7.3920E+001	1.5393E-002	7.4180E+001	1.5753E-002
17	7.8955E+001	1.4474E-002	7.9199E+001	1.4789E-002
18	8.3628E+001	1.3671E-002	8.3890E+001	1.3963E-002
19	9.1914E+001	1.2490E-002	9.1649E+001	1.2851E-002
20	1.0215E+002	1.1290E-002	1.0249E+002	1.1521E-002
21	1.1258E+002	1.0269E-002	1.1307E+002	1.0475E-002
22	1.2286E+002	9.4389E-003	1.2332E+002	9.6292E-003
23	1.3281E+002	8.7555E-003	1.3335E+002	8.9249E-003
24	1.4268E+002	8.1815E-003	1.4314E+002	8.3354E-003
25	1.6178E+002	7.2556E-003	1.6218E+002	7.3901E-003
26	1.8052E+002	6.4680E-003	1.8124E+002	6.5878E-003
27	2.0011E+002	5.8605E-003	2.0069E+002	5.9636E-003
28	2.2047E+002	5.3408E-003	2.2080E+002	5.4349E-003
29	2.4046E+002	4.9150E-003	2.4085E+002	5.0035E-003
30	2.6378E+002	4.5627E-003	2.6248E+002	4.6425E-003
31	2.8129E+002	4.2625E-003	2.8176E+002	4.3364E-003
32	2.9475E+002	4.0756E-003	2.9595E+002	4.1433E-003

Table B.3 Magnetic data for the complex 36 and 37.

36			37	
No.	T (K)	χ (cgsu)	T (K)	χ (cgsu)
1	5.6342E+000	7.1925E-002	5.3680E+000	6.5925E-002
2	7.6008E+000	7.1517E-002	7.7399E+000	6.4488E-002
3	1.2177E+001	6.9415E-002	1.2456E+001	6.1965E-002
4	1.7008E+001	6.5680E-002	1.7099E+001	5.8427E-002
5	2.1802E+001	6.1456E-002	2.1760E+001	5.4587E-002
6	2.6854E+001	5.7178E-002	2.6705E+001	5.0704E-002
7	3.2027E+001	5.3150E-002	3.1680E+001	4.7076E-002
8	3.6761E+001	4.9741E-002	3.6459E+001	4.4040E-002
9	4.1524E+001	4.6635E-002	4.1064E+001	4.1329E-002
10	4.5012E+001	4.4591E-002	4.4177E+001	3.9435E-002
11	4.9232E+001	4.2058E-002	4.8907E+001	3.7233E-002
12	5.4004E+001	3.9746E-002	5.3595E+001	3.5214E-002
13	5.9024E+001	3.7519E-002	5.8448E+001	3.3329E-002
14	6.4254E+001	3.5421E-002	6.3647E+001	3.1464E-002
15	6.9425E+001	3.3548E-002	6.8705E+001	2.9820E-002
16	7.4520E+001	3.1879E-002	7.3720E+001	2.8357E-002
17	7.9735E+001	3.0394E-002	7.8760E+001	2.7064E-002
18	8.4466E+001	2.9051E-002	8.3471E+001	2.5872E-002
19	9.2974E+001	2.7005E-002	9.1848E+001	2.4070E-002
20	1.0330E+002	2.4850E-002	1.0192E+002	2.2157E-002
21	1.1405E+002	2.2912E-002	1.1238E+002	2.0460E-002
22	1.2447E+002	2.1293E-002	1.2240E+002	1.9040E-002
23	1.3455E+002	1.9922E-002	1.3268E+002	1.7835E-002
24	1.4452E+002	1.8743E-002	1.4237E+002	1.6796E-002
25	1.6276E+002	1.6820E-002	1.6139E+002	1.5094E-002
26	1.8362E+002	1.5137E-002	1.8029E+002	1.3601E-002
27	2.0354E+002	1.3798E-002	1.9970E+002	1.2416E-002
28	2.2413E+002	1.2662E-002	2.1974E+002	1.1400E-002
29	2.4431E+002	1.1709E-002	2.3963E+002	1.0551E-002
30	2.6291E+002	1.0907E-002	2.6248E+002	9.8360E-003
31	2.8575E+002	1.0222E-002	2.8081E+002	9.2223E-003
32	3.0074E+002	9.7824E-003	2.9425E+002	8.8354E-003

* Uncertainties in the susceptibility data are of the order of 0.1%

